NASA Contractor Report 3195

Further Investigation of a Finite Difference Procedure for Analyzing the Transonic Flow About Harmonically Oscillating Airfoils and Wings

W. H. Weatherill, F. E. Ehlers,
E. Yip, and J. D. Sebastian

CONTRACT NAS1-15128
MAY 1980

NASA

NASA Contractor Report 3195

Further Investigation of a Finite Difference Procedure for Analyzing the Transonic Flow About Harmonically Oscillating Airfoils and Wings

W. H. Weatherill, F. E. Ehlers,
E. Yip, and J. D. Sebastian
Boeing Commercial Airplane Company
Seattle, Washington

Prepared for
Langley Research Center
under Contract NAS1-15128

NASA
National Aeronautics
and Space Administration

Scientific and Technical
Information Office

1980

CONTENTS

1.0 SUMMARY

A finite difference method for solving the unsteady transonic flow about harmonically oscillating wings is investigated. The procedure is based on separating the velocity potential into steady and unsteady parts and linearizing the resulting unsteady differential equation for small disturbances. The differential equation for the unsteady velocity potential is linear with spatially varying coefficients.

The work of this report is a direct extension of earlier studies and includes the development and application of an out-of-core direct solution.

The main results of this study are as follows:

1. An out-of-core solution procedure has been developed and programmed to provide a capability for solving two-dimensional problems with a sufficient number of mesh points for practical use.

2. Reasonable correlation with more exact linear theory is obtained for airfoils of vanishing thickness at values of Mach number and reduced frequency of direct interest in flutter analyses.

3. Comparison of two-dimensional finite difference solutions with exact analytic solutions indicates the accuracy of the difference solution is dependent on the boundary conditions of the mesh region. A corresponding study with similar results for a simplified one-dimensional problem is described in NASA CR-2933.

2.0 INTRODUCTION

The purpose of the work described in this report is to continue the development of a means for calculating air forces for use in flutter analyses of three-dimensional lifting surfaces in the transonic flight regime. The work concentrates on a particular procedure that assumes small perturbations, the existence of a velocity potential and simple harmonic motion, and uses finite difference theory to solve the resulting set of partial differential equations. This study represents a direct extension of the research described in references 1 through 3.

Recent papers by Tijdeman (ref. 4) and Ashley (ref. 5) have contributed significantly toward understanding the transonic characteristics that are important to the flutter problem. The presence of a shock on an oscillating airfoil results in a pressure pulse in the unsteady pressure distribution. This pressure pulse or "pressure doublet" results from the chordwise movement of the shock. The shock moves chordwise as the airfoil oscillates. The magnitude of the pulse varies as the airfoil moves, and the pulse itself may or may not move chordwise. The important characteristics of the pressure pulse with respect to flutter instabilities appear to be its amplitude, its phasing with respect to the section motion, and its location relative to the section elastic axis. In particular, for airfoils with blunt leading edges such as supercritical sections, the pulse tends to be forward on the section, which increases the likelihood of instabilities.

The procedure of this report divides the velocity potential into steady and unsteady parts. The steady potential is calculated using the classic, nonlinear, small perturbation differential equation. The unsteady potential is then calculated using a linear equation with spatially varying coefficients that depend on the steady flow. The procedure does not appear to include shock motion since the difference operator that is used for each mesh point is determined by the steady flow and does not change during the unsteady calculation.

The results calculated using this procedure do contain the pressure pulse that results from the shock motion (refs. 1 through 3). Figure 1 shows that the pressure coefficient distribution computed by subsonic linearized theory for a Mach number of 0.9 indicates no influence of a shock. The real and imaginary parts of the pressure jump across an NACA 64A006 airfoil are plotted in figure 2 at the same Mach number by the transonic method discussed here. By comparing the location of the sharp peaks in figure 2 with the shock in figure 3, we readily see that these sharp peaks appear at the location of the steady-state shock on the airfoil and hence may well be caused by shock motion induced by the oscillating flow. Since we have assumed harmonic motion (i.e., $e^{i\omega t}$), the shock motion could only be represented to the first harmonic at best.

A major concern at the beginning of the investigation was the lack of correlation between the finite difference results for a purely subsonic configuration and more exact linear theory. Section 6.0 is devoted to this problem, and encouraging results are presented.

The effect of the choice of boundary conditions on solution accuracy for the two-dimensional problem is investigated in section 7. This study parallels an investigation of the one-dimensional problem presented in reference 3.

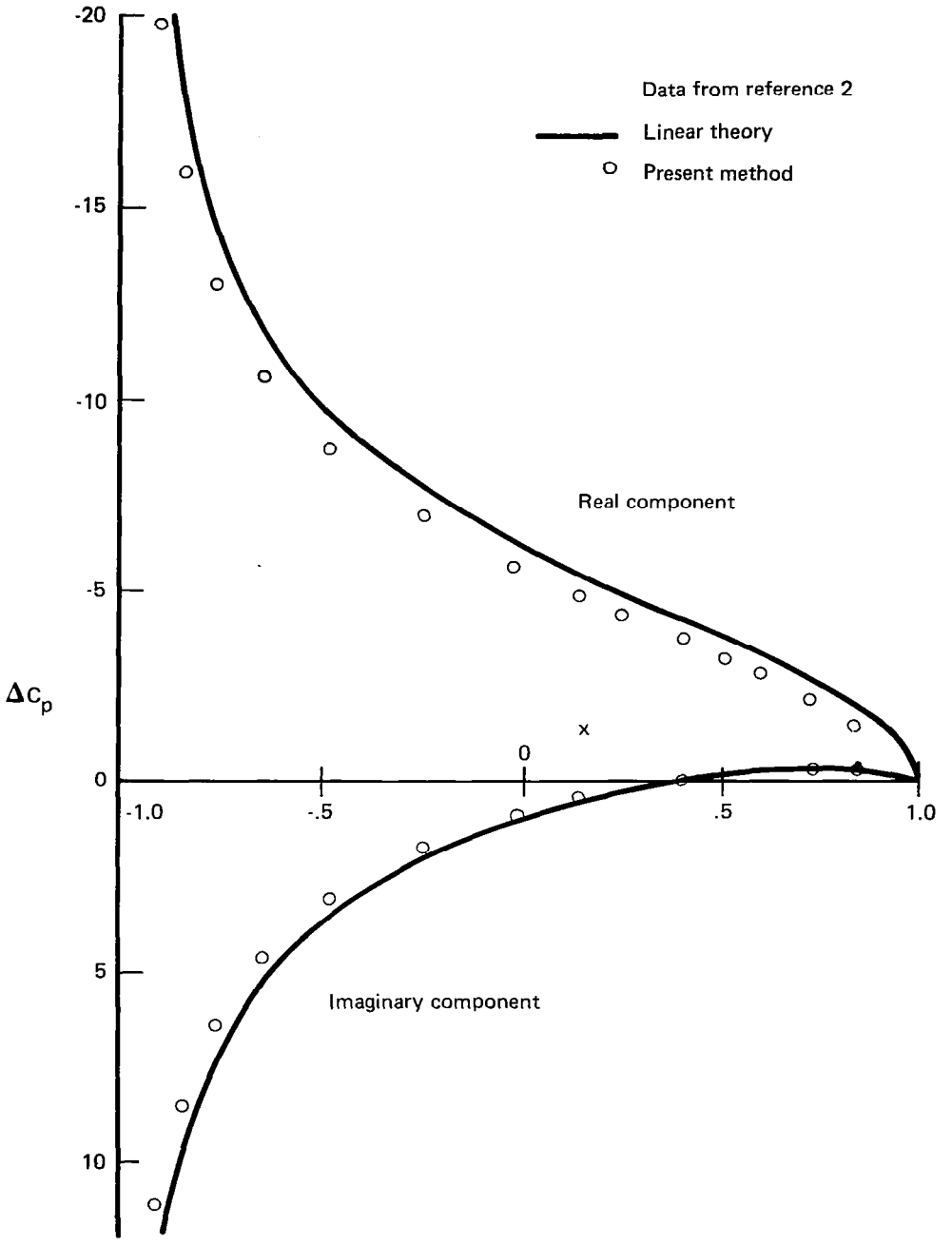

Figure 1.— Jump in Pressure Coefficient Across a Flat Plate Oscillating in Harmonic Pitch; $M = 0.90$, $\omega = 0.06$

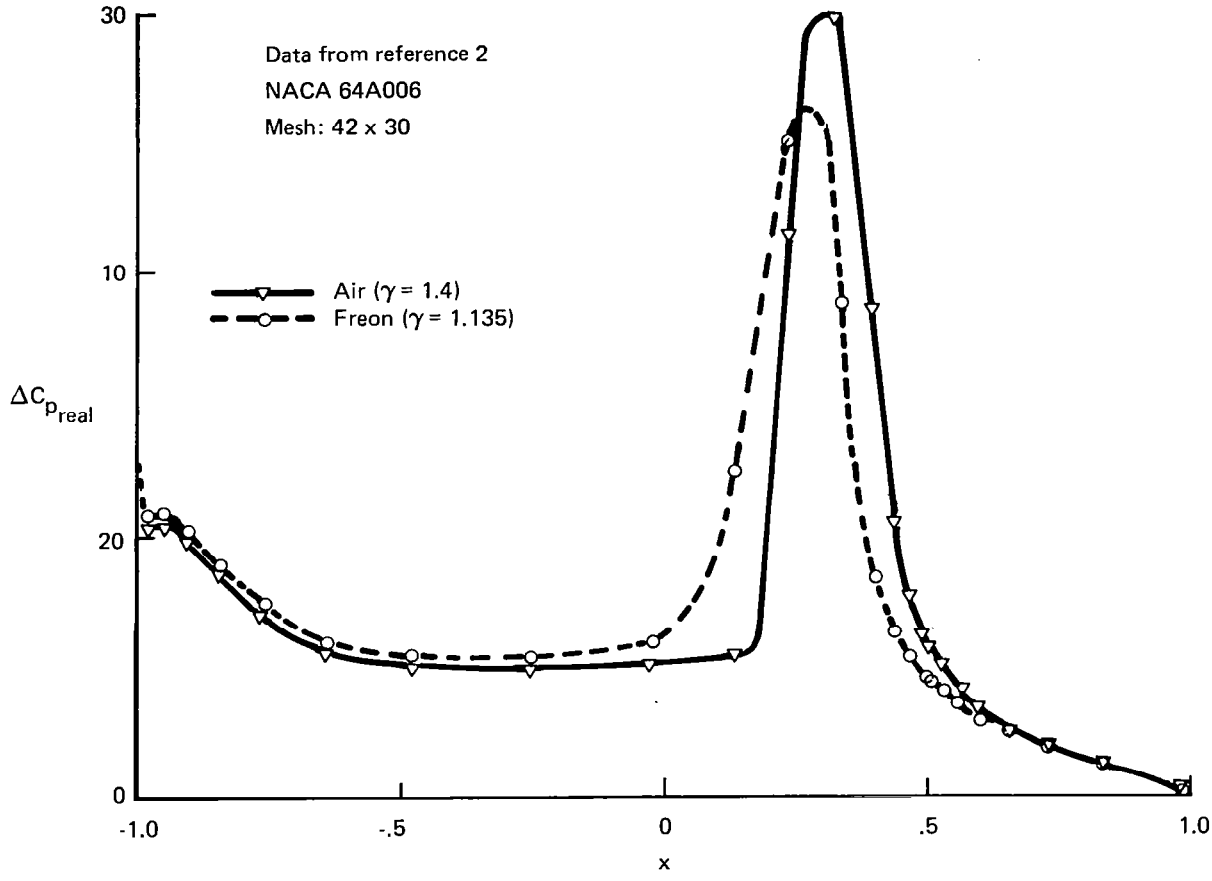

a. REAL PART

Figure 2.– Jump in Pressure Coefficient Across an Airfoil Oscillating in Harmonic Pitch; $M = 0.9$, $\omega = 0.06$

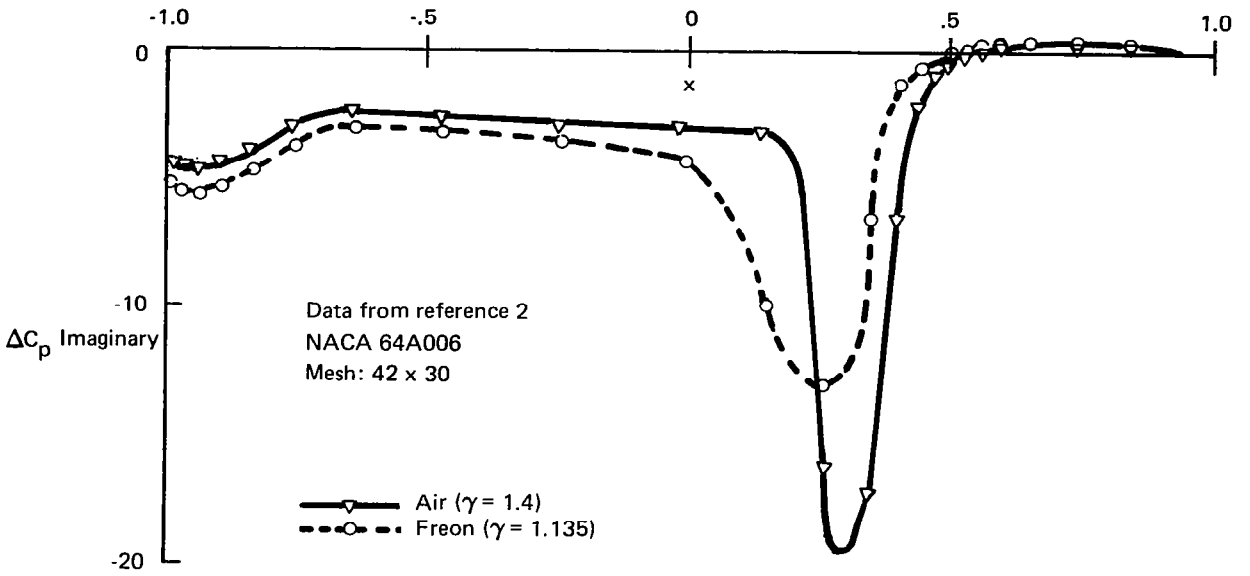

b. IMAGINARY PART

Figure 2.—(Concluded)

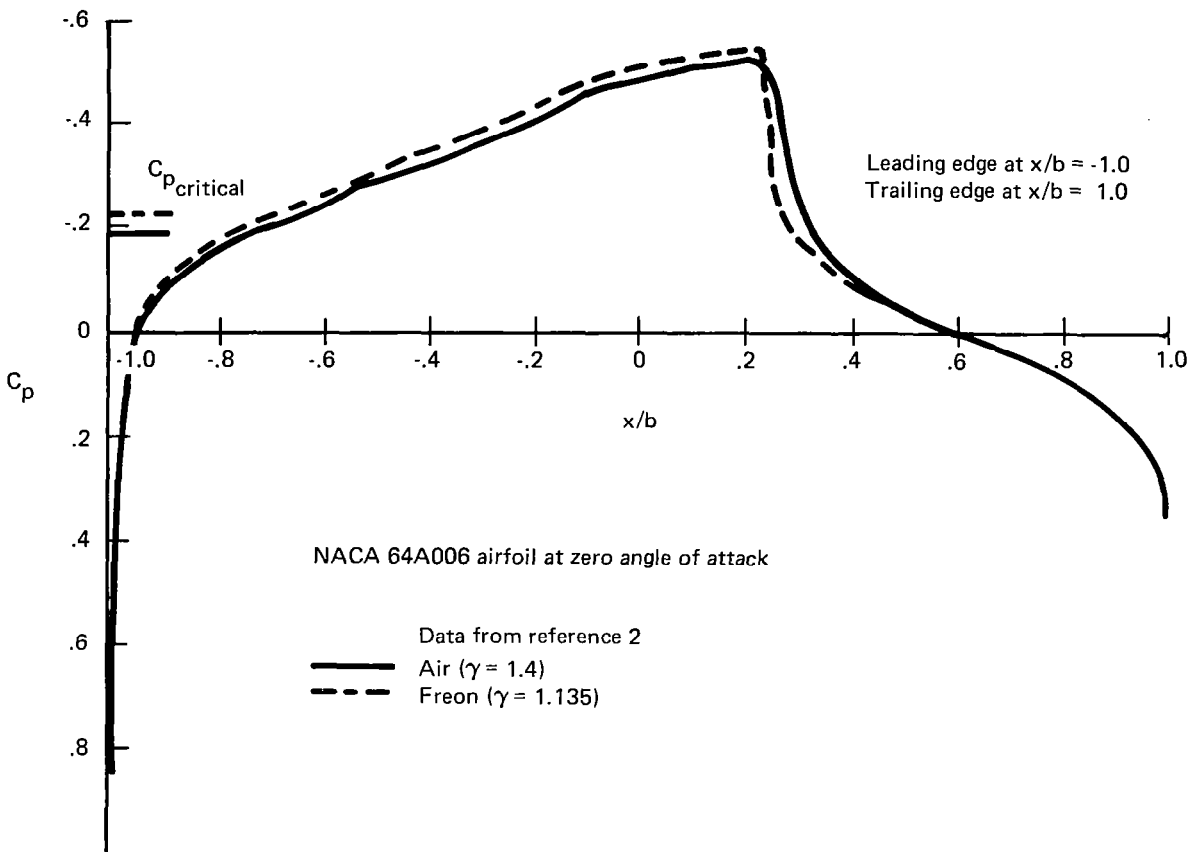

Figure 3.—Steady-State Pressure Coefficient for an Airfoil Section; M = 0.9

Section 8.0 briefly describes several auxiliary investigations that are presented in reference 6. Finally, conclusions are presented in section 9.0.

Other results and studies associated with work presented in this document are given in references 6, 7, and 8. Auxiliary analytical studies are included in reference 6. Reference 7 is the user's manual for the unsteady transonic program used for this report. Reference 8 describes the out-of-core direct solution subroutine.

3.0 ABBREVIATIONS AND SYMBOLS

a	Streamwise dimension of mesh region; also coordinate of downstream boundary
b	Root semichord of wing or semichord of airfoil; also vertical dimension of mesh region
C_p	Pressure coefficient, $(p - p_o) / (1/2\ \rho_o U_o^2)$ where p is the local pressure, p_o the freestream static pressure, and ρ_o the freestream air density
f(x,y,t)	Instantaneous wing shape defined by $z_o = \delta f(x,y,t)$
f_o	Undisturbed wing or airfoil shape
f_1	Unsteady contribution to wing or airfoil shape
i,j,k I,J,K	x,y,z subscripts and indices for points in the mesh
i	$\sqrt{-1}$
K	Transonic parameter, $(1 - M^2) / (M^2\epsilon)$
le, LE	Leading edge
M	Freestream Mach number
n,m	Mesh point indices
q	$\omega^2 / \epsilon - i\omega(\gamma - 1)\varphi_{0_{xx}}$
t	Time in units of b / U_o; also psuedo time defined by iterations in the complex differential equation for the unsteady potential
TE, te	Trailing edge
U_o	Freestream velocity
x_o,y_o,z_o	Physical coordinates, made dimensionless with the root semichord
x,y,z	Scaled coordinates $(x_o,\mu y_o,\mu z_o)$ for the three-dimensional problem; the scaled coordinates for the two-dimensional problem are x and y, with x being the direction of fluid flow

x',y',z'	Variables of integration
x_{le},x_{te}	Coordinates of leading and trailing edges
$\bar{y}$	$\sqrt{K}y$
β	$\sqrt{1 - M^2}$
γ	Ratio of specific heats for air
ΔC_p	Jump in pressure coefficient
$\Delta\varphi_1$	Jump in φ_1 at plane of wing or vortex wake
$\Delta\varphi_{1_{te}}$	Jump in φ_1, at wing trailing edge
δ	Thickness ratio or measure of camber and angle of attack
ϵ	$(\delta / M)^{2/3}$
λ_1	$\omega M / (1 - M^2)$
λ_{1_c}	Critical value of λ_1
μ	Scale factor on y_o and z_o, $\mu = \delta^{1/3} M^{2/3}$; also threshold pivoting factor (sec. 6.1 and separation constant (sec. 7.0 and app. C)
ξ,η,ζ	Coordinates for swept and tapered wing
φ	Complete, scaled perturbation velocity potential; also used for the unsteady potential in finite difference equations
φ_o	Steady scaled perturbation velocity potential
φ_1	Unsteady scaled perturbation velocity potential
ω	Angular reduced frequency (semichord times frequency in radians per second divided by the freestream velocity, $\omega b / U$)

Matrix Notation

[ ]	Rectangular matrix
{ }	Column matrix
[I]	Unit matrix

4.0 FORMULATION AND SOLUTION

A detailed mathematical derivation of the method for the solution of the unsteady velocity potential for the flow about a harmonically oscillating wing is presented in reference 1. The discussion here will be limited to a brief outline of the procedure for the two-dimensional flow.

The complete nonlinear differential equation was simplified by assuming the flow to be a small perturbation from a uniform stream near the speed of sound. The resulting equation for unsteady flow is

$$\left[K - (\gamma - 1)\varphi_t - (\gamma + 1)\varphi_x\right]\varphi_{xx} + \varphi_{yy} - (2\varphi_{xt} + \varphi_{tt}) / \epsilon = 0 \qquad (1)$$

where $K = \left(1 - M^2\right) / \left(M^2\epsilon\right)$, M is the freestream Mach number of velocity U_o in the x-direction, x and y are made dimensionless to the semichord b of the airfoil and the time t to the ratio b / U_o. With the airfoil shape as a function of time defined by the relation

$$y_0 = \delta f(x,t)$$

the linearized boundary condition becomes

$$\varphi_y = f_x(x,t) + f_t(x,t) \qquad (2)$$

The quantity δ is associated with properties of the airfoil (such as maximum thickness ratio, camber, or maximum angle of attack) and is assumed to be small. The coordinate y is scaled to the dimensionless physical coordinate y_o according to

$$y = \delta^{1/3}M^{2/3}y_0$$

and ϵ is given in terms of δ by

$$\epsilon = (\delta / M)^{2/3}$$

The pressure coefficient is found from the relation

$$C_p = -2\epsilon(\varphi_x + \varphi_t)$$

The preceding differential equation is simplified by assuming harmonic motion and by assuming the velocity potential to be separable into a steady-state potential and a potential representing the unsteady effects. We write for a perturbation velocity potential

$$\varphi = \varphi_0(x,y) + \varphi_1(x,y)e^{i\omega t} \qquad (3)$$

and for the body shape

$$y_0 = \delta f(x,t) = \delta\left[f_0(x) + f_1(x)e^{i\omega t}\right]$$

Since the steady-state terms must satisfy the boundary conditions and the differential

equation in the absence of oscillations, we obtain

$$\left[K - (\gamma + 1)\varphi_{0_x}\right]\varphi_{0_{xx}} + \varphi_{0_{yy}} = 0 \tag{4}$$

with

$$\varphi_{0_y} = f_0(x) \quad , \quad y = 0 \quad -1 \leqslant x \leqslant 1 \tag{5}$$

On the assumption that the oscillations are small and products of φ_1 may be neglected, equations (1) and (2) with the aid of equations (4) and (5) yield

$$\left\{\left[K - (\gamma + 1)\varphi_{0_x}\right]\varphi_{1_x}\right\}_x + \varphi_{1_{yy}} - (2i\omega / \epsilon)\varphi_{1_x} + q\varphi_1 = 0 \tag{6}$$

where

$$q = \omega^2 / \epsilon - i\omega(\gamma - 1)\varphi_{0_{xx}}$$

subject to the wing boundary conditions

$$\varphi_{1_y} = f_{1_x} + i\omega f_1(x) \quad , \quad y = 0 \quad -1 \leqslant x \leqslant 1 \tag{7}$$

A computer program for solving the steady-state transonic flow about lifting airfoils based on equations (4) and (5) was developed by Krupp and Murman (refs. 9 and 10). The output of this program or a similar program can be used in computing the coefficients for the differential equation of the unsteady potential. The similarity of the unsteady differential equation to the steady-state equation suggests that the method of column relaxation used by Murman and Krupp for the nonlinear steady-state problem should be an effective way to solve equation (6) for the unsteady potential φ_1. Note that equation (6) is of mixed type, being elliptic or hyperbolic whenever equation (4) is elliptic or hyperbolic. Central differencing was used at all points for the y derivative and all subsonic or elliptic points for the x derivatives. Backward (or upstream) differences were used for the x derivatives at all hyperbolic points.

The boundary condition that the pressure be continuous across the wake from the trailing edge was found in terms of the jump in potential $\Delta\varphi_1$ to be

$$\Delta\varphi_1 = \Delta\varphi_{1_{te}} e^{-i\omega(x - x_{te})} \tag{8}$$

where $\Delta\varphi_{1_{te}}$ is the jump in the potential at $x = x_{te}$ just downstream of the trailing edge and is determined to satisfy the Kutta condition that the jump in pressure vanish at the trailing edge. The quantity $\Delta\varphi_1$ is also used in the difference formulation for the derivative $\varphi_{1_{yy}}$ to satisfy continuity of normal flow across the trailing edge wake.

For the set of difference equations to be determinate, the boundary conditions on the

outer edges of the mesh must be specified. In the original unsteady formulation, these boundary conditions were derived from asymptotic integral relations in a manner parallel to that used by Klunker (ref. 11) for steady flow. A later formulation (ref. 3) applies an outgoing plane wave boundary condition to the outer edges of the mesh. This boundary condition is numerically simpler to apply and, on the basis of limited experience, appears to provide equally good correlation.

The preferred numerical approach to solving the resulting large-order set of difference equations is a relaxation procedure, which permits the calculation to be made as a sequence of relatively small problems. However, as discussed in preceding NASA reports by the authors (refs. 2 and 3), a significant problem of convergence with the relaxation procedure was encountered that severely limits the range of Mach number and reduced frequency for which solutions may be obtained. The authors currently believe the only practical technique for circumventing these instabilities is a full direct solution where the difference equations are solved "all at once" rather than by line relaxation.

5.0 REPRESENTATION OF THE PRESSURE PULSE

Consider an airfoil submerged in a flow that is subsonic but of relatively high Mach number. With appropriate conditions, the usual subsonic pressure distribution differs from that at lower Mach numbers by the presence of shocks attached to the airfoil. For the simple case of a symmetrical airfoil, and with the airfoil at zero angle of attack, these shocks would be of equal strength and symmetrically placed top and bottom. As the airfoil oscillates in pitch, the shocks move in opposite directions, resulting in a pressure pulse that will oscillate in amplitude. In this particular case, although the shocks move fore and aft, the resulting pressure pulse is fixed at a point on the chord. It is also possible, of course, for the location of the pulse to move if the airfoil section is not symmetrical or if the airfoil is at a nominal angle of attack. Also, if the oscillation is very slow, the pulse is in phase with the motion. As the frequency is increased, oscillation of the pulse may lag the motion of the wing. This pressure pulse, called a "pressure doublet" by Ashley, is described in some detail by Tijdeman (ref. 4) and analyzed in a general fashion for its potential effects on flutter by Ashley (ref. 5). The important characteristics of the pressure pulse with respect to flutter instabilities appear to be its amplitude, its phasing with respect to the section motion, and its location relative to the section elastic axis. In particular, for airfoils with blunt leading edges such as supercritical sections, the pulse tends to be forward on the section, which increases the likelihood of instabilities.

An illustration of how the moving shock pulse may be represented in the frequency domain solution of the type discussed here is obtained by considering the Fourier expansion of the pressure pulse produced by two unit step functions oscillating back and forth 90° out of phase on opposite sides of a plate. The resulting lift pulse oscillates in width and the center position oscillates along the plate. In addition, the amplitude of the pulse changes sign in the manner of a square wave. These properties are easily seen in the graphs of figure 4. The Fourier coefficients of the sine and cosine of the first harmonic are shown as a function of position along the plate in figure 5. This is seen to be very similar to the sharp peaks observed in figure 2 which appear at the mean shock location in figure 3. Thus it appears that the present frequency domain method may well produce the pulse amplitude and movement of the fundamental resulting from the moving shock system without additional treatment such as computing the actual shock motion by a nonlinear theory and performing the Fourier analysis. The derivation of the equations for this analysis is included in appendix D.

Tijdeman (ref. 4) has performed a similar analysis for a single shock wave on one side of the airfoil. He showed that the major part of the unsteady pressure pulse is due to the first harmonic.

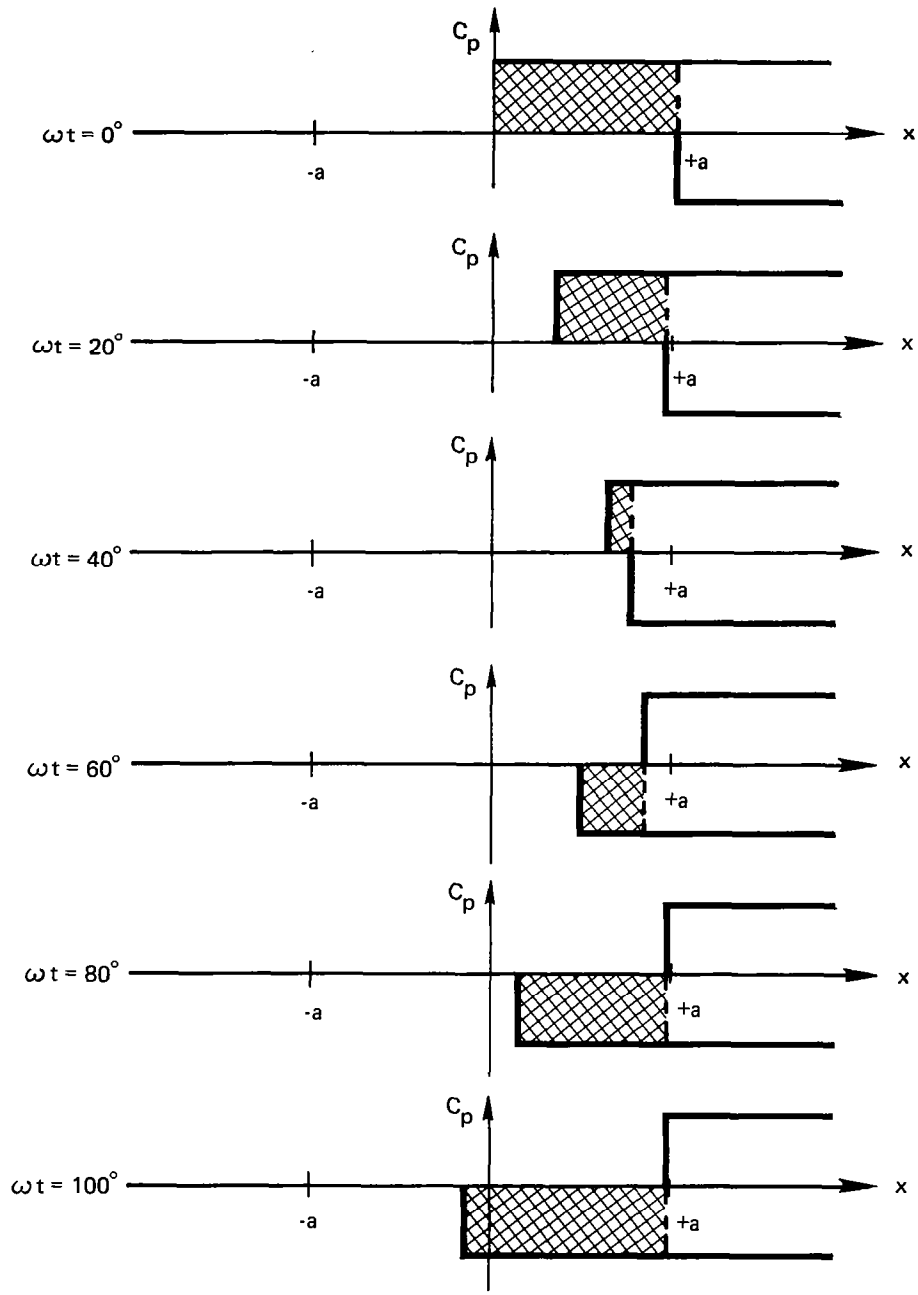

Figure 4.—Pressure Distribution Resulting From Two Pressure Step Functions Oscillating 90° Out of Phase on Opposite Sides of a Plate

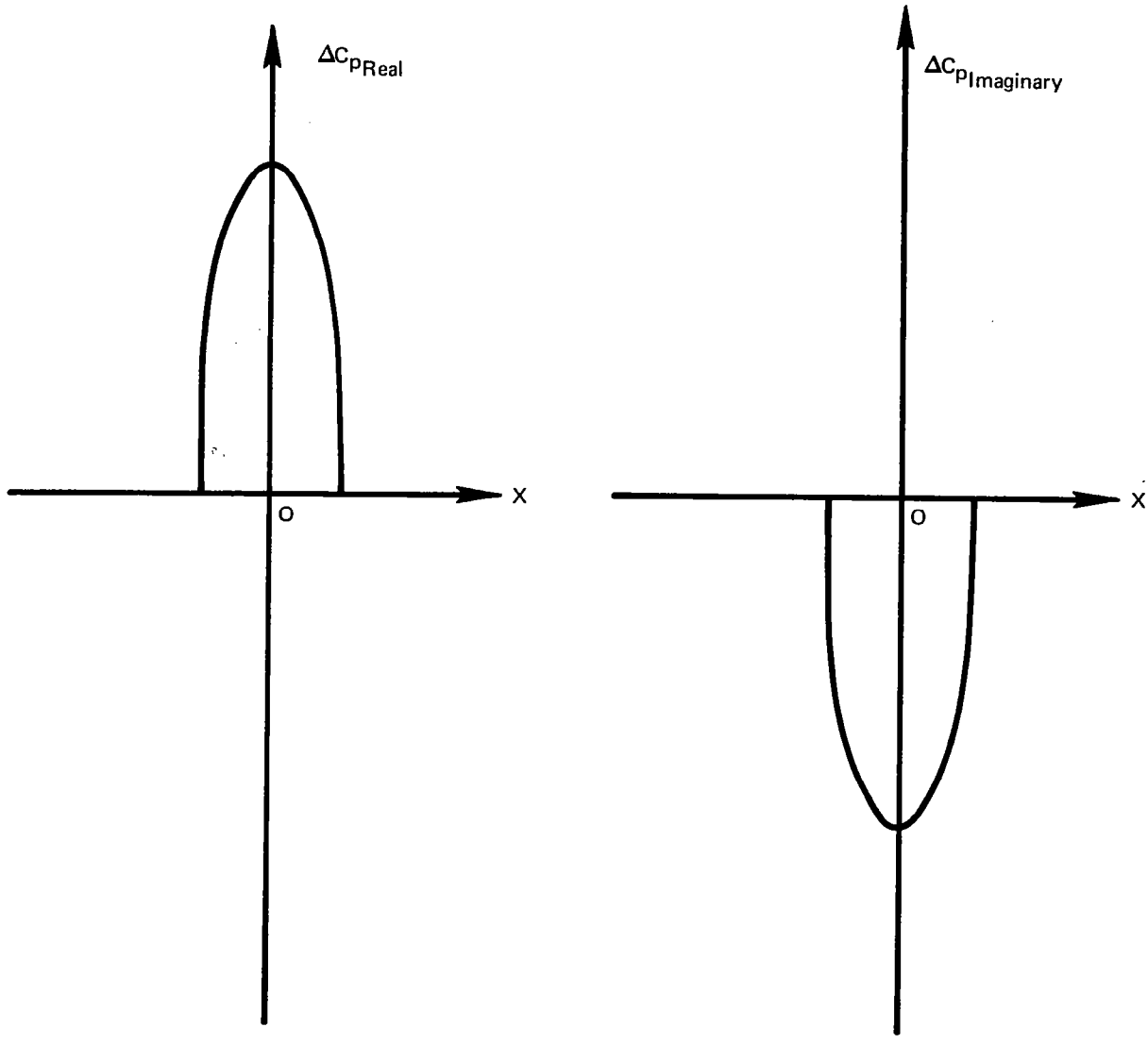

Figure 5.—Real and Imaginary Parts of the Amplitude of the Fundamental Frequency of ΔC_p from Two Step Functions Oscillating 90° out of Phase on Opposite Sides of a Plate

6.0 THE DIRECT SOLUTION

The full direct solution of the finite difference formulation of equation (6) was explored in reference 3 as a means for circumventing the solution instability problems associated with the relaxation procedure. These initial studies were successful in that solutions could be obtained for values of $\lambda_1 = \omega M / (1 - M^2)$ well above the critical value. However, the accuracy of the solutions (as measured by comparing solutions for a flat plate with subsonic kernel function solutions) rapidly decreased with increasing λ_1. This accuracy problem was at first assumed to be due to an insufficient number of mesh points resulting from the use of an in-core solution routine. An out-of-core solution has been developed under the current contract, and the number of mesh points to be handled can now be increased to the number used in the relaxation procedure.

The new program has proved successful although all the improvement in correlation has not been due solely to increasing the number of mesh points. Other modifications that have contributed significantly to obtaining better results include removing a coordinate transformation, which provided for applying the boundary conditions at infinity to the outer boundaries of the finite difference region, and redistributing the mesh points vertically to more uniformly span the solution region.

The out-of-core solution procedure, which is developed in detail by Yip (ref. 8), is discussed in the following section.

6.1 THE OUT-OF-CORE SUBROUTINE

The out-of-core solution routine is set up to solve the matrix expression

$$[A]\{x\} = \{R\} \tag{8}$$

The coefficient matrix, [A], is complex, of the order 2000 to 4000, sparse and banded. The right-hand-side matrix, $\{R\}$, is a column matrix that introduces the internal boundary condition (i.e., the boundary conditions on the wing) and for the general flutter problem may have as many as 20 different values for each [A]. The forms of the matrices of equation (8) that result from using outgoing wave boundary conditions are shown in appendix A.

The coefficient matrix, [A], of equation (8) can be written as the sum of two matrices

$$[A] = [B] + [D] \tag{9}$$

where [B] is a banded matrix and [D] is such that its upper triangular part is all zero, and its lower triangular part has four columns of nonzeroes. The matrix [D] can be written as

$$[D] = [U][V]^T \tag{10}$$

where [U] and [V] are nx4 matrices. If the solution is for

$$[A]\{x\} = \{R\} \tag{11}$$

then, by a variant of the Sherman-Morrison formula, we have

$$\{x\} = [A]^{-1}\{R\} = [B]^{-1}\{R\} - [B]^{-1}[U]\left[I_4 + V^T B^{-1} U\right]^{-1}[V]^T[B]^{-1}\{R\} \tag{12}$$

upon noting that $\left[I_4 + V^T B^{-1} U\right]$ is a 4x4 matrix.

A two-step method is used where

1. [B] is decomposed into a product of a lower and an upper triangular matrix by an algorithm for block banded (or profile) matrices. Then $[B]^{-1}\{R\}$ and $[B]^{-1}\{U\}$ are solved by forward and backward substitutions.
2. Equation (12) is used to compute $[A]^{-1}\{R\}$.

The matrix is partitioned into blocks (as described in app. A) with the order of each block equal to the number of vertical mesh points. Only nonzero blocks are stored as a record in a random access file. Since any algorithm for LU factorization of banded matrices ultimately fills in zeroes between bands, all the nonzero blocks of the coefficient matrix are stored as full matrices. A "threshold" pivoting strategy is used. That is, a nonnegative number, μ, is chosen so that

$$0 \leqslant \mu \leqslant 1$$

and if

$$|a_{kk}| \geqslant \mu \cdot |a_{jk}| \qquad j > k$$

then there is no pivoting in the k^{th} pivotal step. If μ is set equal to zero, there is no pivoting; if $\mu = 1$, there is the usual row pivoting. Our experience shows that using $\mu = 0.01$ has been very satisfactory.

The numerical stability of the solution procedure is monitored by comparing the actual solution with a computed solution. A new right-hand side $\{\bar{R}\}$ can be generated where the element $\bar{R}_i$ is the row sum of the i^{th} row of [A]. Therefore, if $\{\bar{X}\}$ is the actual solution of $[A]\{\bar{X}\} = \{\bar{R}\}$, then the deviation of $\{\bar{X}\}$ from $\{1\}$ will give some indication of the quality of the solution. In all solutions run so far, this error has been of the order 10^{-10}. The program has the capability of treating several wing motions for the same frequency and Mach number with considerable economy in computing resources.

6.2 PROCEDURAL MODIFICATIONS

As will be noticed by examining section 6.3, the direct solution program provides relatively good solutions for the two-dimensional airfoil section of vanishing thickness at relatively

large values of λ_1, i.e., for values well above the critical value of λ_1 for relaxation procedures. This represents a significant improvement over the direct solution results discussed in reference 3. Although development of the out-of-core solution subroutine is the largest single modification made during the current work, several other changes have contributed to the better results.

First, the coordinate transformation that applied the physical boundary conditions at infinity to the outer boundaries of the finite difference solution region failed to yield good results for higher λ_1 values and was removed. Although this transformation – which works well for steady state and small values of λ_1 but does not work for larger values of λ_1 – has not been studied, we assume that the problem lies with trying to analyze a set of waves extending to infinity with a limited number of mesh points. That is, it appears to be important to have enough mesh points to define properly all the waves within the finite difference region. This is demonstrated by the better results obtained by spreading the mesh points out rather uniformly in the crossflow direction. Points are still stacked close to the wing surface where the gradients in φ_1 are known to be large. However, increasing adjacent intervals going away from the wing by a factor of 1.4 did not provide a good point distribution.

Outgoing wave boundary conditions have been used and appear to be adequate. However, the equations given in reference 3 for the upper and lower boundaries are in error and should be as follows:

$$\varphi_{1_y} + \frac{i\omega M\sqrt{K}}{1 - M^2}\,\varphi_1 = 0 \qquad \text{UPPER BOUNDARY}$$

$$\varphi_{1_y} - \frac{i\omega M\sqrt{K}}{1 - M^2}\,\varphi_1 = 0 \qquad \text{LOWER BOUNDARY}$$

An alternative downstream boundary condition has been developed and applied. This involves replacing the outgoing wave boundary condition with the value φ_1 on the downstream boundary as determined from the flow induced by the doublet sheet shed from the trailing edge of the airfoil. The calculated pressure distributions at $M = 0.9$ and $\omega = 0.6$, for example, are essentially the same for both downstream boundary conditions.

There have been no apparent problems with numerical instabilities resulting from the presence of eigenvalues of the coefficient matrix. The pressure distributions appear to be smoothly varying with small changes in reduced frequency.

6.3 ANALYTICAL RESULTS

This section presents and discusses some results from the direct solution program described in the preceding section. These examples include both subsonic and supersonic freestream conditions and are for airfoil sections only. That is, all the examples are two-dimensional. The following section examines the purely subsonic problem in some detail as it is imperative that good correlation be obtained here if the full mixed flow condition is to be

successfully handled. The succeeding section presents some supersonic freestream results for a circular-arc airfoil.

6.3.1 SUBSONIC FREESTREAM EXAMPLES

The flow around an airfoil of vanishing thickness is purely subsonic and corresponds to the problem solved by conventional subsonic unsteady flow programs such as that developed for NASA by Rowe et al. in references 12 and 13. This latter program is considered to provide very accurate pressure distributions, and the finite difference results should approach those of the current NASA study as the number of mesh points increases to infinity. Thus, the criterion for evaluating pressure distributions is the correlation of the finite difference calculations with the results from the NASA program of references 12 and 13.

The first point to be made is that good pressure distributions have been obtained from the direct solutions for values of λ_1 well above the critical value for which relaxation solutions fail to converge. Results for a section oscillating in pitch about the leading edge at a free-stream Mach number of 0.9 and four reduced frequencies are presented in figures 6 through 9. At this Mach number and for our standard sized finite difference solution region, the critical reduced frequency would be about 0.1. As can be seen, very good correlation is obtained up to a reduced frequency of 0.9.

Results for a second example for the same motion at Mach 0.4 are shown in figures 10 and 11. Here, correlation with the more exact theory is good at both $\omega = 0.9$ and $\omega = 3.0$ The critical value of λ_1 is about 1.0.

Finally, results are presented for a section having an oscillating quarter-chord control surface at M = 0.5 in figures 12, 13, and 14. Here, correlation is seen to be good for reduced frequencies of 0.5, 1.0, and 1.6.

Experience to date indicates a number of characteristics are important in setting up a satisfactory mesh point distribution. Nonuniform mesh point distributions are used in order to concentrate points where the gradients in φ_1 are largest and still keep the number of points to a minimum for calculation purposes. In the x-direction (direction of flow), a high density of points are located in the vicinity of the airfoil leading edge, the control surface hinge-line, and the trailing edge where the Kutta condition is to be satisfied. Having met these conditions, the pressure seems relatively insensitive to the particular distribution of points. In the crossflow direction, grid points are located very close to the wing surface to accurately define φ_1 directly adjacent to the wing surface. It is also important to keep enough points distributed in the outer parts of the flow to properly define the wave shapes.

An example of a distribution with good correlation at relatively high values of λ_1 is shown in figure 15. The complete grid is not shown, but it is symmetric about a line halfway between the j = 30 line and the j = 31 line. Here, the finite difference points are the intersections of the lines. The φ_1 distributions for this grid with the airfoil at a Mach number of 0.9 and four different reduced frequencies are shown in figures 16 through 19. A description of the φ_1 plots is given in appendix B. The potential, which in this case is antisymmetric

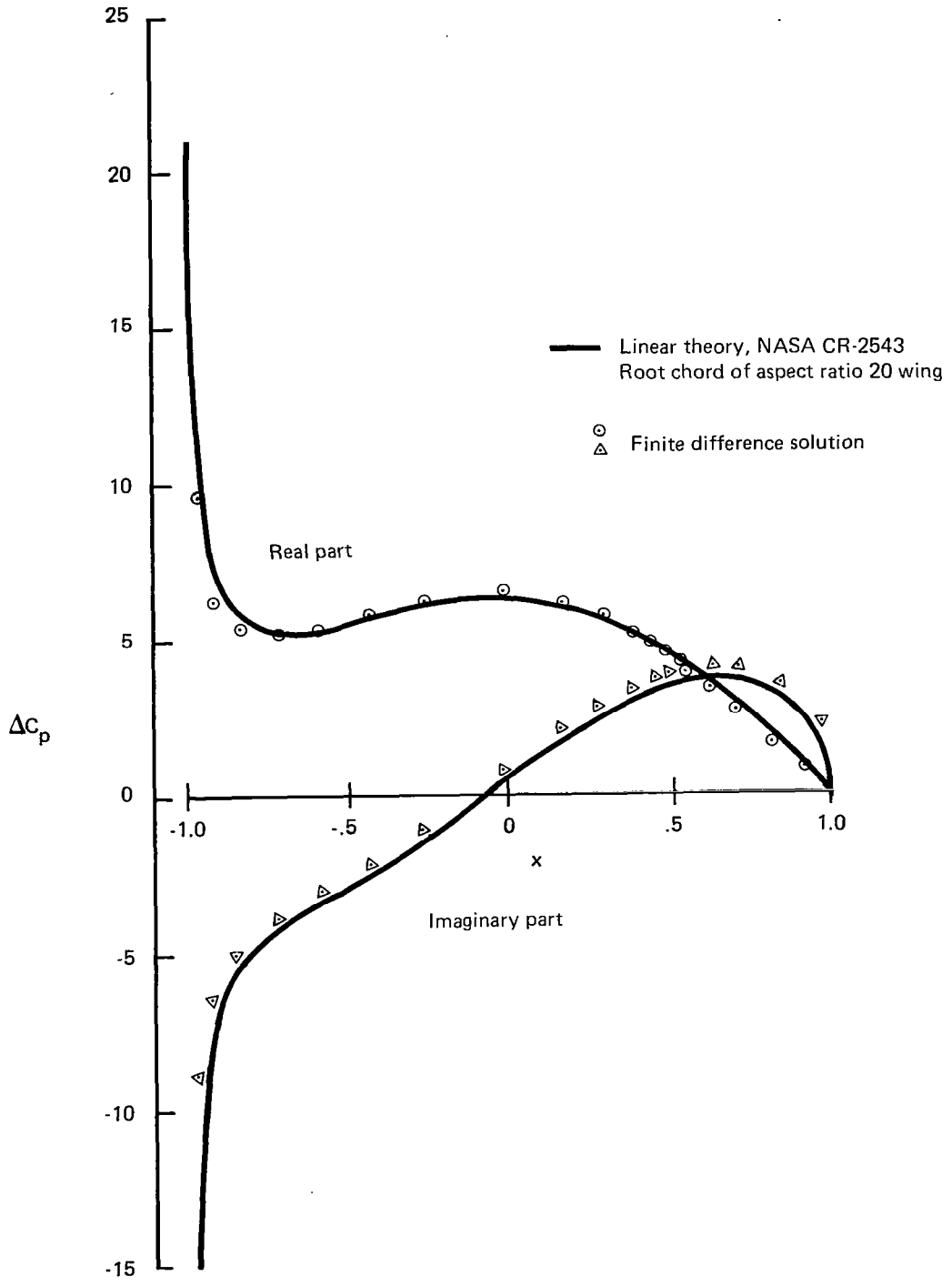

Figure 6.—Jump in Pressure Coefficient Across a Flat Plate Oscillating in Pitch; M = 0.9, ω = 0.3

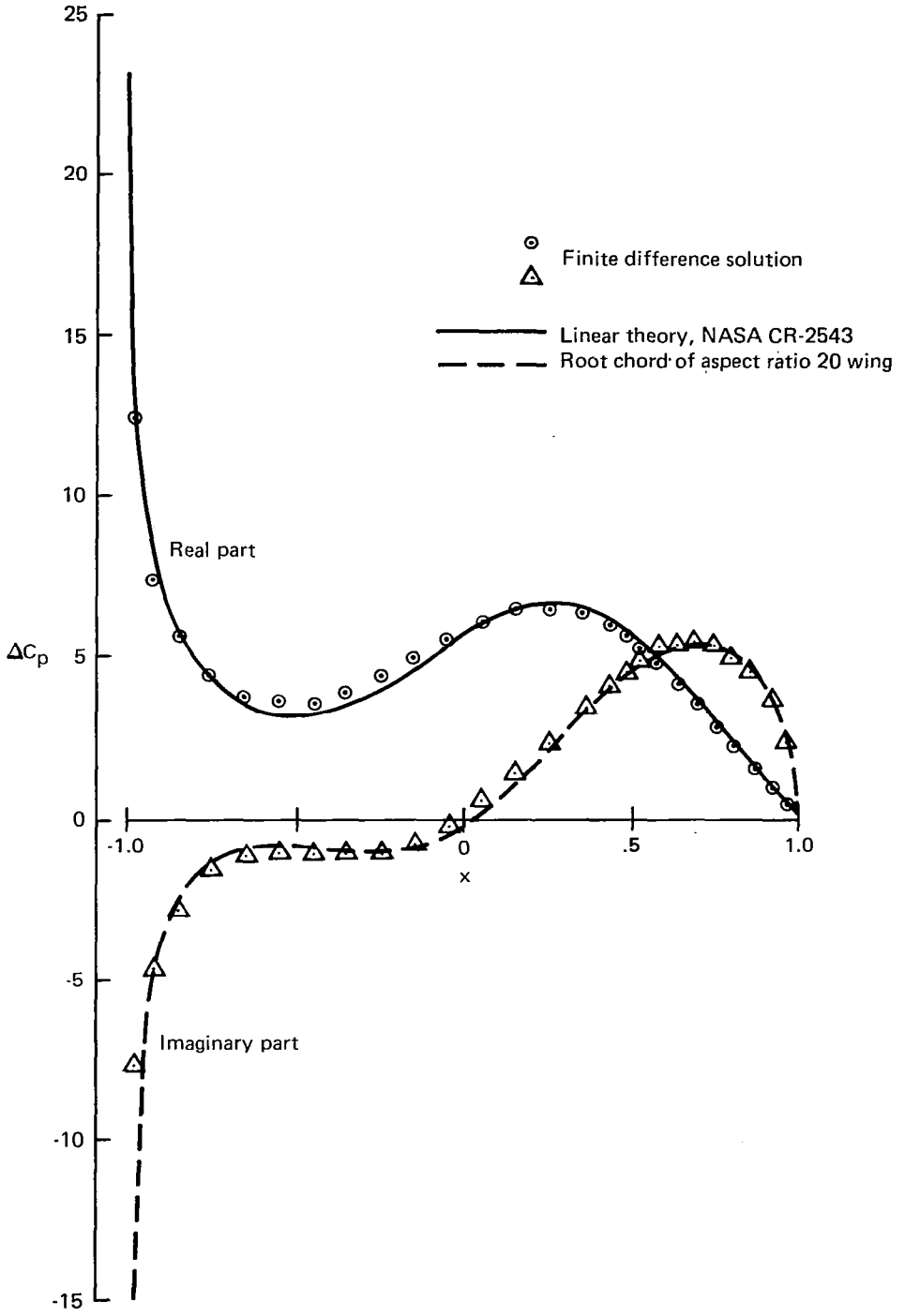

Figure 7.--Jump in Pressure Coefficient Across a Flat Plate Oscillating in Pitch; $M = 0.9$, $\omega = 0.45$

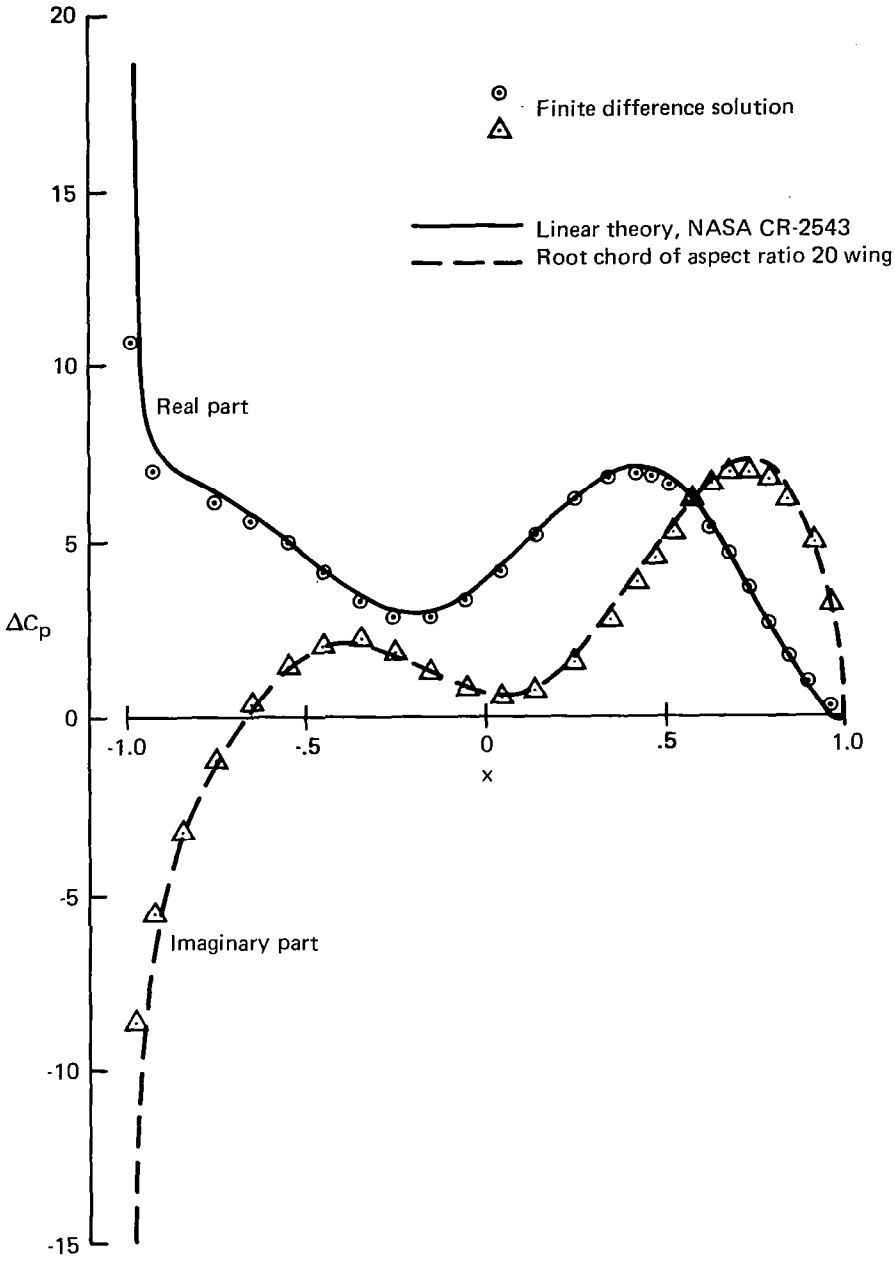

Figure 8.—Jump in Pressure Coefficient Across a Flat Plate Oscillating in Pitch; $M = 0.9$, $\omega = 0.6$

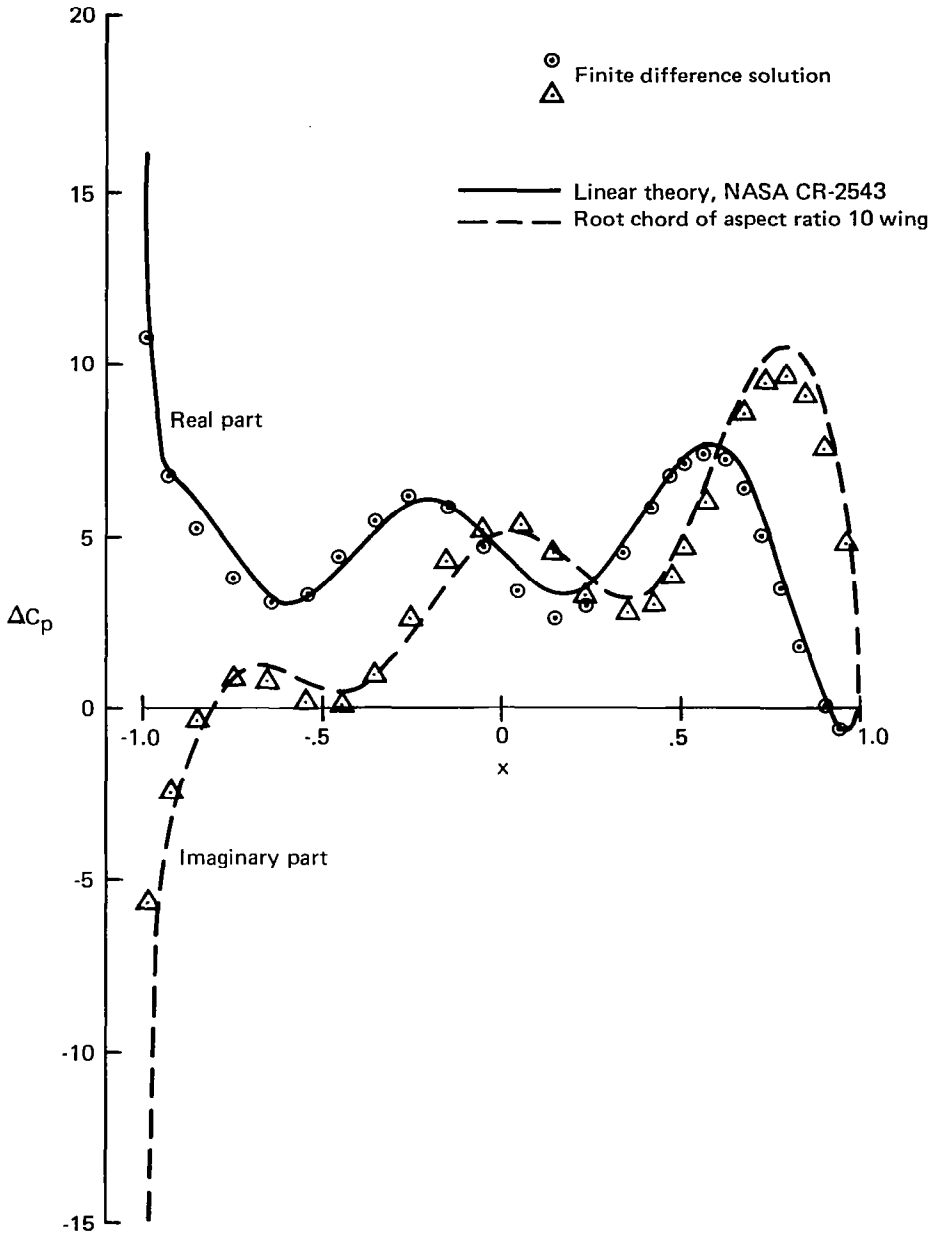

Figure 9.—Jump in Pressure Coefficient Across a Flat Plate Oscillating in Pitch; $M = 0.9$, $\omega = 0.9$

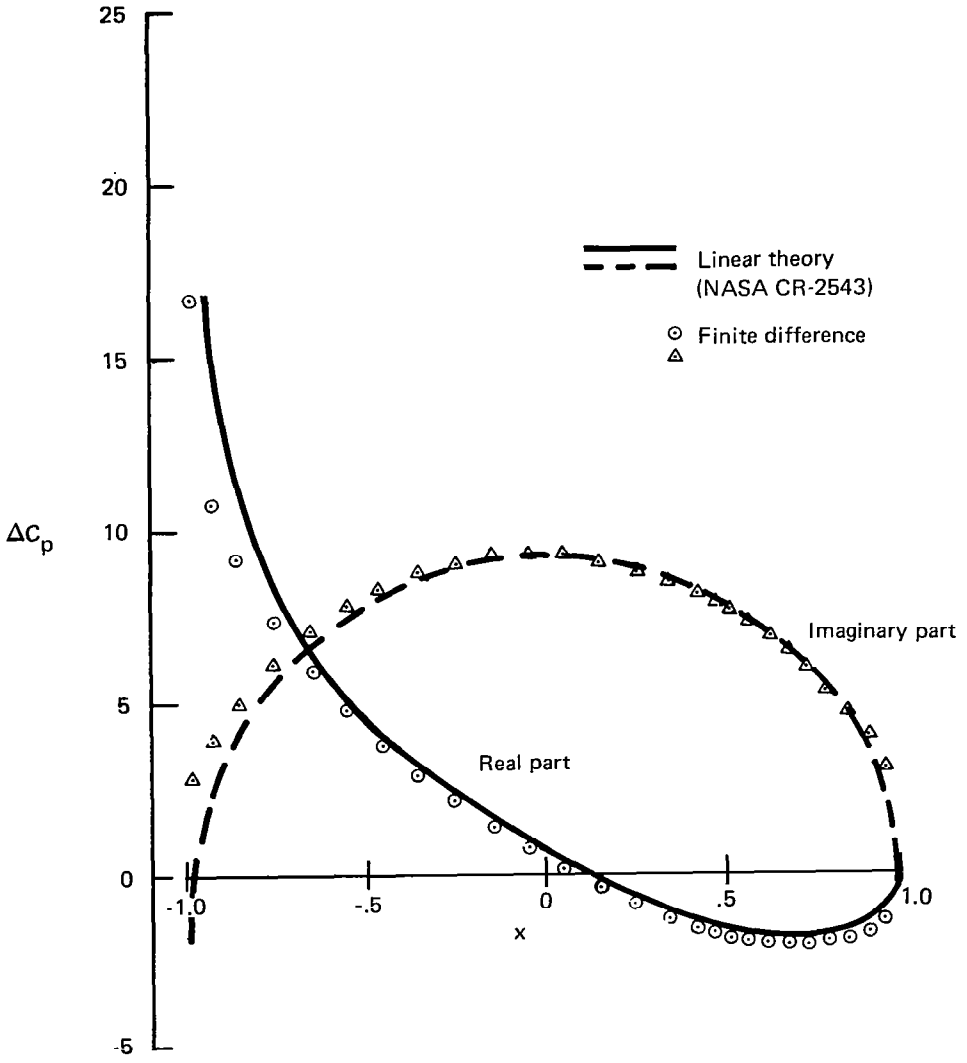

Figure 10.– Jump in Pressure Coefficient Across a Flat Plate Oscillating in Pitch; $M = 0.4$, $\omega = 0.9$

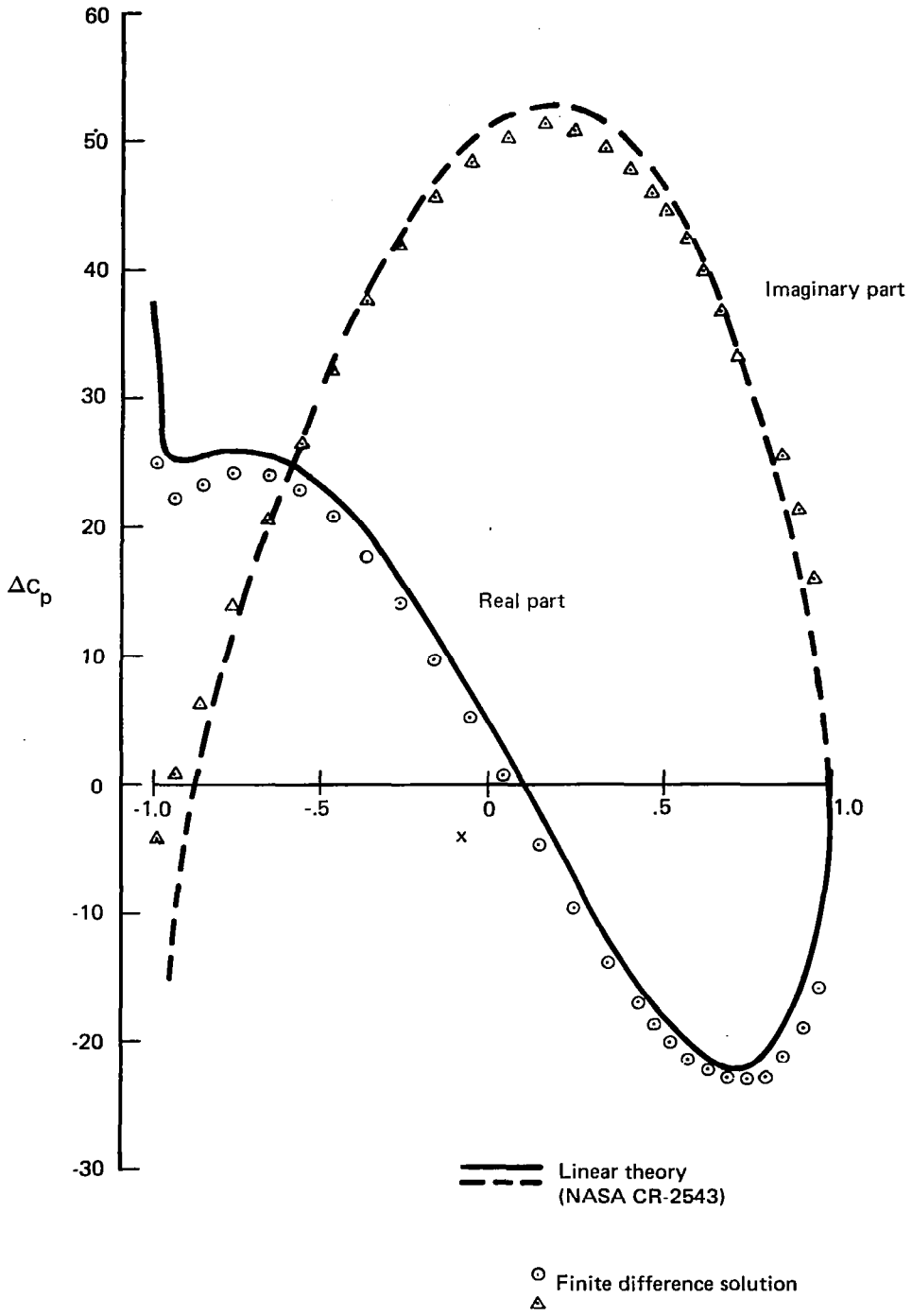

Figure 11.— Jump in Pressure Coefficient Across a Flat Plate Oscillating in Pitch; $M = 0.4$, $\omega = 3.0$

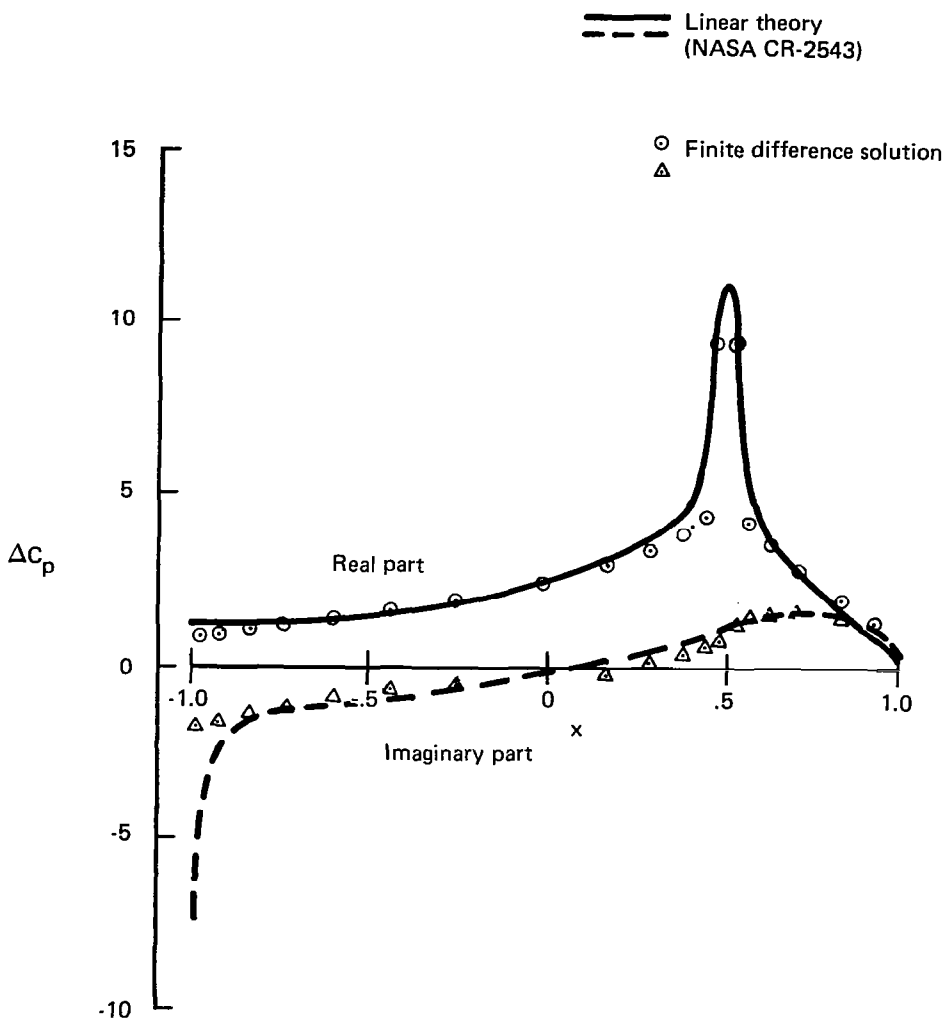

Figure 12.– Jump in Pressure Coefficient Across a Flat Plate With Oscillating Quarter-Chord Control Surface; M = 0.5, ω = 0.5

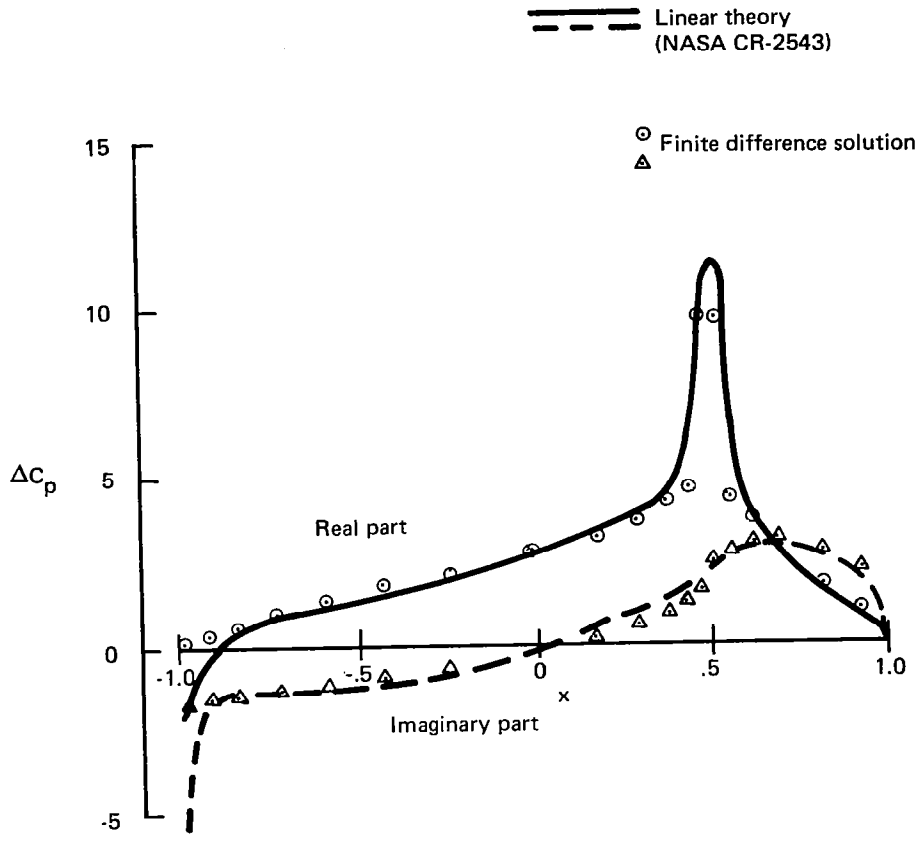

Figure 13.– Jump in Pressure Coefficient Across a Flat Plate With Oscillating Quarter-Chord Control Surface; M = 0.5, ω = 1.0

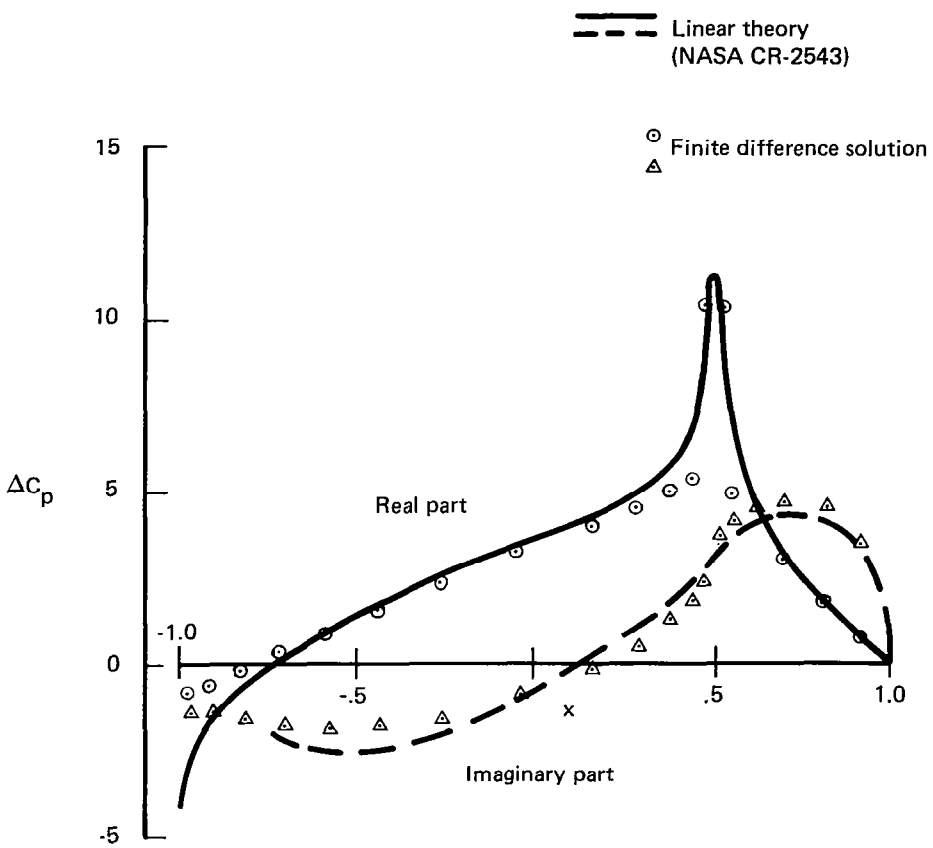

Figure 14.– Jump in Pressure Coefficient Across a Flat Plate With Oscillating Quarter-Chord Control Surface; M = 0.5, ω = 1.6

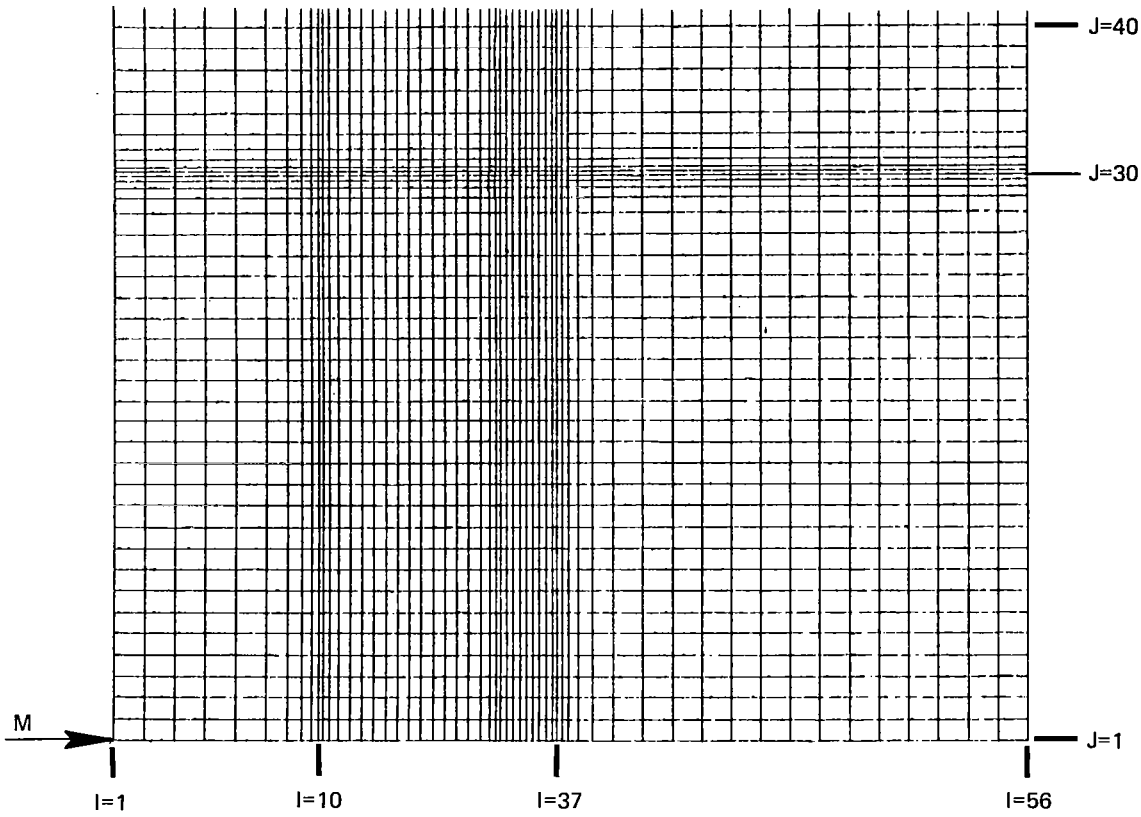

Leading edge between X(I=10) and X(I=11)
Trailing edge at X(I=37)
Airfoil between Y(J=30) and Y(J=31)

Figure 15.— Mesh Pattern for 56 x 60 Grid

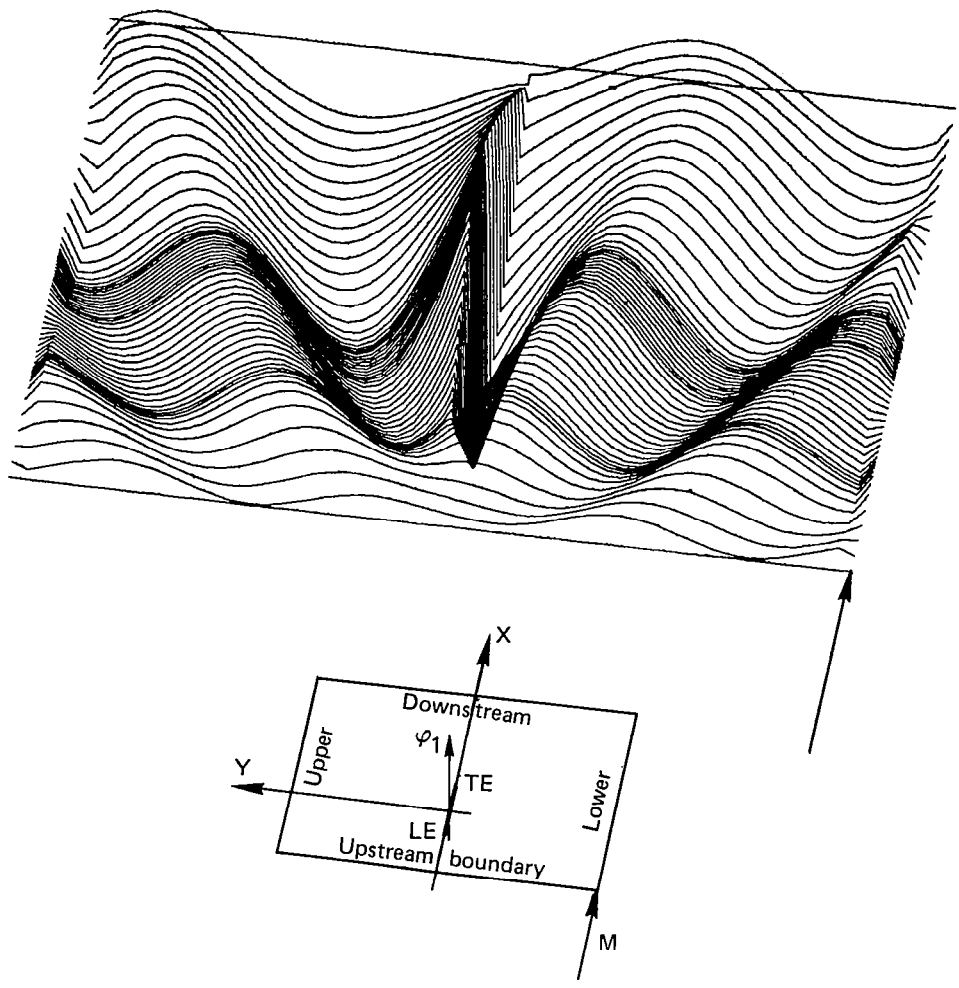

a. REAL PART

Figure 16.— Velocity Potential for a Flat Plate Oscillating in Pitch; $M = 0.9$, $\omega = 0.3$

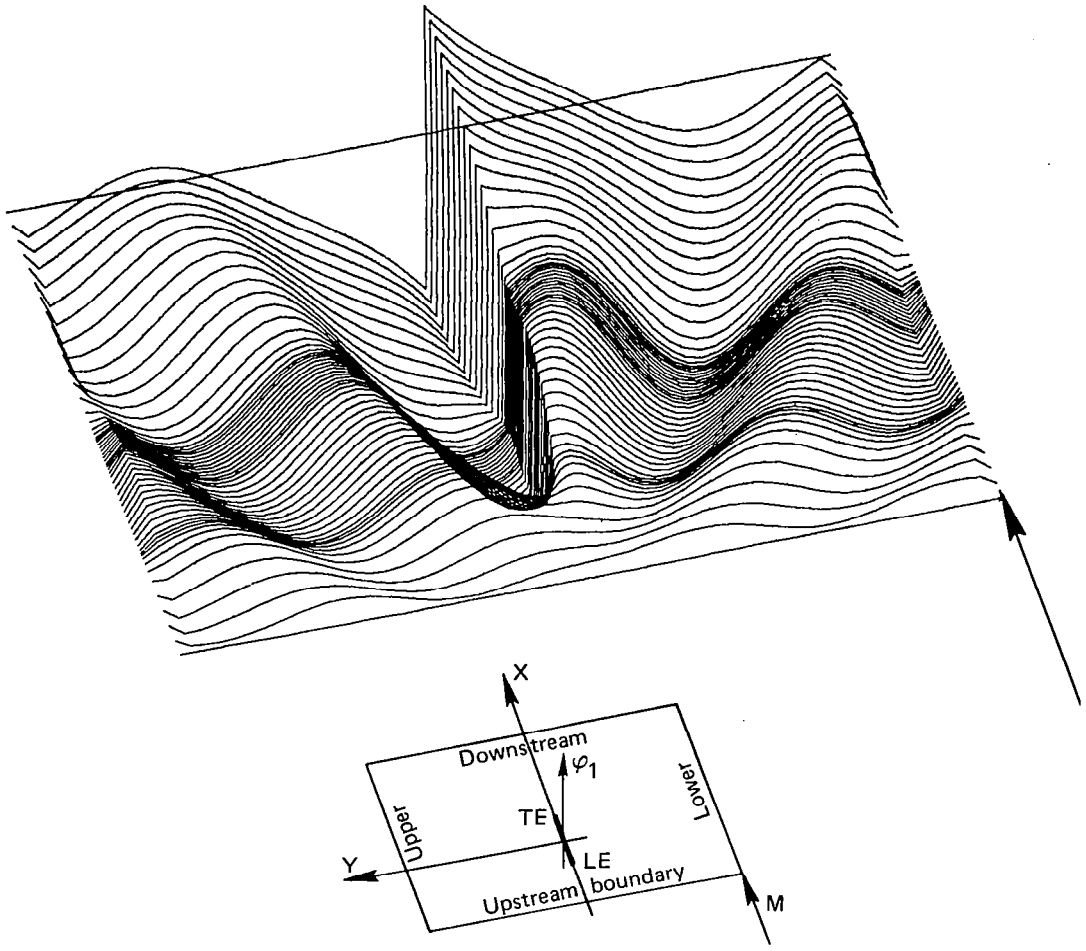

b. IMAGINARY PART

Figure 16.– (Concluded)

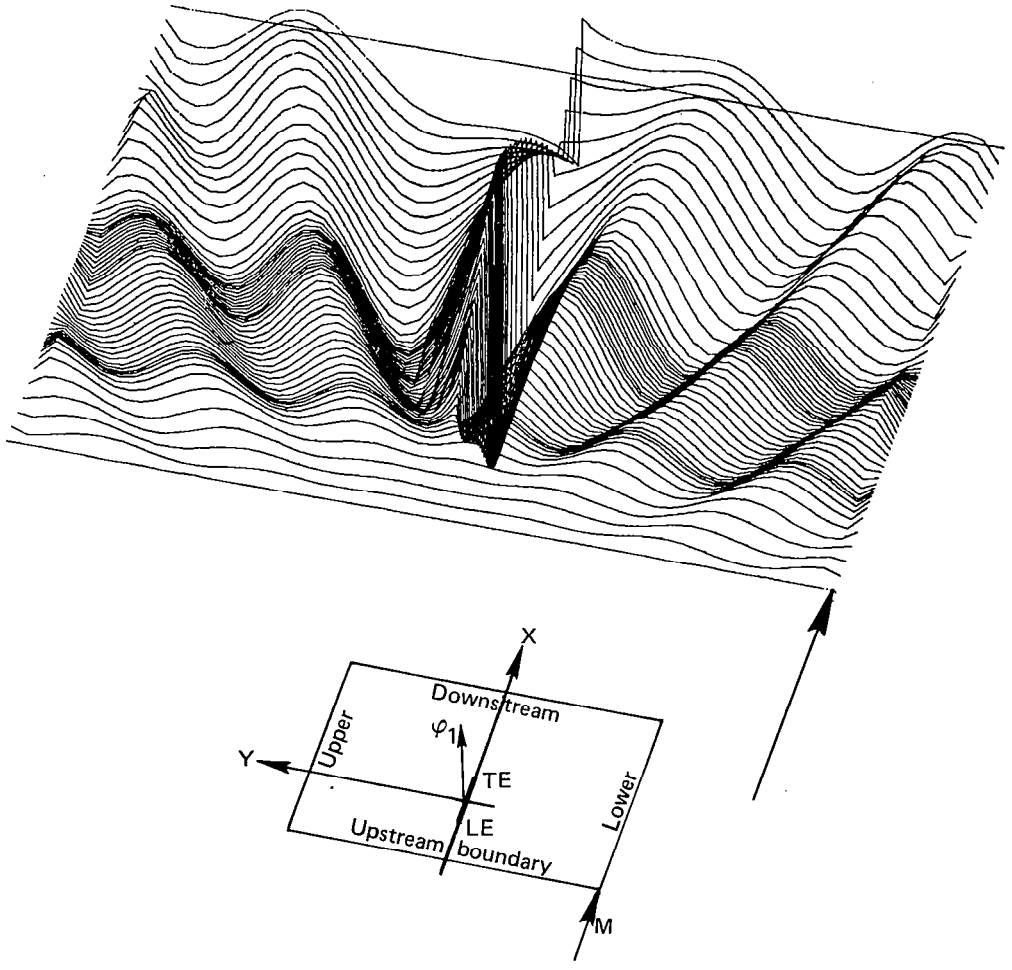

a. REAL PART

Figure 17.—Velocity Potential for a Flat Plate Oscillating in Pitch; M = 0.9, ω = 0.45

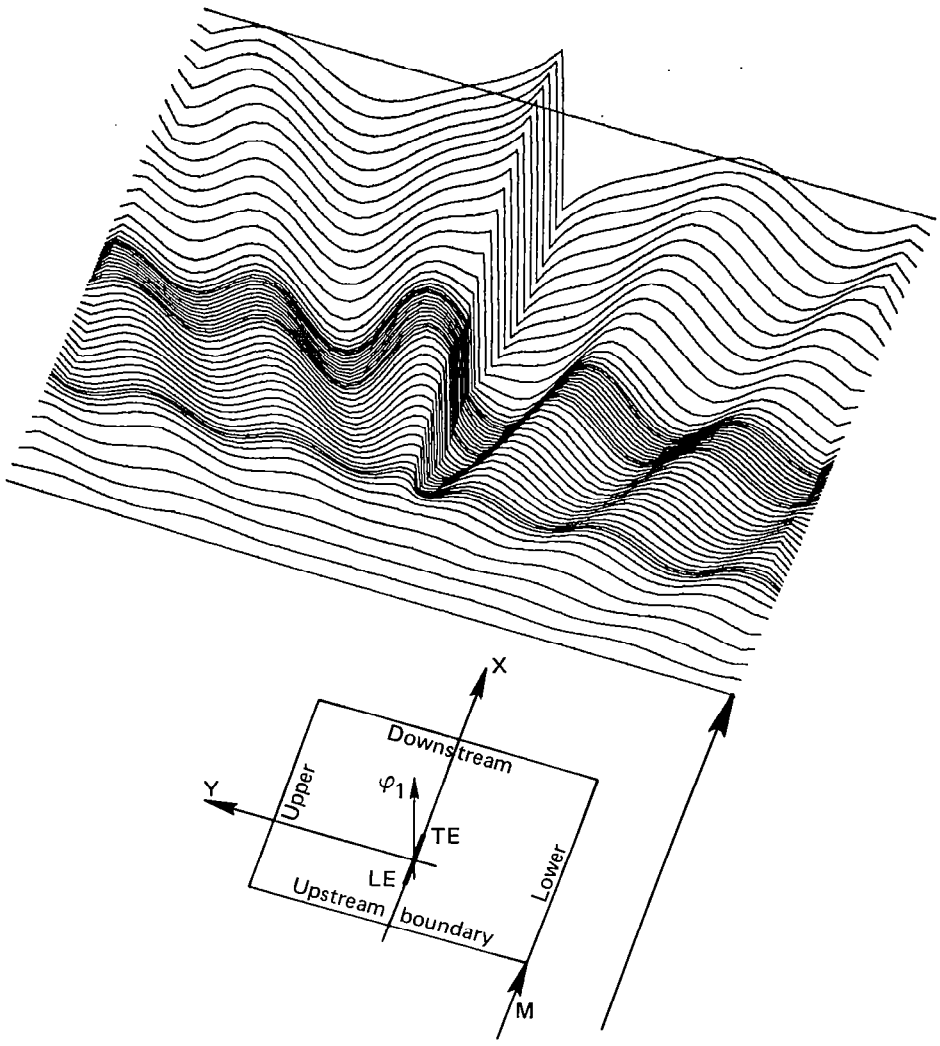

b. IMAGINARY PART

Figure 17.– (Concluded)

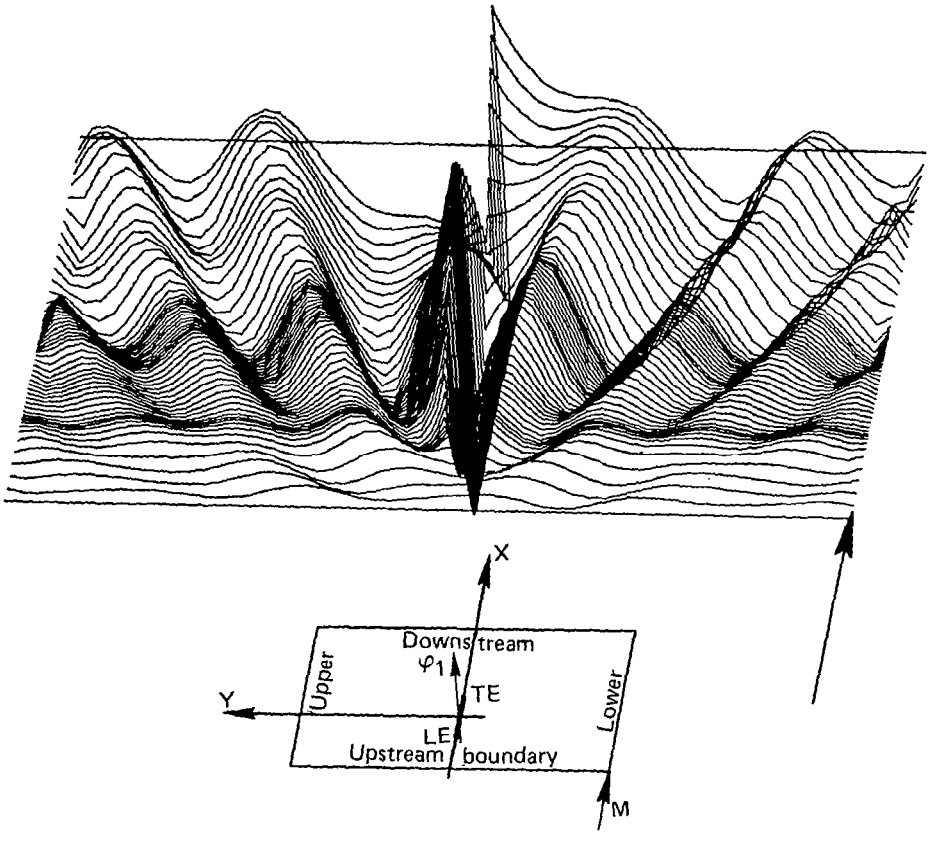

a. REAL PART

Figure 18.– Velocity Potential for a Flat Plate Oscillating in Pitch; M = 0.9, ω = 0.6

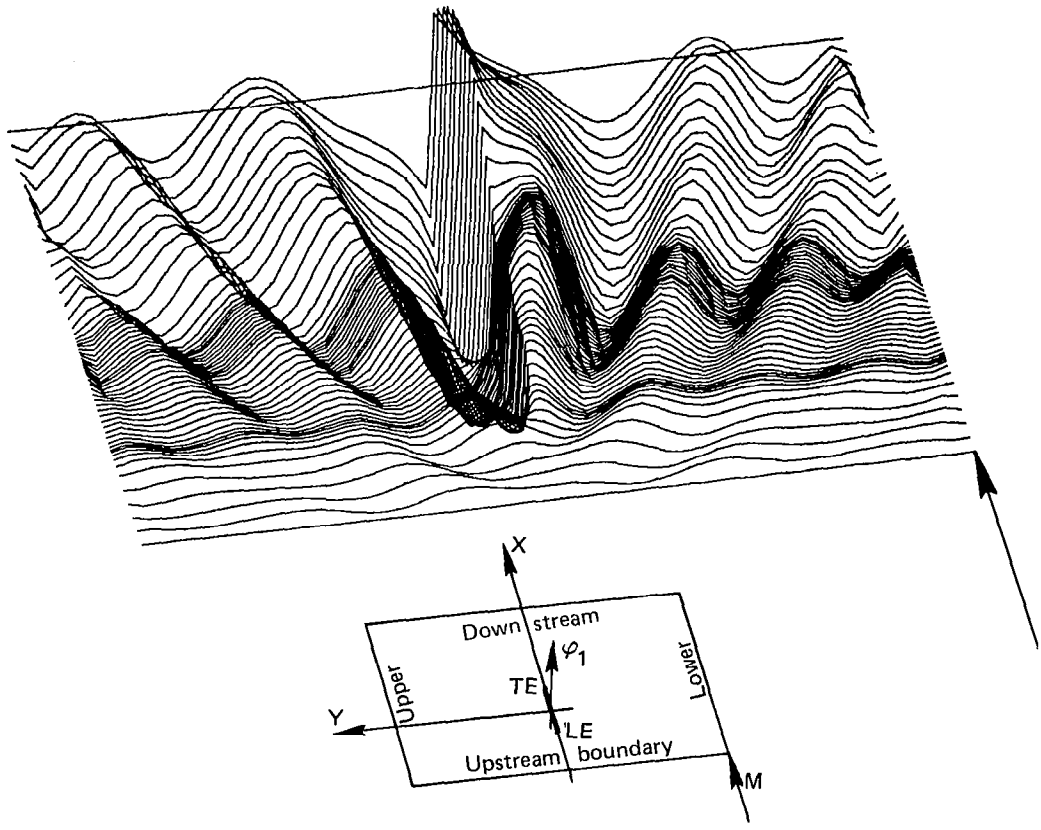

b. IMAGINARY PART

Figure 18.– (Concluded)

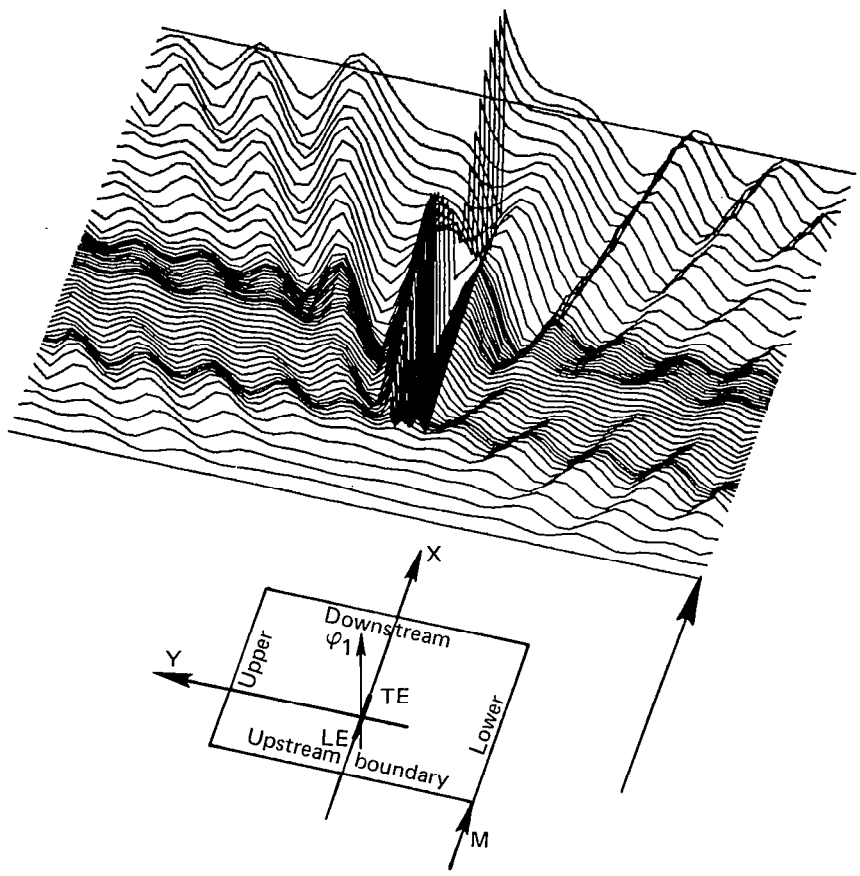

a. REAL PART

Figure 19.– Velocity Potential for a Flat Plate Oscillating in Pitch; M = 0.9, ω = 0.9

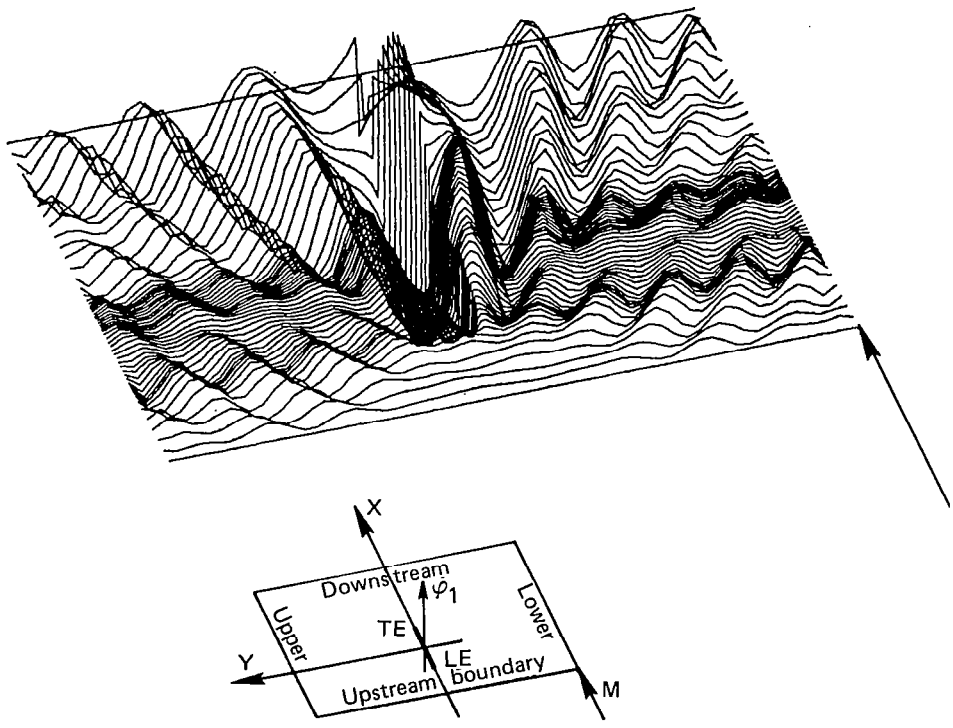

b. IMAGINARY PART

Figure 19.– (Concluded)

about y = 0, is continuous in the crossflow direction ahead of the leading edge. The discontinuity in φ_1 across the airfoil from which the lift is calculated shows clearly, as does the continuing discontinuity across the wake. The boundary conditions across the wake ensure that the pressure difference across the wake is zero.

It will be noted that the gradients in the flow direction, even adjacent to the plane of the wing (there are no mesh points along y = 0), are, in all cases, relatively mild except at the airfoil leading edge. The most noticeable characteristic of the distribution is the development of bow-type waves, with the wavelength decreasing as the reduced frequency is increased. The waves appear to be well defined by the grid of figure 15 for $\omega = 0.3$ and $\omega = 0.45$. 0.45. However, waves at $\omega = 0.6$ are not as smooth as those obtained for smaller frequencies.

Several different grids were used for $\omega = 0.45$ and $\omega = 0.6$ in an attempt to improve the pressure distribution results. The pressure results were relatively insensitive to movement of the upstream and downstream boundaries, as well as to the addition of points close to the upper and lower boundaries.

A grid resulting in less accuracy is shown in figure 20 for which rows of mesh points are stacked very closely against the wing and spread out toward the upper and lower boundaries. Although good results are obtained at small values (e.g., $\omega \doteq 0.18$ at M = 0.9), the quality of results decreases rapidly with increasing reduced frequency. Also, at the higher values of reduced frequency where the pressures are bad, the results are sensitive to the location of the downstream boundary. The velocity potential for the grid of figure 20 and $\omega = 0.9$ and $\omega = 0.3$ is shown in figure 21. Although the velocity potential is smooth in the region adjacent to the airfoil, the wave pattern in the outer field is not well defined and is distinctly different from that of figure 16. The downstream flow pattern appears different because the downstream boundaries are at different locations; 4.0 semichords aft of the trailing edge in figure 16 and 1.75 semichords in figure 21. A great variety of point distributions in the x-direction were tried with this type of distribution in the crossflow direction. The resulting pressures proved to be sensitive to the location of the downstream boundary. Also, good correlation was never achieved for this combination of Mach number and reduced frequency using this crossflow pattern.

The velocity potential for another pitch case is shown in figure 22 with the grid of figure 15. Here the Mach number is 0.4 and the reduced frequency is 3.0. The λ_1 for this case matches that for M = 0.9 and $\omega = 0.3$. The upper and lower boundaries are at the same scaled distance from the airfoil surface (6.25 semichords above and below the wing), but this length transforms into a larger physical length at M = 0.4 than at M = 0.9: hence, the additional number of waves in the crossflow direction. Despite the number of waves, the pressure distribution correlates well with more exact theory (see fig. 11).

The velocity potential for a section of vanishing thickness with an oscillating quarter-chord control surface is shown in figure 23. The freestream Mach number is 0.5 and the reduced frequency is 1.6. The downstream boundary is 9 semichords aft of the trailing edge. Again, despite the number of waves in the crossflow direction, correlation with more exact theory is good, (see fig. 14).

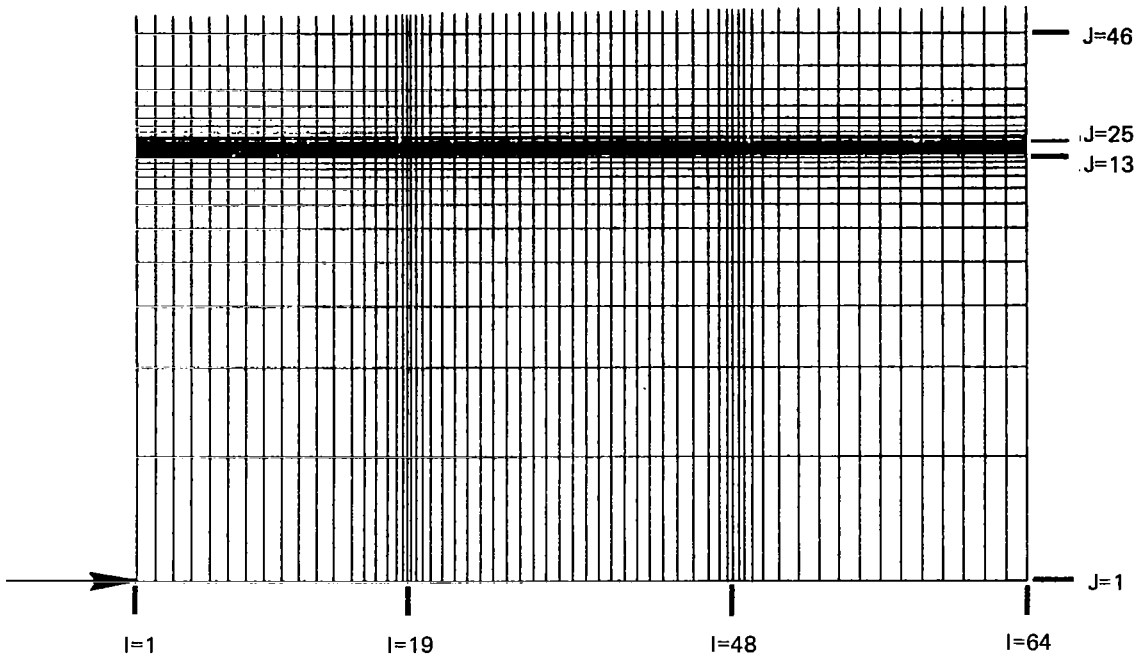

Leading edge between X(I=19) and X(I=20)
Trailing edge at X(I=48)
Airfoil between Y(J=25) and Y(J=26)

Vertical spacing: $Y(J=27)-Y(J=26)=Y(J=26)-Y(J=25)=Y(J=25)-Y(J=24)$

$Y(J)-Y(J-1)=1.4*[Y(J+1)-Y(J)] \quad 2 \leq J \leq 24$

$Y(J+1)-Y(J)=1.4*[Y(J)-Y(J-1)] \quad 27 \leq J \leq 49$

Figure 20.— Mesh Pattern for 64 x 50 Grid

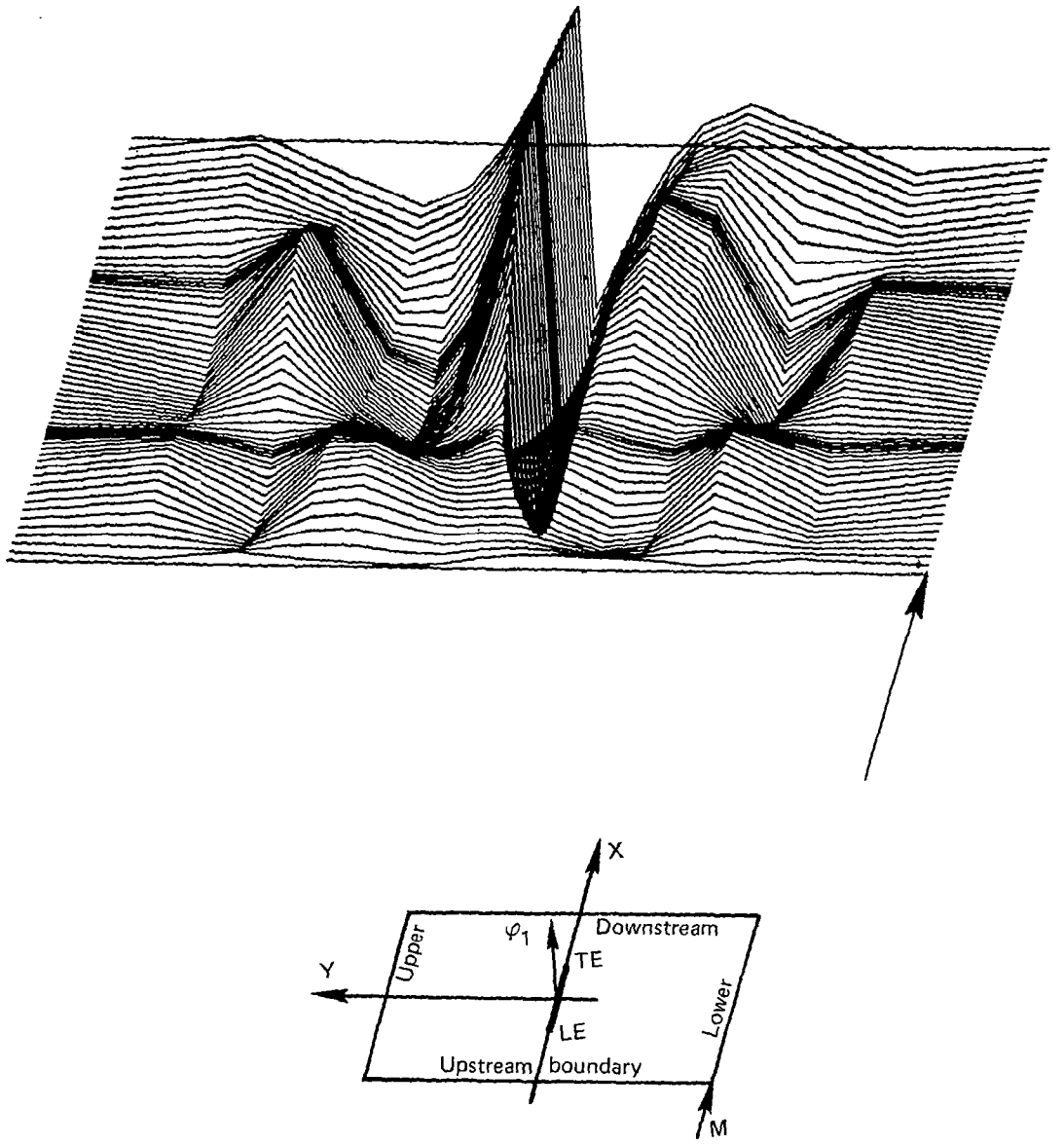

a. REAL PART

Figure 21.— Velocity Potential for a Flat Plate Oscillating in Pitch; $M = 0.9$, $\omega = 0.3$

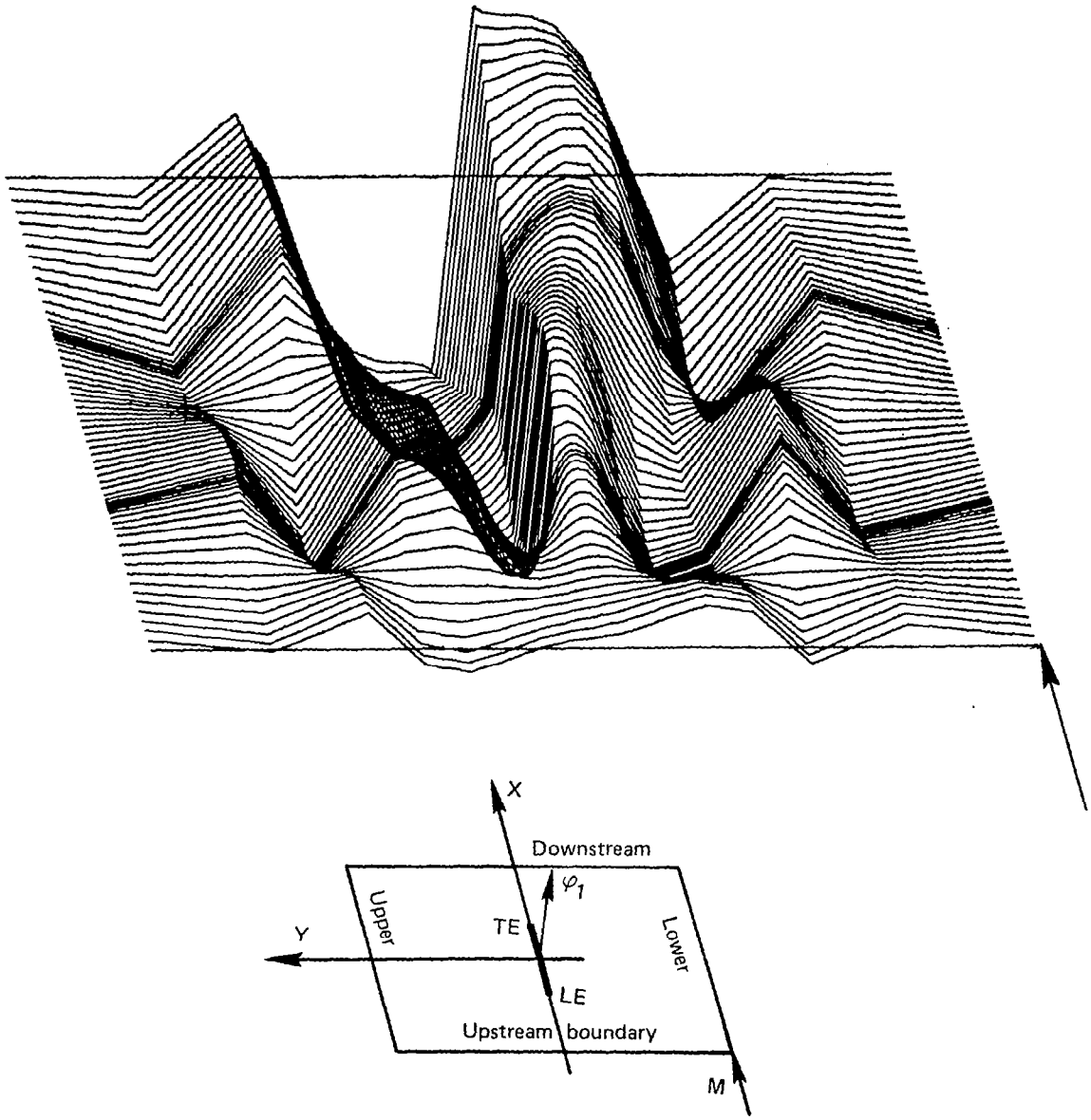

b. IMAGINARY PART

Figure 21.– (Concluded)

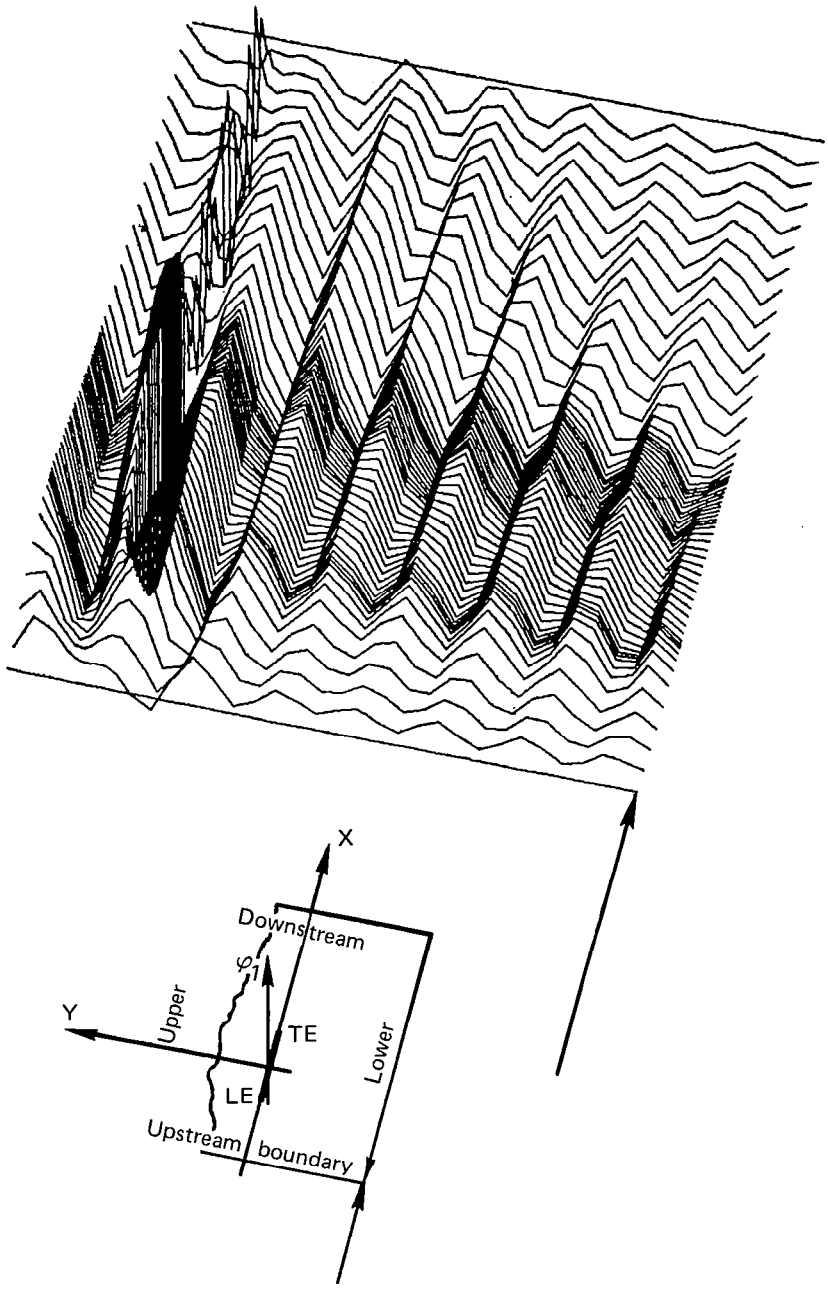

a. REAL PART

Figure 22.— Velocity Potential for a Flat Plate Oscillating in Pitch; M = 0.4, ω = 3.0

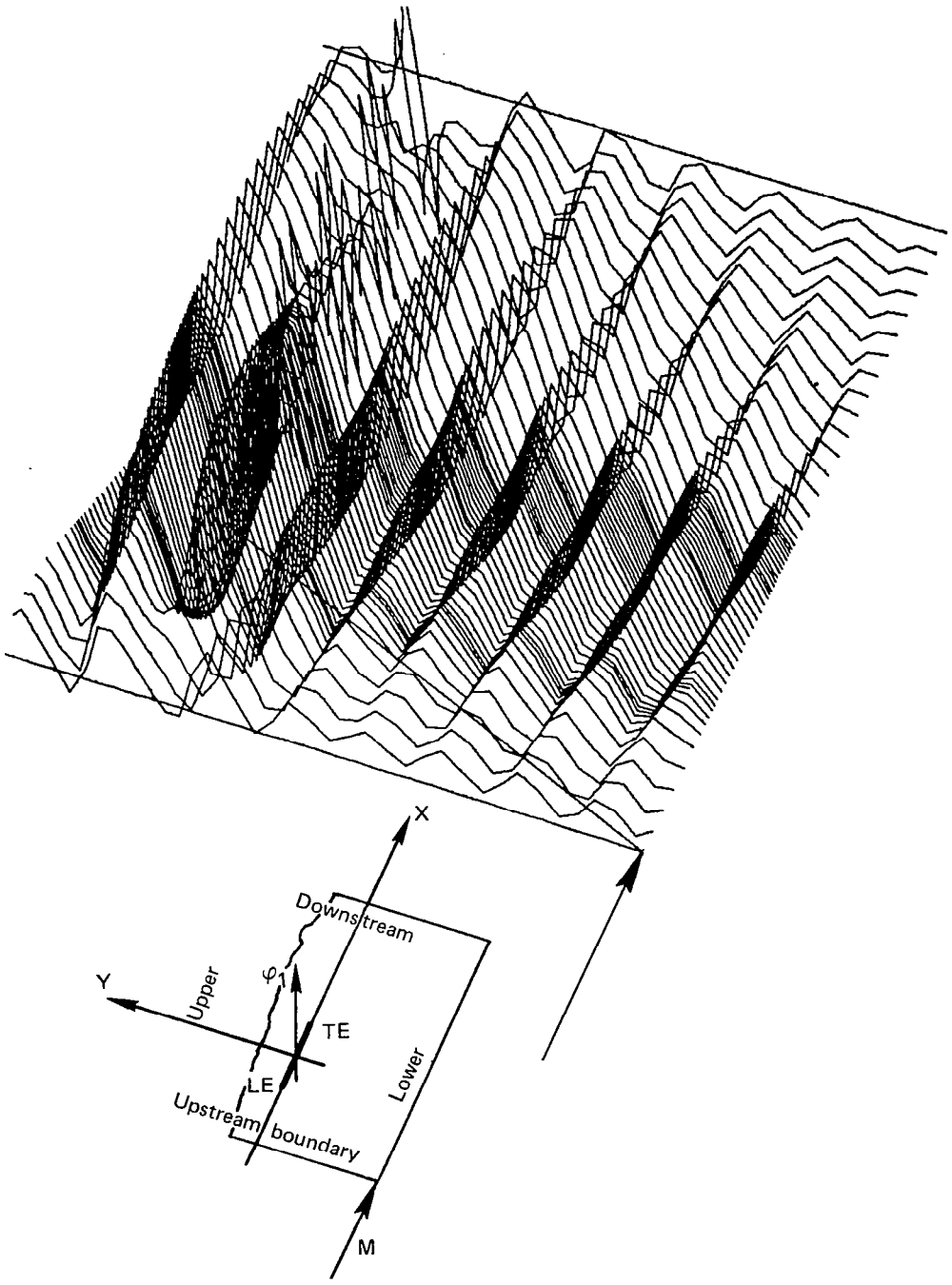

b. IMAGINARY PART

Figure 22.— (Concluded)

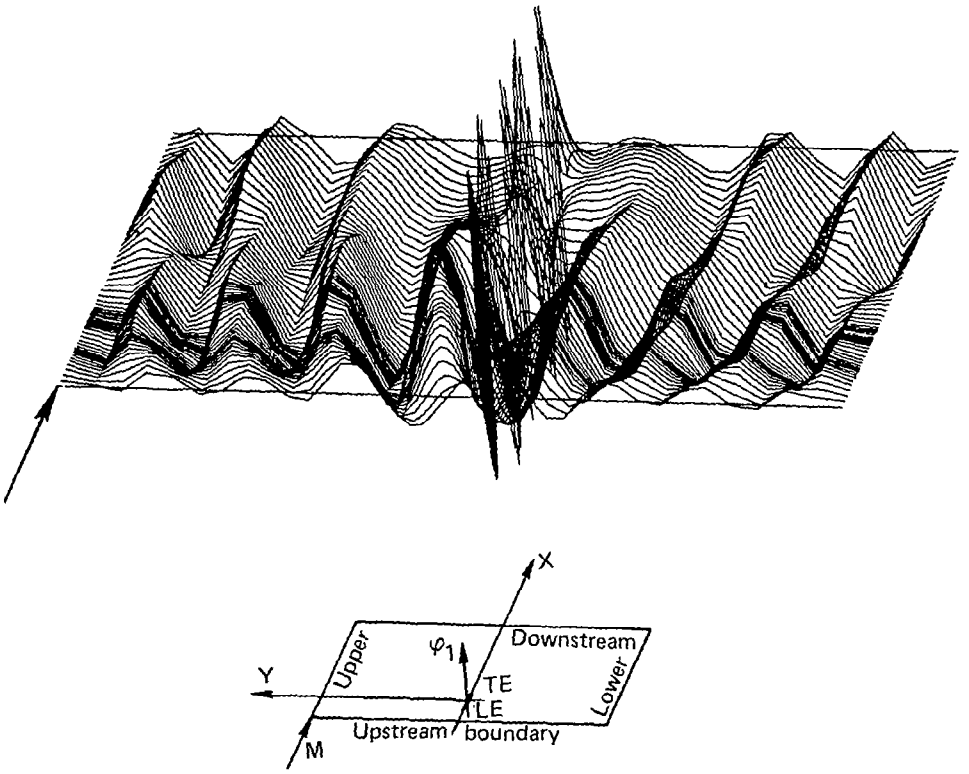

a. REAL PART

Figure 23.– Velocity Potential for a Flat Plate Oscillating in Pitch; $M = 0.5$, $\omega = 1.6$

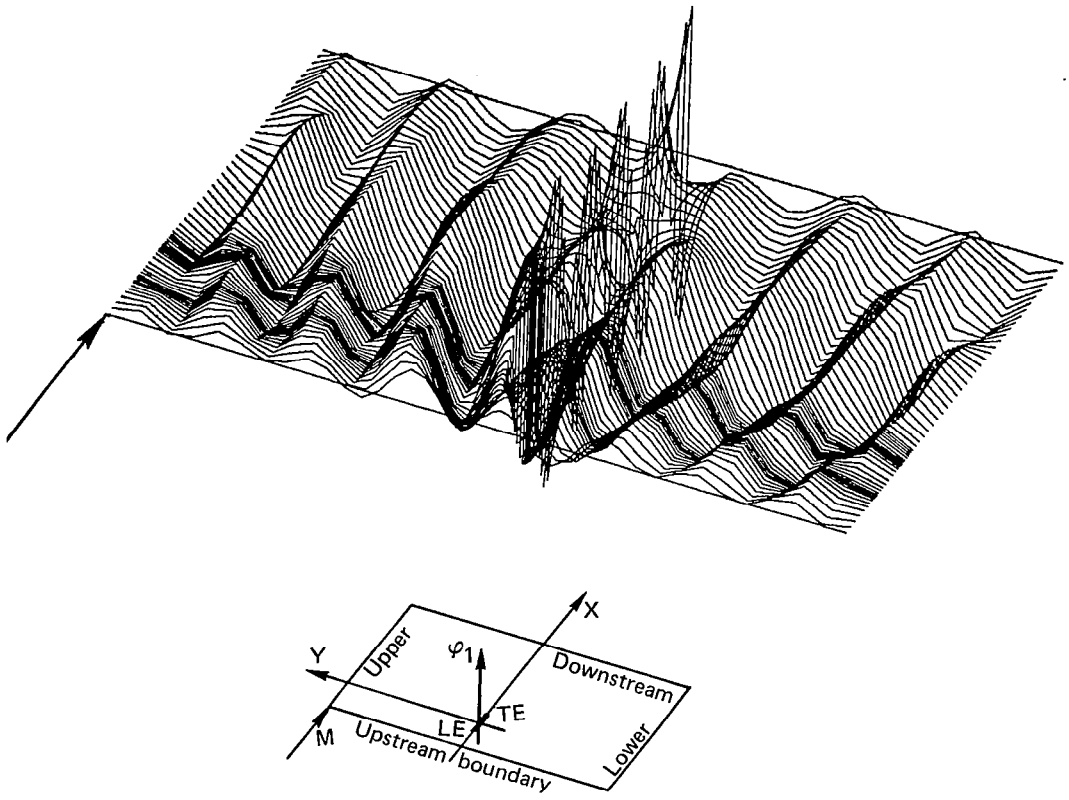

b. IMAGINARY PART

Figure 23.— (Concluded)

6.3.2 SUPERSONIC FREESTREAM EXAMPLES

The pilot two-dimensional program with the full direct solution procedure has been adapted to the supersonic freestream condition. For demonstration purposes, sample calculations have been made at two Mach numbers and for a range of reduced frequencies. The results appear to be reasonable, although we have nothing with which to correlate them. No numerical problems were encountered.

As a trial example, pressure distributions were calculated for a 6% thick circular-arc airfoil oscillating in pitch with freestream Mach numbers of 1.05 and 1.15 and for a range of reduced frequencies up to 0.72. The steady-state pressure and velocity potential distributions were calculated using a Boeing routine that was derived from a program developed by Murman at NASA Ames (ref. 14). The procedure is fully conservative. Plots of pressure coefficients for the M = 1.15 calculations are given in figures 24 through 27.

The steady-state pressure coefficient is given in figure 24. The corresponding data from Traci et al. (ref. 15) is also shown, with the difference in location of the bow shock between the two procedures being attributed to differences in point spacing ahead of the leading edge, although this effect has not been investigated.

The unsteady pressure distributions for ω = 0.06, 0.18, 0.36, and 0.72 are presented in figure 25. The results include the singularity in the pressure distribution at the leading edge, reflecting the effect of the subsonic bubble attached to the leading edge. The pressure aft is relatively constant as would be expected in purely supersonic flow.

The steady-state velocity potential is presented in figure 26. The size of the finite difference region used for the unsteady calculation is much larger than that used for the steady calculation to ensure that the boundary conditions used on the outer boundary did not affect the pressures on the wing. The region used for the steady calculation is small enough to truncate the full crossflow extent of the φ_1 distribution. This truncation occurs only in the regions that do not influence the pressures on the wing itself.

The unsteady velocity potential distribution for M = 1.15 and ω = 0.06 is shown in figure 27. This distribution is relatively smooth considering the small number of grid points in the portion of the flow that actually affects the airfoil section. There are a couple of sharp breaks in the distribution at the outer edges of the region of influence. One irregularity shows clearly in the plot of the the imaginary part. It is assumed these breaks are due to the truncation of the φ_0 distribution discussed above and the relatively small number of mesh points used.

The results for the M = 1.05 calculation are presented in figures 28 and 29. A plot of the pressure coefficient for steady flow is shown in figure 28. The subsonic bubble about the leading edge extends further in the upstream direction than that for the M = 1.15 case, but only slightly further aft of the leading edge. The unsteady pressures are shown in figure 29 for ω = 0.06 and 0.12, and have the same characteristics as those at M = 1.15.

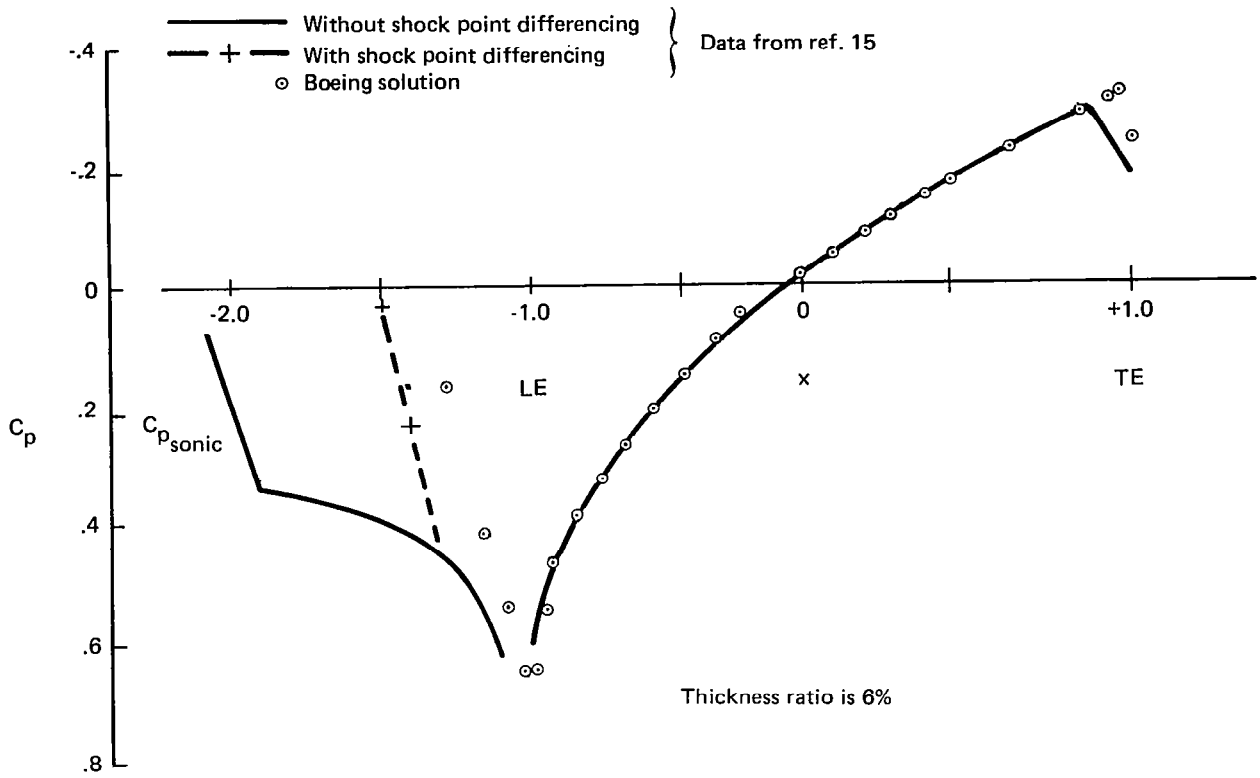

Figure 24.— Jump in Pressure Coefficient Across a Circular-Arc Airfoil; M = 1.15

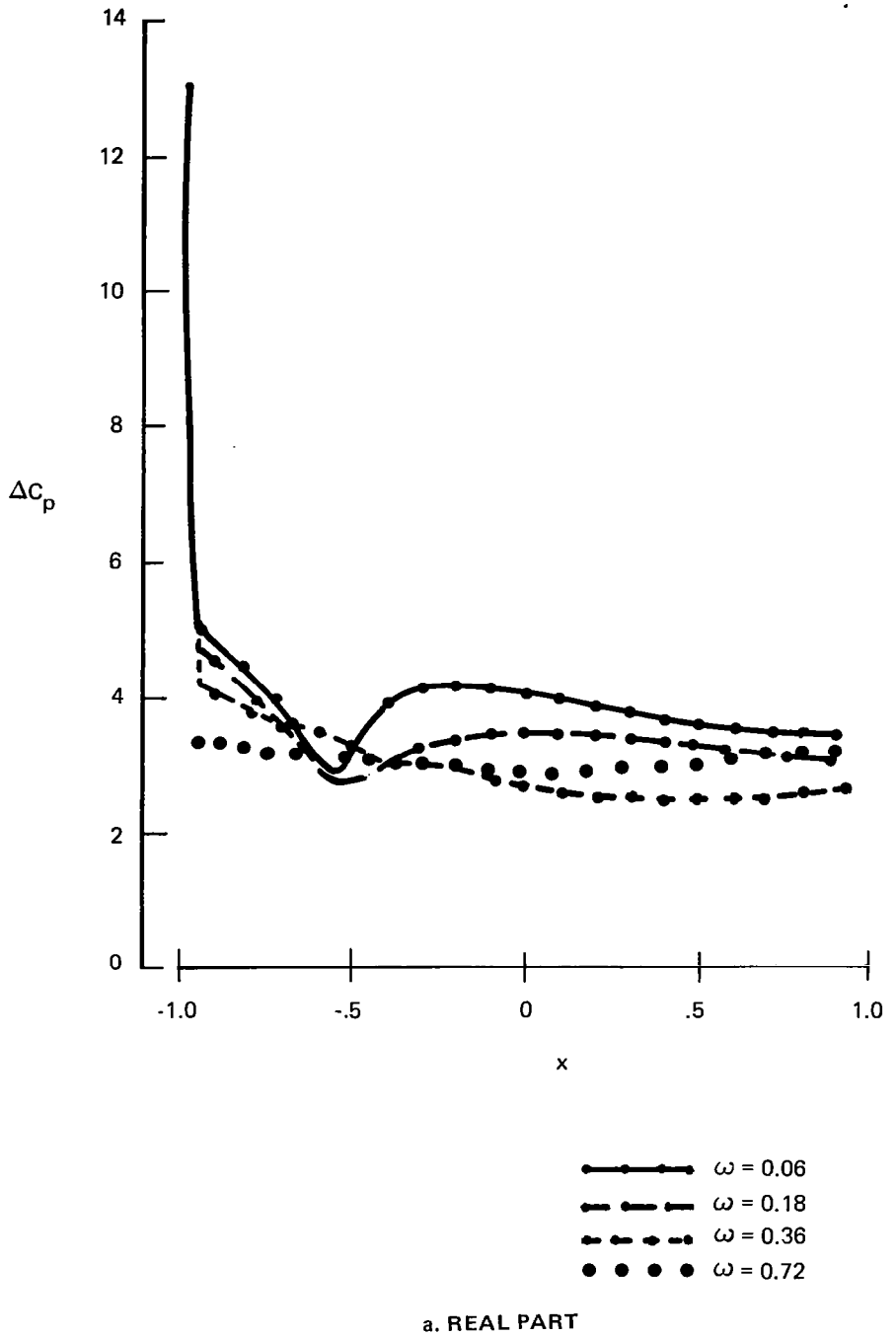

Figure 25.— Jump in Pressure Coefficient Across a Circular-Arc Airfoil Oscillating in Pitch; M = 1.15

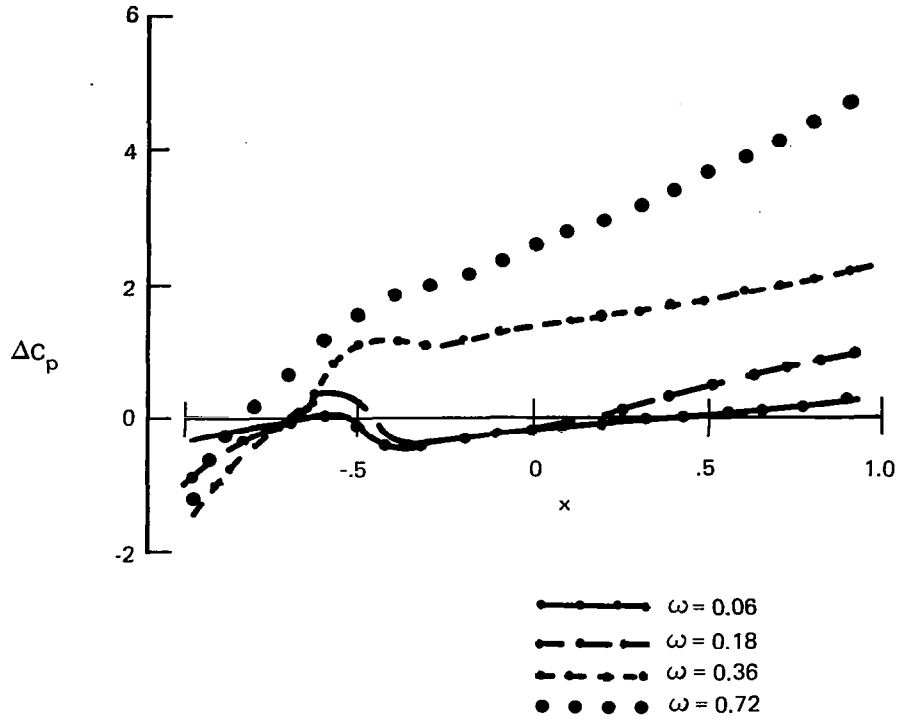

b. IMAGINARY PART

Figure 25.— (Concluded)

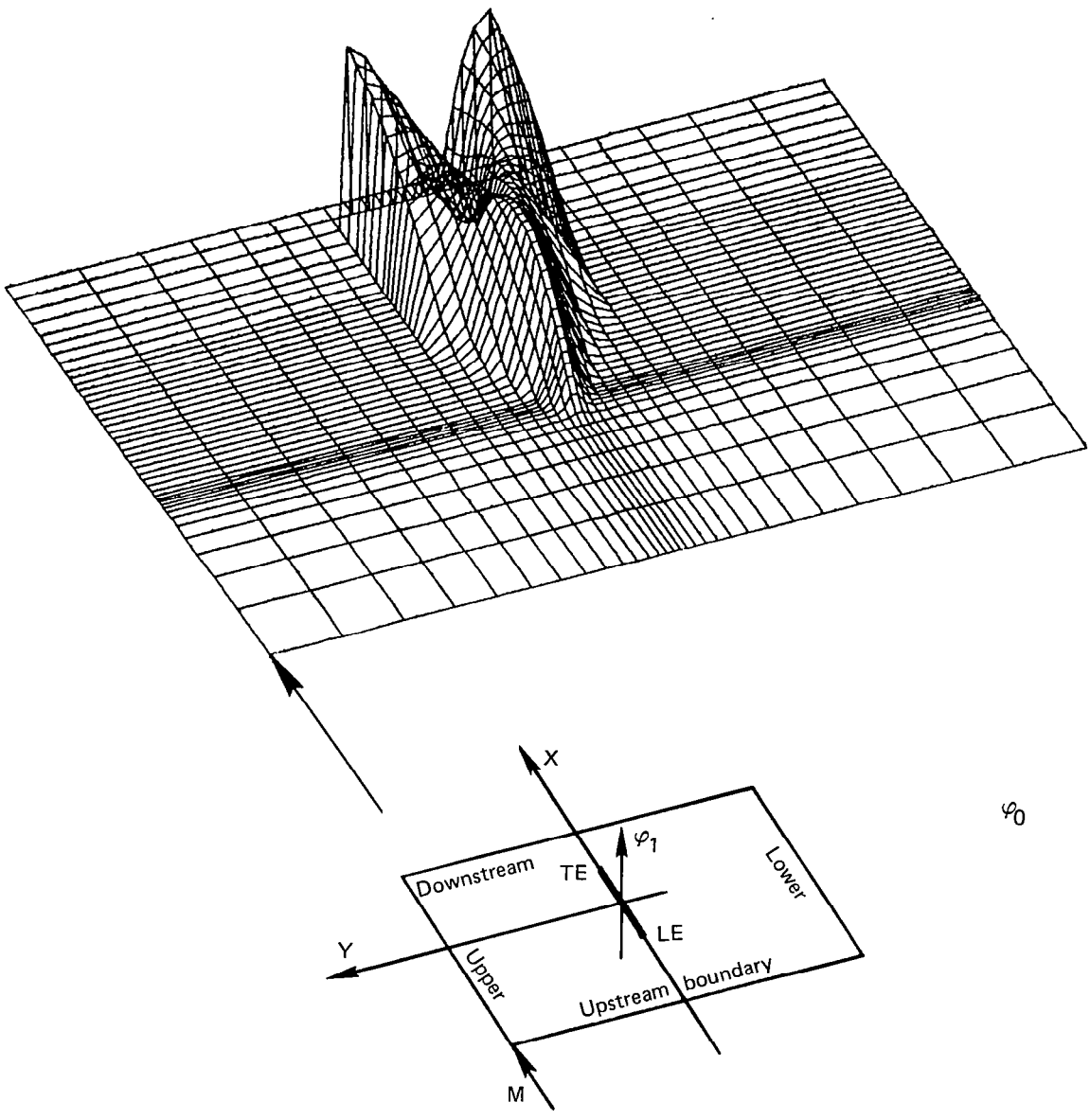

Figure 26.— Steady-State Velocity Potential for a Circular-Arc Airfoil; M = 1.15

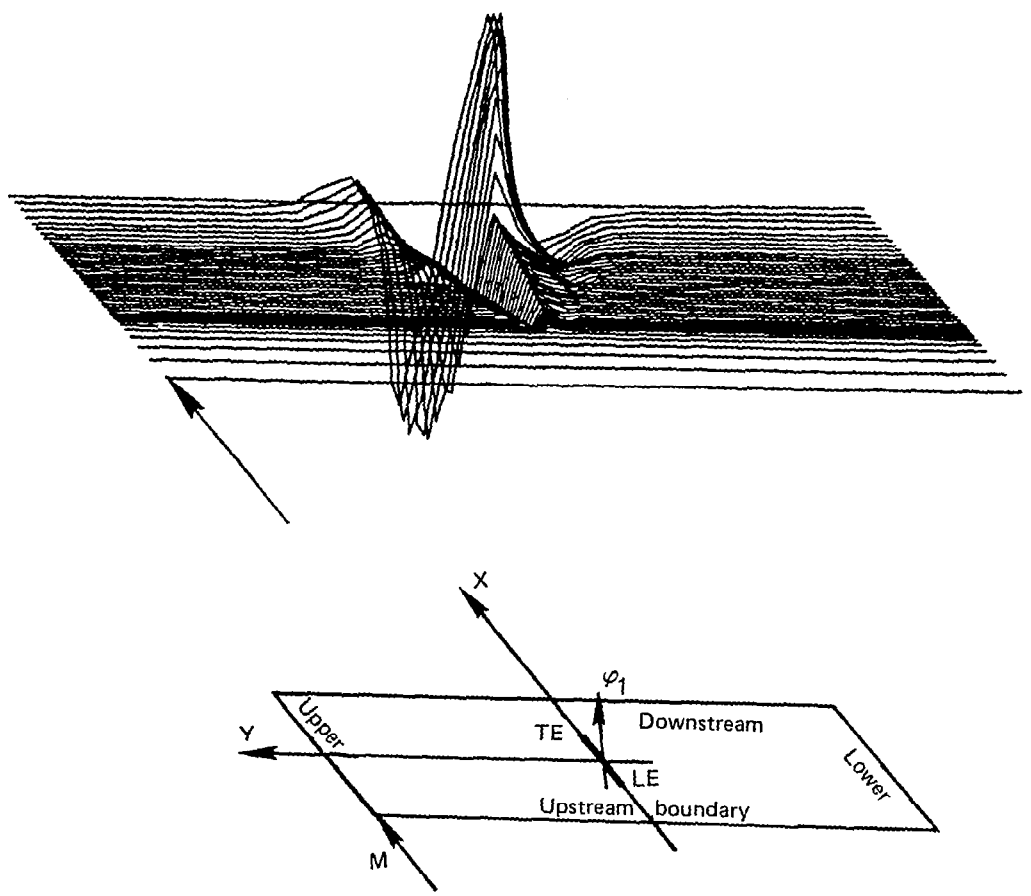

a. REAL PART

Figure 27.– Velocity Potential for a Flat Plate Oscillating in Pitch; $M = 1.15$, $\omega = 0.06$

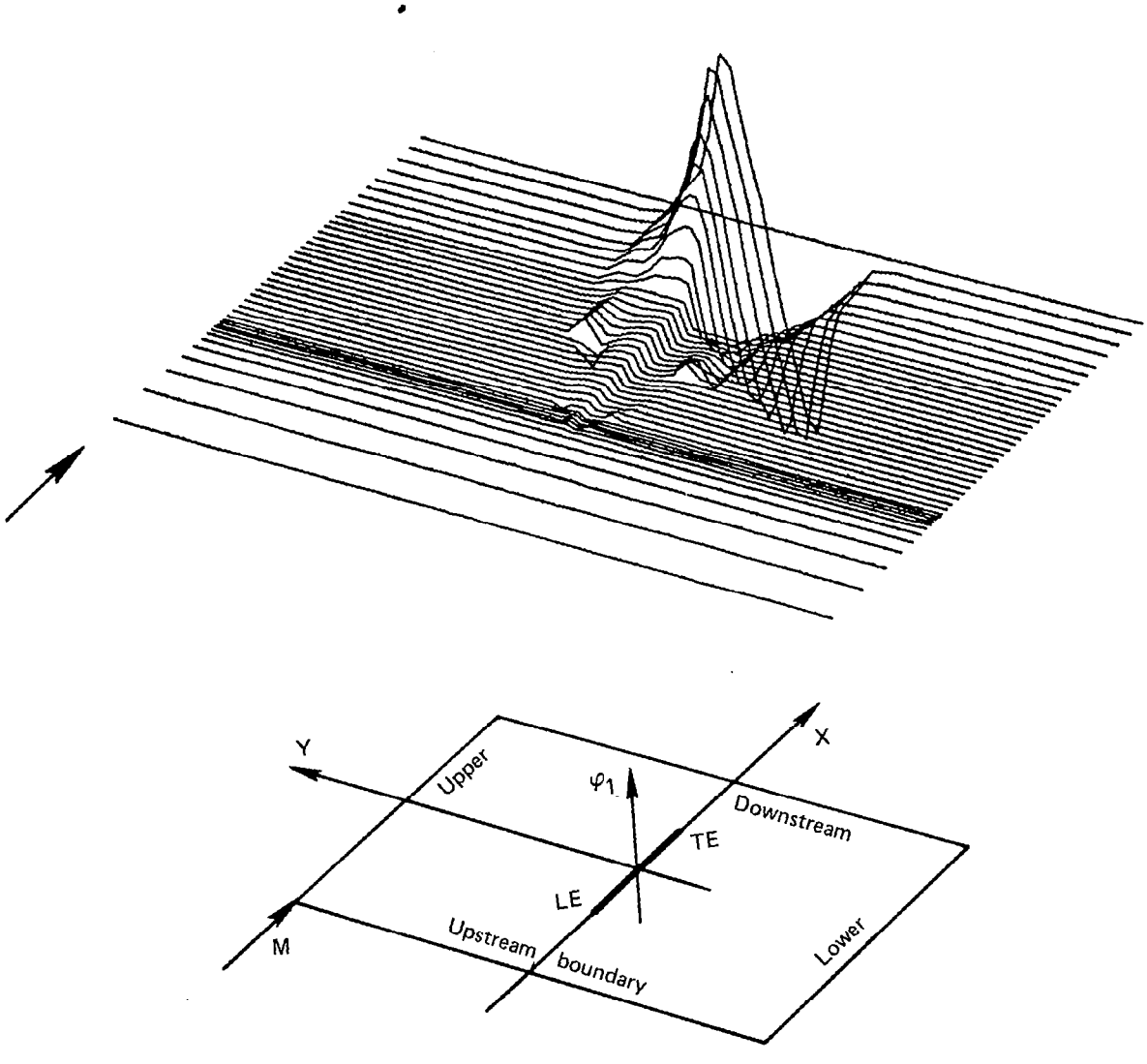

b. IMAGINARY PART

Figure 27.– (Concluded)

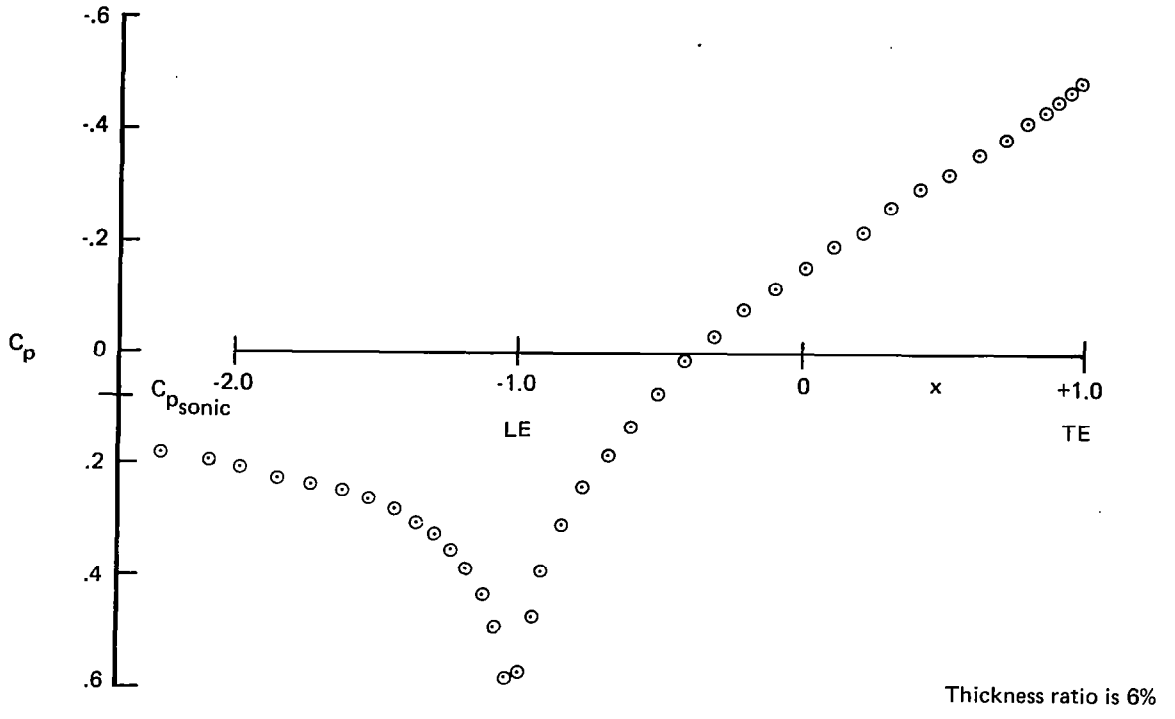

Figure 28.— Pressure Coefficient Distribution for a Circular-Arc Airfoil; M = 1.05

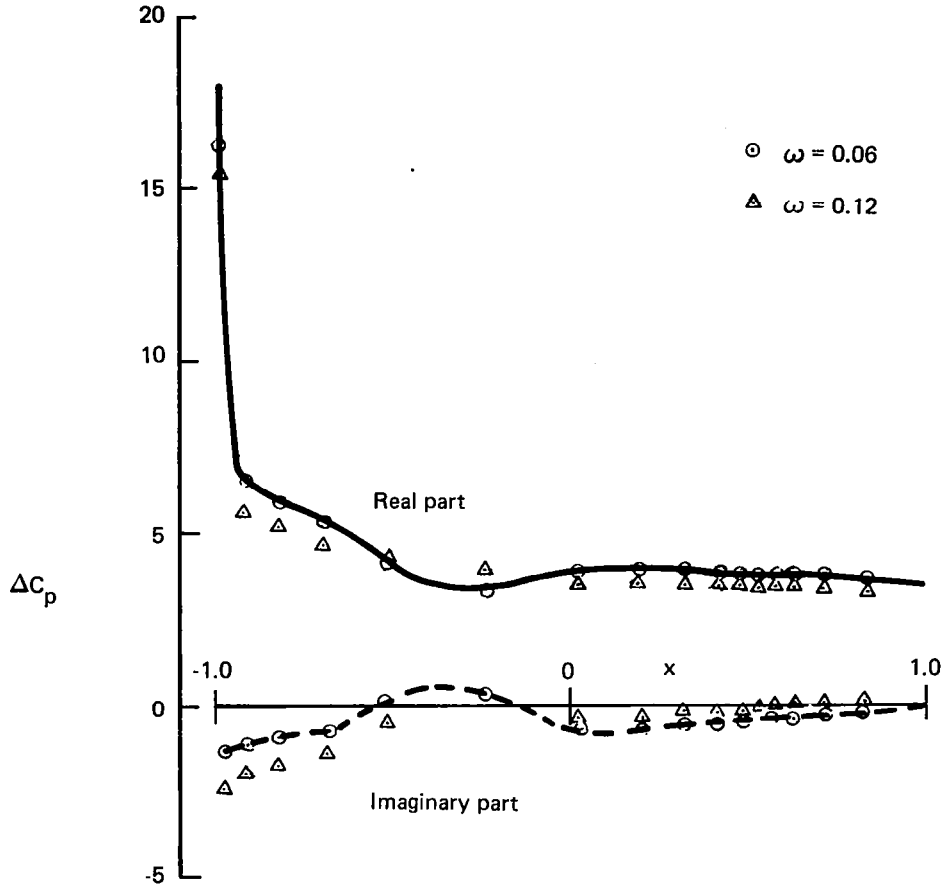

Figure 29.— Jump in Pressure Coefficient Distribution for a Circular-Arc Airfoil Oscillating in Pitch; M = 1.05

6.4 FUTURE APPLICATIONS

The frequency limitation on convergence occurs for the relaxation solution of three-dimensional transonic unsteady harmonic flow as well as two-dimensional flow, although it is not quite as severe due to the extra dimension. Nevertheless, to cover the required range of frequency, a direct solution seems to be the only practical approach.

Approximate solutions of the three-dimensional problem may be obtained by using a strip theory approach where the two-dimensional direct solution is applied to each spanwise cross-section, with the steady-state potential derived from the actual three-dimensional steady-state transonic small-perturbation method of Bailey and Ballhaus (ref. 16). Reference 6 discusses this procedure in greater detail regarding its application to aeroelastic analyses.

The matrix derived from the system of difference equations for the full three-dimensional problem is extremely large. For example, if the numbers of mesh points in the x, y, z direction are, respectively, 50, 40, 60, then the order of the coefficient matrix is 120 000. If the present out-of-core linear equation solver is used, the immediate problem will be insufficient disk storage. In the present example, it will take 1.06×10^{10} sectors to store the factored matrix. Another problem would be the amount of central processor unit (CPU) time required for the computations. For this example, it would take approximately 144×10^{5} CPU seconds on the Cyber 175 (assuming one multiplication takes 3.4 nano-seconds).

However, there are several possible practical approaches to solving the matrix equation for the three-dimensional problem. It should be noted that the generalized conjugate gradient method provides a means for solving large matrix equations with practically no disk storage and within a reasonable amount of CPU time. The generalized conjugate gradient method, like iterative procedures, uses the original matrix in such a way as to eliminate the problem of "fill-ins" of zero elements, as in the case of Gaussian elimination. This is a very good feature for the application under discussion because the original matrix can be recomputed from time to time quite economically. In the example cited here, it is estimated that it would take 576 CPU seconds to arrive at the solution (excluding the CPU time taken to recompute the matrix). However, the biggest concern in using the generalized conjugate method is that the condition number of the required matrix $[A]^{T}[A]$ is the square of the condition number of [A]. This means that if [A] is only fairly well conditioned, the solution obtained might not be satisfactory. Yet, recently, numerical analysts have been studying preconditioning techniques (e.g., ref. 17) to improve the condition number of [A] before applying the generalized conjugate gradient method.

The vector processors such as the CDC Star 100 and the more advanced CRAY machine may also provide a practical means for obtaining direct solutions to the unsteady transonic problem. The difficulty with the application of vector processors to the matrix of the difference equations is the sparseness of the resulting nonzero vectors of the coefficients. These machines are especially suited for large systems of equations for which the matrices are full, and they may be the only feasible approach to such large-scale problems. Rodrique,

Madsen, and Karush (ref. 18) propose an odd-even reduction method for banded linear equations. The three-dimensional problem, unlike the two-dimensional one, has a strictly banded matrix. If the x, y, z grid is 40 x 40 x 60, then the band width is 50 x 60 x 3 = 9000 and the method of Rodrigue et al. is applicable. By the application of permutation matrices P, the odd variables are decoupled from the even variables. For example, consider an even-order matrix equation

$$[A]\{x\} = \{b\}$$

If $[P]$ is a permutation matrix and $[P][A][P]^T$ has the form

$$[P][A][P]^T = \left[\begin{array}{c|c} A_1 & A_2 \\ \hline A_3 & A_4 \end{array}\right]$$

then the approach is to construct a matrix $[Q]$ such that

$$[Q][P][A][P]^T = \left[\begin{array}{c|c} D & U \\ \hline O & \bar{A} \end{array}\right]$$

where $[D]$ is an easily invertible matrix and $[A]$ has the same band structure as $[A]$. The solution of $[A]\{x\} = \{b\}$ is equivalent to

$$[Q][P][A][P]^T[P]\{X\} = [Q][P]\{b\}$$

Letting $\{y\} = [P]\{x\} = \begin{Bmatrix} y_1 \\ y_2 \end{Bmatrix}$ and $\{\bar{b}\} = [Q][P]\{b\} = \begin{Bmatrix} b_1 \\ b_2 \end{Bmatrix}$

the solution of the system

$$[Q][P][A][P]^T\{y\} = \{\bar{b}\}$$

is seen to be

$$\{y_2\} = [\bar{A}]^{-1}\{b_2\}$$

$$\{y_1\} = [D]^{-1}\left(\{b_1\} - [U]\{y_2\}\right)$$

and the final solution of $[A]\{x\} = \{b\}$ is given by

$$\{x\} = [P]^T\{y\}$$

The system $[A]\{Y\} = \{b_2\}$ still needs to be solved, but it is of the same form as the original equations and hence the odd-even reduction may be applied to this set to reduce still further the order of the system. Reference 18 presents some sufficient conditions which guarantee that odd-even reduction can be performed, but conditions which guarantee that the algorithm can be applied in a cyclical manner still need to be established. The overall stability of the method, moreover, needs to be analyzed theoretically.

7.0 AN EXACT TWO-DIMENSIONAL ANALYSIS

In reference 3, the one-dimensional version of the flat plate problem for unsteady transonic flow was solved by a finite difference procedure and the results compared with the analytical solution. One of the main results of this study was that the outer mesh boundary conditions could significantly affect the accuracy of finite difference solutions. This result may be described as follows: The unknown constants in the general solution for the exact partial differential equations are determined by using the boundary conditions to write a set of simultaneous equations. This set of equations forms a characteristic value problem with λ_1 as an eigenvalue. The characteristic values of λ_1 may be real and/or complex. In the finite difference procedure, solutions are calculated only for real values of λ_1. A plot of error (the maximum difference between the analytical and finite difference solutions) versus ω is shown in figure 30, which is reproduced from reference 3. It is seen that if the boundary conditions are such that the eigenvalues (the characteristic values of λ_1) are complex, a smooth error curve is generated. If the boundary condition results in eigenvalues that are real, the error curve tends to infinity at values of ω corresponding to the eigenvalues. A parallel study for this report shows that this same phenomenon also occurs for the two-dimensional problem.

The general form of the equation for a flat plate oscillating in two-dimensional flow is

$$K\varphi_{1_{xx}} + \varphi_{1_{yy}} - 2i(\omega / \epsilon)\varphi_{1_x} + (\omega^2 / \epsilon)\varphi_1 = 0 \tag{13}$$

Three exact solutions of equation (13) are derived in appendix C for the purpose of studying the effects of mesh boundary conditions on the accuracy of finite difference solutions. These are:

$$\begin{aligned}
\varphi_1 &= \left\{\exp\left[i\lambda_1 M(x - x_1)\right] \cdot \sin(\pi y / b) \cdot \sinh[\mu(a - x)]\right\} / \sinh\left[\mu(a - x_1)\right], \quad \lambda_1 < \pi / (b\sqrt{K}) \\
&= \left\{\exp\left[i\lambda_1 M(x - x_1)\right] \cdot \sin(\pi y / b) \cdot \sin[\mu(a - x)]\right\} / \sin\left[\mu(a - x_1)\right], \quad \lambda_1 > \pi / (b\sqrt{K}) \\
&= \exp\left[i\lambda_1 M(x - x_1)\right] \cdot \sin(\pi y / b) \cdot \left\{\frac{\mu \cosh[\mu(a - x)] + i\lambda_1 \sinh[\mu(a - x)]}{\mu \cosh\left[\mu(a - x_1)\right] + i\lambda_1 \sinh\left[\mu(a - x_1)\right]}\right\}, \quad \lambda_1 < \pi / (b\sqrt{K}) \\
&= \exp\left[i\lambda_1 M(x - x_1)\right] \cdot \sin(\pi y / b) \cdot \left\{\frac{\mu \cos[\mu(a - x)] + i\lambda_1 \sin[\mu(a - x)]}{\mu \cos\left[\mu(a - x_1)\right] + i\lambda_1 \sin\left[\mu(a - x_1)\right]}\right\}, \quad \lambda_1 > \pi / (b\sqrt{K})
\end{aligned} \tag{14}$$

where $\mu = \sqrt{\left|\lambda_1^2 - \pi^2 / \left(b^2 K\right)\right|}$ (15)

$$\varphi_1 = \exp\left[i\lambda_1 M(x - x_1)\right] \cdot \left[\exp\left(i\lambda_1 zy\sqrt{K}\right) + \frac{z + 1}{z - 1}\exp\left(-i\lambda_1 zy\sqrt{K}\right)\right] \cdot \left\{\frac{(\mu_1 - \lambda_1)\exp[i\mu_1(x - a)] + (\mu_1 + \lambda_1)\exp[-i\mu_1(x - a)]}{(\mu_1 - \lambda_1)\exp[i\mu_1(x_1 - a)] + (\mu_1 + \lambda_1)\exp[-i\mu_1(x_1 - a)]}\right\} \tag{16}$$

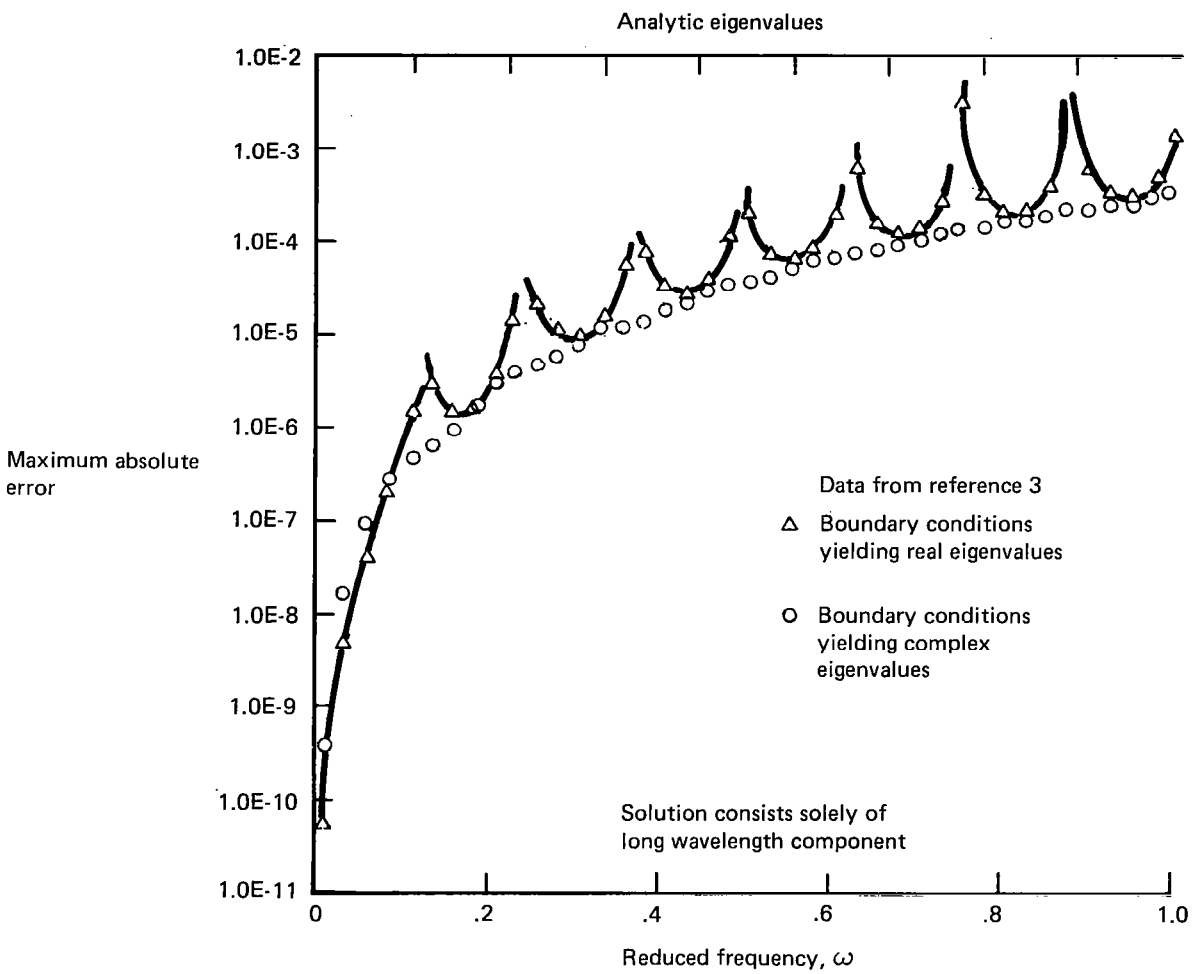

Figure 30.— Comparison of Error Curves for Boundary Conditions Yielding All-Real and Complex Eigenvalues

and $\mu_1 = i\lambda_1\sqrt{1 + z^2}$ and z is a root of

$$(z - 1)^2 - (z + 1)^2 \exp\left[- 2iz\lambda_1 b\sqrt{K} \right] = 0 \qquad (17)$$

The coordinate $x = x_1$ is the upstream boundary, x = a the downstream boundary, while y = 0 and -b are the upper and lower mesh boundaries.

Three types of boundary conditions were considered. In all three cases, the unsteady potential was prescribed on the upstream boundary. For the first solution (eq. (14)), the perturbation potential was set to zero on the other three boundaries. For the second solution (eq. (15)), the potential was set to zero on the upper and lower boundaries, and outgoing wave boundary conditions were applied on the downstream boundary. For the third solution (eq. (16)), outgoing wave boundary conditions were prescribed on all three boundaries. The first leads to real eigenvalues, the second leads to imaginary eigenvalues, while the third set of boundary conditions yields complex eigenvalues.

The direct finite difference solutions are compared with the exact analytic solutions in figure 31. As expected, for the first case the error peaks at those reduced frequencies that correspond to the eigenvalues of the zero potential boundary conditions. Surprisingly, considerable error also occurs for the second solution about these same resonant frequencies, although the eigenvalues for this solution are imaginary.

Outgoing waves on all three boundaries eliminate this difficulty, and the error in the third solution is smooth and considerably less than that for the solution with the zero potential boundary conditions. The improved accuracy for the outgoing wave boundary conditions on all three boundaries is even better than the graph indicates. The curves in figure 31 are absolute magnitude of error. Since the maximum value on the upstream boundary for the first two solutions is unity while the maximum value for the third solution is about three, all three boundary conditions yield about the same relative error in the range of reduced frequency: 0.1 to 0.2.

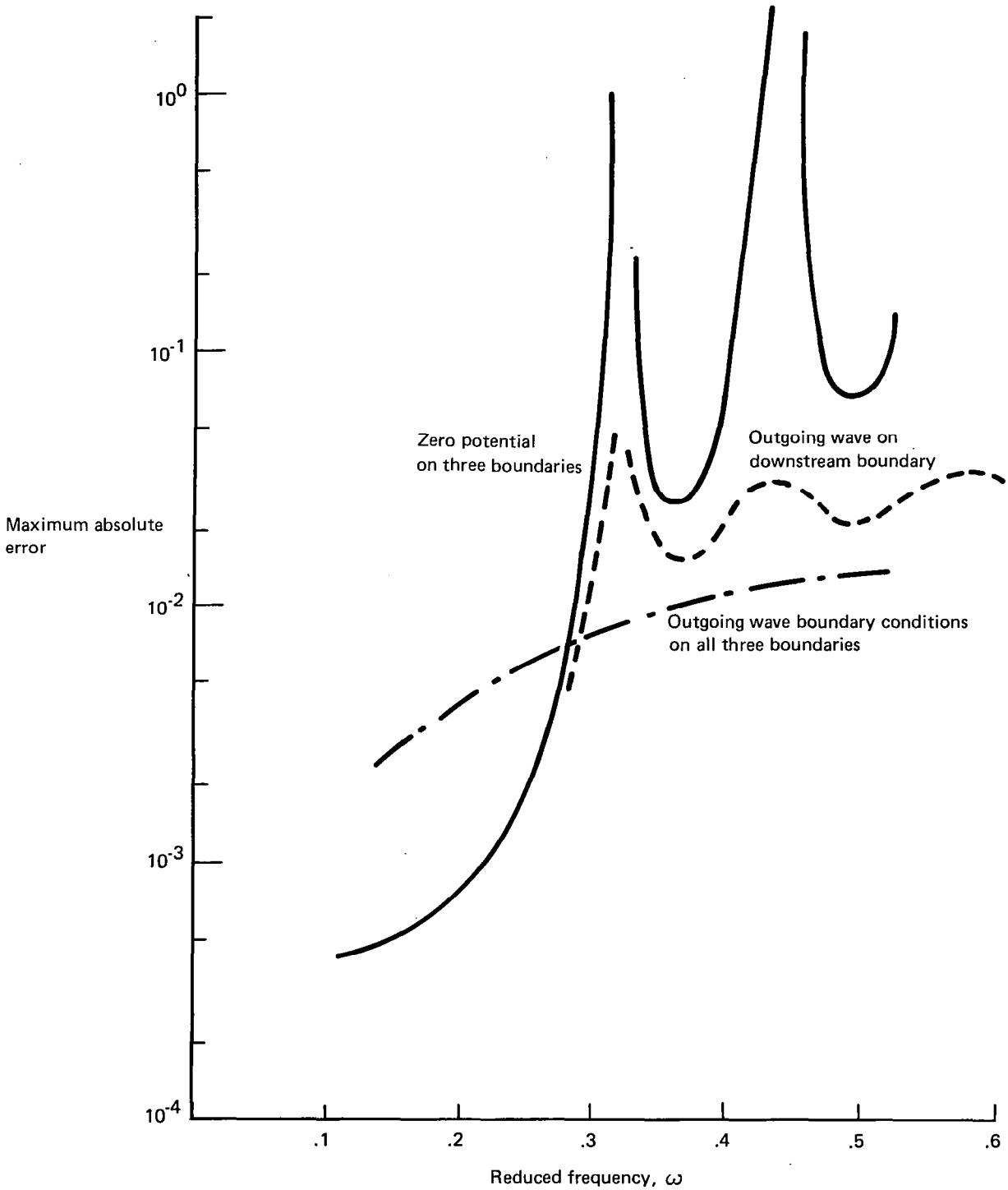

Figure 31.– Influence of Mesh Boundary Conditions on the Accuracy of the Finite Difference Solution of the Linearized Differential Equation for Unsteady Subsonic Flow

8.0 ADDITIONAL STUDIES

Additional studies performed as part of the investigations for this report are presented in a separate report (ref. 6). These studies are either theoretical in nature and were not implemented, or are concerned with concepts that were tried and did not significantly affect either the solution or the solution procedure.

1. An analysis is made of the finite difference operator applied to supersonic mesh points. The usual five-point upwind difference operator is found to be over-stable. This means that, although the numerical solution approaches the true solution as the mesh (step size) is refined, for a given mesh the correct numerical solution is distorted by being attenuated as the disturbance propagates through the mesh. A new nine-point operator is derived which is stable and thus does not attenuate the disturbances.

2. The effect on relaxation solution convergence of adding a viscous term is investigated. It is found that the addition of viscosity has very little effect on convergence, even when large amounts of viscosity are used.

3. An alternate downstream boundary condition is applied in which the velocity potential on the downstream boundary is set equal to the potential due to the wake. The resulting pressures are not significantly different from those obtained by assuming a plane outgoing wave.

4. The three-dimensional differential equation for unsteady transonic flow, as used in this report, is rederived using an oblique coordinate system appropriate for use with swept and tapered wings.

5. In reference 2 it was shown that for the two-dimensional problem, row relaxation converged more rapidly than column relaxation, but that additional terms were required for mesh points at which the flow equation was hyperbolic. These additional terms are derived for the three-dimensional problem.

6. Equations are derived and presented for implementing a procedure that matches the finite difference solution over an inner mesh region to an outer linearized solution that has the appropriate outgoing wave properties. This procedure should reduce the size of the finite difference region as well as provide a more accurate mesh boundary condition.

7. A three-dimensional aeroelastic solution procedure is described that uses two-dimensional unsteady transonic air forces at each cross section. The two-dimensional air forces are calculated using the three-dimensional steady-state velocity potential distribution.

9.0 CONCLUSIONS

The direct finite difference method of this report appears to yield sufficient accuracy for two-dimensional subsonic flow at Mach numbers and reduced frequencies of interest to flutter analysts. The most pressing problem at the start of the investigation had been lack of accuracy at higher values of the parameter λ_1. As shown by examples in section 6.0, this inaccuracy seems to have been overcome by removing a coordinate transformation that placed the outer boundaries of the finite difference region at infinity, by using a more uniformly spaced grid in the crossflow direction, and by increasing the number of finite difference points to provide a finer grid in the field away from the wing. The correlation of the finite difference method with the more exact linear theory is good and no numerical difficulties have been encountered. As a result of this investigation, we have also concluded that the simple outgoing plane wave boundary condition yields sufficient accuracy.

Two concerns of immediate interest remain. First, there is a question of correlating the analytic results of the harmonic procedure with valid experimental data. Preliminary correlation studies with the experimental studies of Tijdeman (ref. 4) have been encouraging but not conclusive. The forthcoming availability of the NASA-Ames data for two-dimensional sections provides an opportunity to further these studies. Second, there is the problem of extending the direct solution to three-dimensional flow. The two possible procedures discussed in section 6 warrant further investigation.

There is controversy over whether the harmonic procedure as formulated for this report includes the characteristics of transonic flow that are of most importance to flutter instability. As of now, the main concern is whether the effects of moving shocks are properly included in the calculation. The most obvious effect – the oscillating pressure pulse that results from the moving shock system – is contained in the numerical results. We believe that this pulse is the first harmonic of the Fourier expansion of the solution for the full nonlinear system and probably incorporates the most significant effects of the moving shock system with respect of the flutter instability. This is an important point and certainly worthy of further investigation.

APPENDIX A

FORM OF DIRECT SOLUTION MATRICES

The matrix of coefficients, [A], of equation (8), is a large, relatively sparse, banded matrix with complex elements. The two-dimensional solution region with the index conventions used in reference 1 is shown in figure A-1. Each mesh point interior to the boundaries is numbered in sequence starting with the first point inside the lower left-hand (upstream) corner. The points on the boundary are eliminated with the outer boundary conditions. The mesh points are numbered by column, bottom to top, and upstream to downstream. The resulting coefficient matrix is of the order* (IMAX - 2) · (JMAX - 2) and is conveniently partitioned into blocks, with each block associated with a column of mesh points from the solution plane. There are thus (IMAX - 2) · (IMAX - 2) blocks each of order (JMAX - 2). The block matrix is shown in figure A-2. Block matrix [A] is a tridiagonal matrix with elements that are coefficients of $\varphi 1_{i,j-1}$, $\varphi 1_{ij}$, and $\varphi 1_{i,j+1}$. Arrangement of the elements in [A] is shown in figure A-3. Block matrix [B] is a diagonal matrix whose nonzero elements are coefficients of $\varphi 1_{i-1,j}$. Block matrix [C] is a diagonal matrix whose elements are coefficients of $\varphi 1_{i+1,j}$. If a mesh point is supersonic, as determined from the steady velocity potential distribution, the corresponding diagonal element in [C] is zero. The block matrix [D] is a diagonal whose elements are coefficients of $\varphi 1_{i-2,j}$. If a mesh point is subsonic, the corresponding diagonal element in [D] is zero. Block matrix [E], illustrated in figure A-4, is a diagonal matrix with elements from the wake calculation included. Block matrix [F] has four nonzero elements as shown in figure A-5. Block matrix [G] is shown in figure A-6.

* The dimensions given in this paragraph are for full-space solutions. For half-space solutions, (JMAX - 2) is replaced by (JM -1).

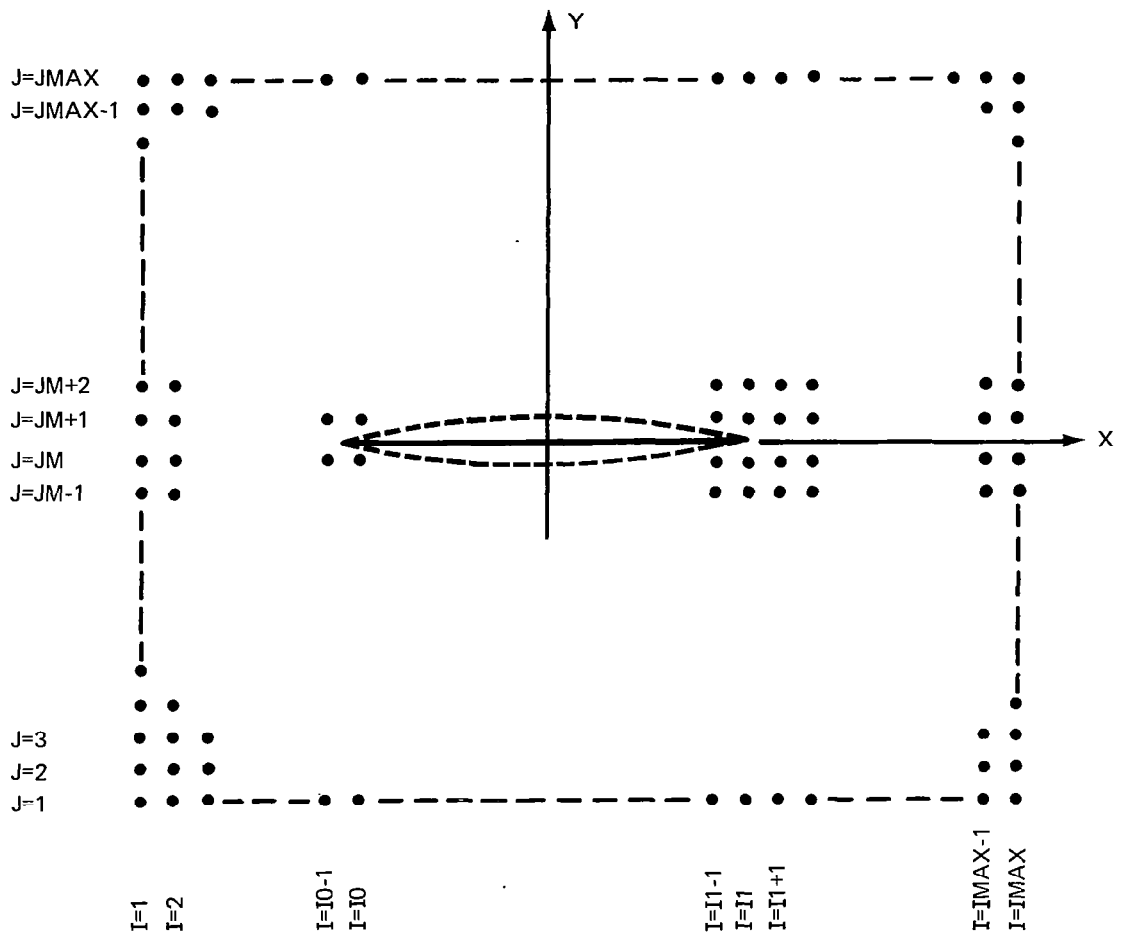

Figure A-1.—Solution Mesh for Two-Dimensional Problem

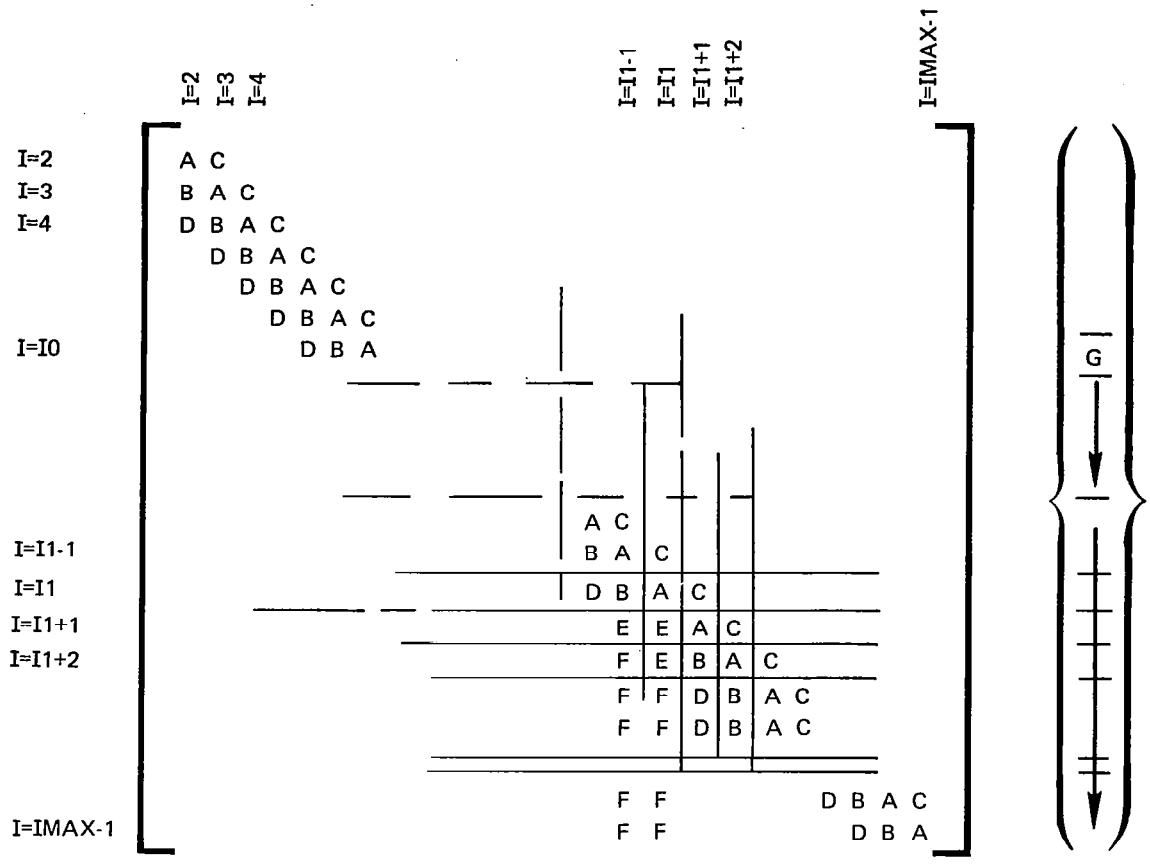

Coefficient matrix

Right-hand-side matrix

Figure A-2.— Form of Matrices for Direct Solution

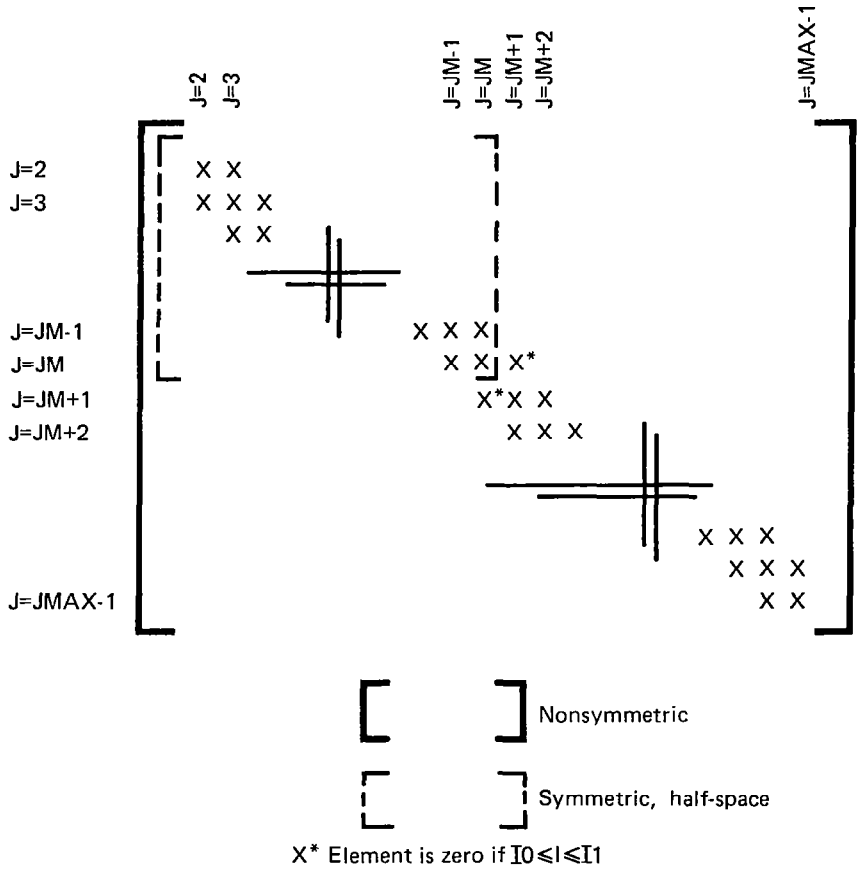

Figure A-3.— Form of Block Matrix A

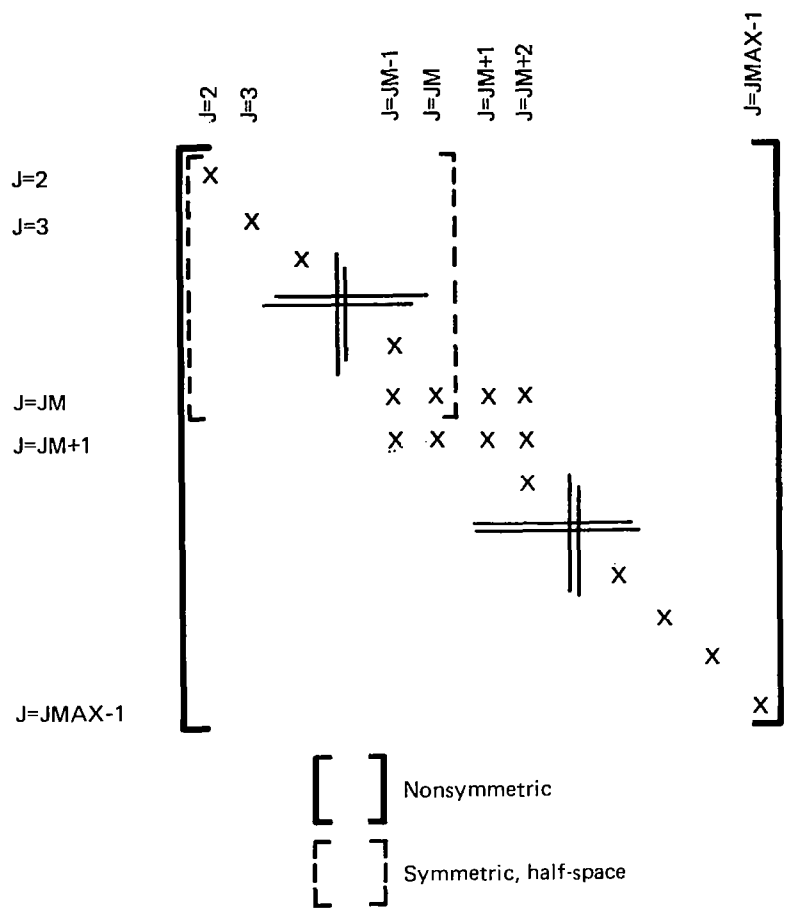

Figure A-4.—Form of Block Matrix E

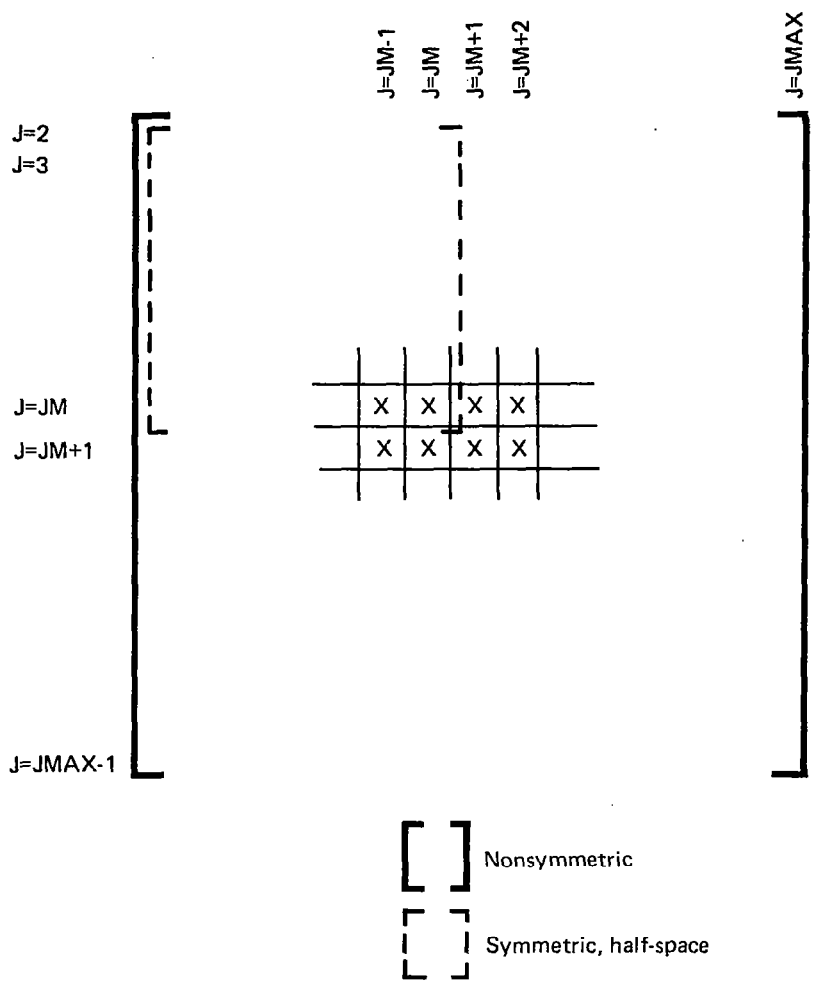

Figure A-5.— Form of Block Matrix F

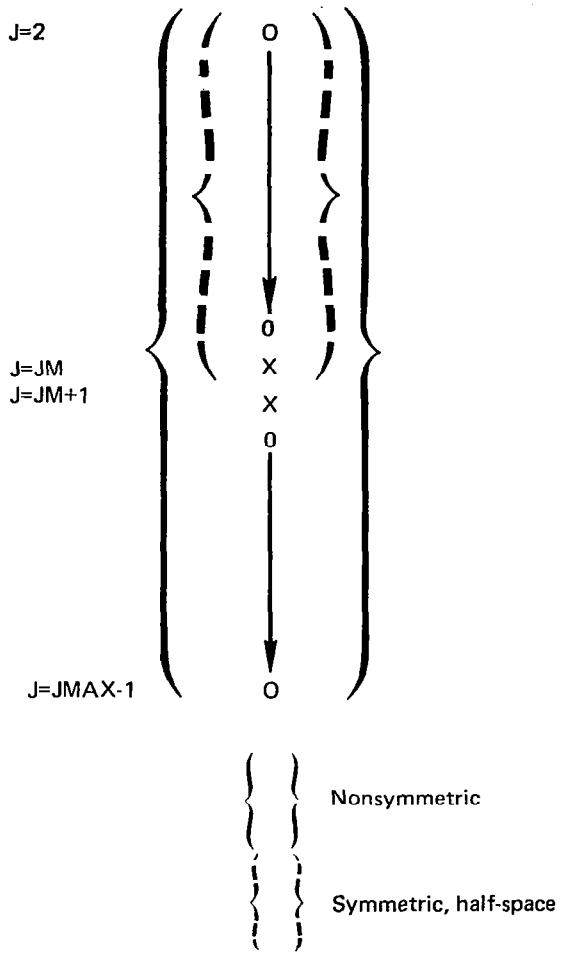

Figure A-6.— Form of Block Matrix G

APPENDIX B

PLOTS OF VELOCITY POTENTIAL DISTRIBUTIONS

A capability for plotting the complex velocity potential distributions calculated with the pilot two-dimensional program of this report has been developed. This capability has been implemented on the PDP-11/70 computer system. These plots have permitted visual study of the potential distributions and provide a basis for estimating the number of points required and the distribution of the points within the solution space for a given case. The real and imaginary parts of the velocity potential are plotted as separate distributions. Each distribution is plotted as a three-dimensional surface over the solution region. The figures appear on a scope and may be manipulated by the observer (i.e., rotated about any of the three axes and regions of particular interest may be enlarged) in order to examine the characteristics of the distribution. In practice, the distributions for the problems of this study are so complicated that no single view provides a clear understanding of the total field, and the ability to change the view continuously has proved invaluable. Hard copies may be obtained; examples are included in section 6.0. A schematic of these plots is shown in figure B-1.

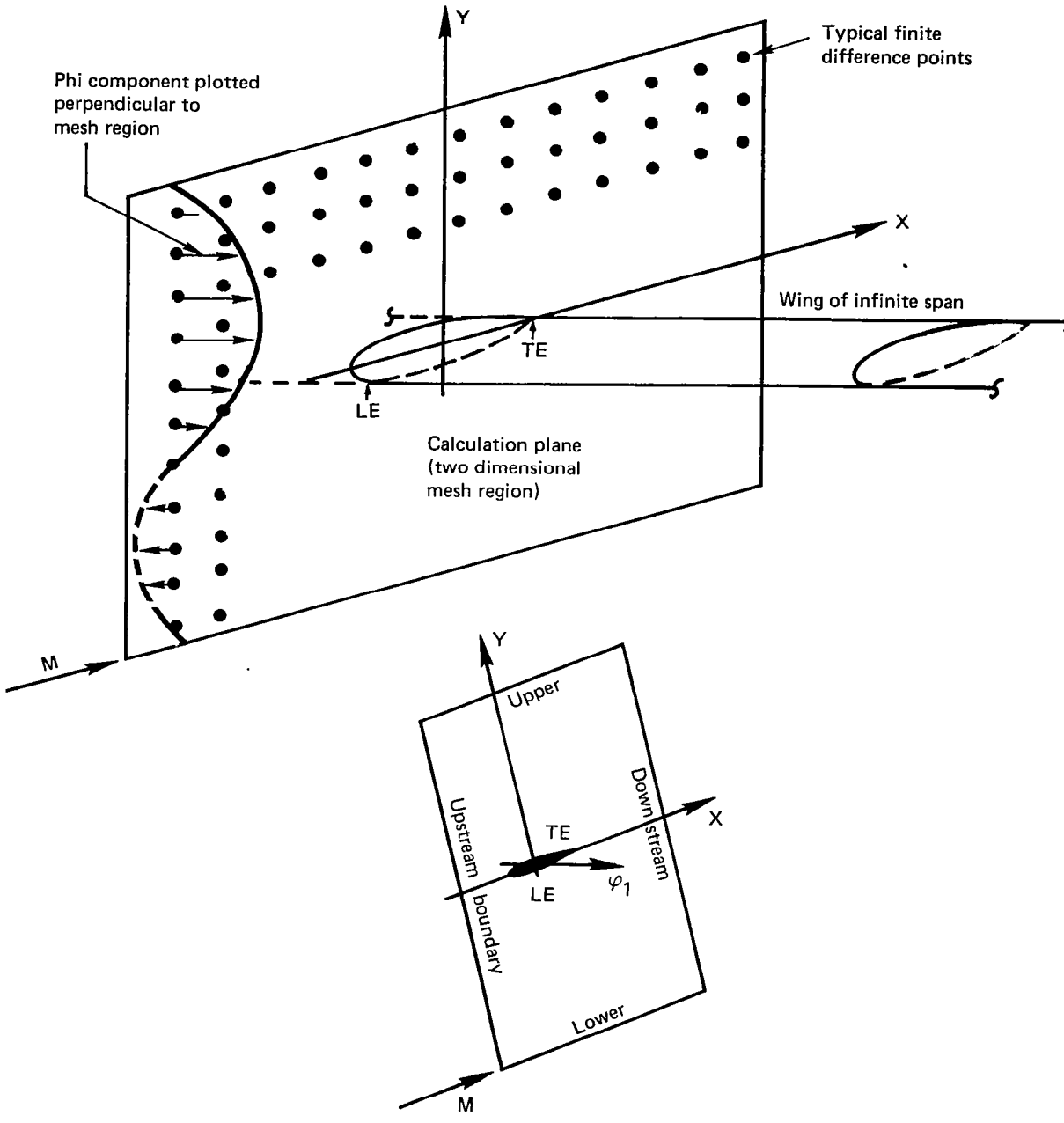

Figure B-1.— Schematic of Velocity Potential Figures

APPENDIX C

EIGENFUNCTION ANALYSIS FOR A FLAT PLATE IN TWO-DIMENSIONAL FLOW

The partial differential equation for the harmonically oscillating flat plate (see eq. (6)) is

$$K\varphi_{1_{xx}} + \varphi_{1_{yy}} - 2i(\omega / \epsilon)\varphi_{1_x} + \left(\omega^2 / \epsilon\right)\varphi_1 = 0$$

Substituting $K = \left(1 - M^2\right)/ M^2\epsilon$ yields

$$\varphi_{1_{xx}} + \varphi_{1_{\bar{y}\bar{y}}} - \frac{2iM^2\omega}{1 - M^2}\varphi_{1_x} + \frac{\omega^2 M^2}{1 - M^2}\varphi_1 = 0 \qquad \text{(C-1)}$$

where $\bar{y} = \sqrt{K}\ y$. We can eliminate the first derivative term by substituting

$$\varphi_1 = \exp\left[i\left(\omega M^2 / \beta^2\right)x\right]\psi = e^{i\lambda_1 Mx}\psi \qquad \text{(C-2)}$$

where $\lambda_1 = \omega M / \beta^2$ and $\beta^2 = 1 - M^2$. Substituting equation (C-2) into equation (C-1) reduces the differential equation to

$$\psi_{xx} + \psi_{\bar{y}\bar{y}} + \lambda_1{}^2\psi = 0 \qquad \text{(C-3)}$$

The boundary condition representing an outgoing plane wave in the x-direction is given by

$$\varphi_{1_x} + i\omega\left(\frac{M}{1 + M}\right)\varphi_1 = 0 \qquad \text{(C-4)}$$

or

$$\varphi_{1_x} + i\lambda_1(1 - M)\varphi_1 = 0$$

Since $\varphi_{1_x} = \left[i\lambda_1 M\psi + \psi_x\right]e^{i\lambda_1 Mx}$, the downstream boundary conditions for ψ becomes

$$\psi_x + i\lambda_1\psi = 0 \qquad \text{(C-5)}$$

Similarly, the upstream boundary condition for an outgoing plane wave in the negative x-direction is given by

$$\varphi_{1_x} - i\lambda_1(1 + M)\varphi_1 = 0 \qquad \text{(C-6)}$$

and in terms of ψ becomes

$$\psi_x - i\lambda_1\psi = 0 \qquad \text{(C-7)}$$

Consider a rectangular region with boundary conditions as shown in figure C-1.

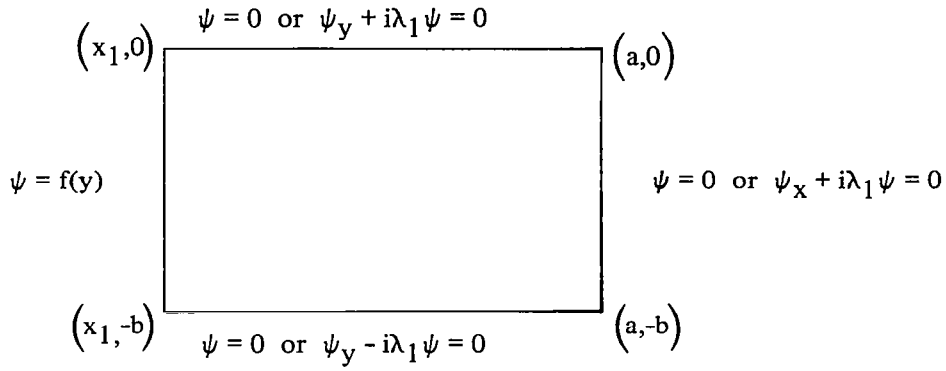

Figure C-1.—Boundary Conditions for Error Analysis

We use separation of variables to solve equation (C-3) and obtain the general solution

$$\psi = (A_1 \sin \mu x + B_1 \cos \mu x)(A_2 \sin \nu\bar{y} + B_2 \cos \nu\bar{y}) \qquad \lambda_1^2 > \nu^2$$

$$\psi = (A_1 \sinh \mu x + B_1 \cosh \mu x)(A_2 \sin \nu\bar{y} + B_2 \cos \nu\bar{y}) \qquad \lambda_1^2 < \nu^2 \qquad \text{(C-8)}$$

where μ and ν are related to λ_1 by

$$\lambda_1^2 + \mu^2 + \nu^2 = 0$$

Consider first the case of $\lambda_1^2 > \nu^2$. To satisfy the boundary conditions $\psi = 0$ at $\bar{y} = 0$ and $\bar{y} = b\sqrt{K}$, the parameter ν must equal $\frac{n\pi}{b\sqrt{K}}$ with $B_2 = 0$.

Thus

$$\psi = \sin \frac{n\pi\bar{y}}{b\sqrt{K}} \cdot [B_1 \cos \mu x + A_1 \sin \mu x] \qquad \text{(C-9)}$$

where

$$\mu = \sqrt{\lambda_1^2 - \frac{n^2\pi^2}{b^2K}} \qquad \text{(C-10)}$$

Eigenfunctions for which $\psi = 0$ on all boundaries occur when $B_1 = 0$

$$\mu = \frac{m\pi}{a}, \quad m = 0,1,2,3... \qquad \text{(C-11)}$$

or

$$\lambda_1^2 = \left(\frac{m\pi}{a}\right)^2 + \left(\frac{n\pi}{b\sqrt{K}}\right)^2 \qquad \text{(C-12)}$$

We take n = 1 and set $\psi = \sin(\pi\bar{y} / b\sqrt{K})$ on $x = x_1$.

For $\psi = 0$ at $x = a$, we use

$$\psi = \frac{\sin \frac{\pi \bar{y}}{b\sqrt{K}} \cdot \sin \mu(a - x)}{\sin \mu(a - x_1)} \tag{C-13}$$

When $\lambda_1 < \frac{\pi}{b}$,

$$\psi = \left[\sin \left(\pi \bar{y} / b\sqrt{K}\right) \cdot \sinh \mu(a - x)\right] / \sinh \mu(a - x_1) \tag{C-14}$$

where

$$\mu = \sqrt{\left|\lambda_1^2 - n^2 \pi^2 / \left(b^2 K\right)\right|} \tag{C-15}$$

We now consider the boundary conditions

$$\psi_x + i\lambda_1 \psi = 0 \qquad \text{at } x = a \tag{C-16}$$

Then equation (C-9) leads to

$$\psi = \sin \frac{\pi y}{b} \cdot \left\{ \frac{\mu \cos \mu(a - x) + i\lambda_1 \sin \mu(a - x)}{\mu \cos \mu(a - x_1) + i\lambda_1 \sin \mu(a - x_1)} \right\} \tag{C-17}$$

We now consider a solution of equation (C-3) with outgoing wave boundary conditions on the three boundaries, i.e.,

$$\begin{aligned} &\psi_x + i\lambda_1 \psi = 0 \text{ at } x = a \\ &\psi_{\bar{y}} + i\lambda_1 \psi = 0 \text{ at } \bar{y} = 0 \\ &\psi_{\bar{y}} - i\lambda_1 \psi = 0 \text{ at } \bar{y} = -\sqrt{K}\, b \end{aligned} \tag{C-18}$$

In place of the form of the solution given in equation (C-8) we write

$$\psi = \left[c_1 e^{i\alpha \bar{y}} + c_2 e^{-i\alpha \bar{y}}\right] \cdot \left[d_1 e^{i\mu(x-a)} + d_2 e^{-i\mu(x-a)}\right]$$

where $\lambda_1^2 + \alpha^2 + \mu^2 = 0$

To satisfy the conditions at $x = a$ we obtain for the second bracketed term

$$\frac{(\mu - \lambda_1) e^{i\mu(x-a)} + (\mu + \lambda_1) e^{-i\mu(x-a)}}{(\mu - \lambda_1) e^{i\mu(x_1-a)} + (\mu + \lambda_1) e^{-i\mu(x_1-a)}} \tag{C-19}$$

Here, we normalized the factor to make it unity at the upstream boundary $x = x_1$.

The constants c_1 and c_2 are now determined to satisfy the boundary conditions in equation (C-18) for the boundaries $\bar{y} = 0$ and $-b\sqrt{K}$. The first boundary condition yields

$$c_2 = \frac{(\alpha + \lambda_1)}{(\alpha - \lambda_1)} c_1$$

while the second boundary condition leads to

$$i\alpha\left[e^{-i\alpha b\sqrt{K}} - \frac{\alpha+\lambda_1}{\alpha-\lambda_1} e^{i\alpha b\sqrt{K}}\right] - i\lambda_1\left[e^{-i\alpha b\sqrt{K}} + \frac{\alpha+\lambda_1}{\alpha-\lambda_1} e^{i\alpha b\sqrt{K}}\right] = 0$$

or

$$(\alpha-\lambda_1)^2 - (\alpha+\lambda_1)^2 e^{2i\alpha b\sqrt{K}} = 0$$

Substituting $\alpha = \lambda_1 z$ we choose a nonzero root of the equation

$$(z-1)^2 - (z+1)^2 e^{-2iz\lambda_1 b\sqrt{K}} = 0 \qquad \text{(C-20)}$$

for each value of λ_1. With this specific value of z, the solution to the flat plate equation (C-1) is found by multiplying the solution to equation (C-3) by the factor $\exp(i\lambda_1 M(x - x_1))$. Thus we obtain

$$\varphi_1 = e^{i\lambda_1 M(x-x_1)} \cdot \left\{ e^{i\lambda_1 zy\sqrt{K}} + \left(\frac{z+1}{z-1}\right) e^{-i\lambda_1 zy\sqrt{K}} \right\}$$

$$\cdot \left\{ \frac{(\mu-\lambda_1)\cdot\exp[i\mu(x-a)] + (\mu+\lambda_1)\cdot\exp[-i\mu(x-a)]}{(\mu-\lambda_1)\cdot\exp[i\mu(x_1-a)] + (\mu+\lambda_1)\cdot\exp[-i\mu(x_1-a)]} \right\} \qquad \text{(C-21)}$$

where z is a root of equation (C-20) and $\mu \Rightarrow i\lambda_1\sqrt{1+z^2}$.

In the difference solution, the first bracketed term is used as boundary conditions on the mesh line $x = x_1$. Similarly, solutions of the flat plate equation are obtained from equations (C-13), (C-14), and (C-17). We then have

$$\varphi_1 = \left\{\exp[i\lambda_1 M(x-x_1)] \cdot \sin(\pi y/b) \cdot \sinh[\mu(a-x)]\right\} / \sinh[\mu(a-x_1)], \quad \lambda_1 < \pi/(b\sqrt{K})$$

$$= \left\{\exp[i\lambda_1 M(x-x_1)] \cdot \sin(\pi y/b) \cdot \sin[\mu(a-x)]\right\} / \sin[\mu(a-x_1)], \quad \lambda_1 > \pi/(b\sqrt{K}) \qquad \text{(C-22)}$$

$$\varphi_1 = \exp[i\lambda_1 M(x-x_1)] \cdot \sin(\pi y/b) \cdot \left\{\frac{\mu\cosh[\mu(a-x)] + i\lambda_1\sinh[\mu(a-x)]}{\mu\cosh[\mu(a-x_1)] + i\lambda_1\sinh[\mu(a-x_1)]}\right\}, \quad \lambda_1 < \pi/(b\sqrt{K})$$

$$= \exp[i\lambda_1 M(x-x_1)] \cdot \sin(\pi y/b) \cdot \left\{\frac{\mu\cos[\mu(a-x)] + i\lambda_1\sin[\mu(a-x)]}{\mu\cos[\mu(a-x_1)] + i\lambda_1\sin[\mu(a-x_1)]}\right\}, \quad \lambda_1 > \pi/(b\sqrt{K}) \qquad \text{(C-23)}$$

where $\mu = \sqrt{\left|\lambda_1^2 - \pi^2/(b^2K)\right|}$

The solutions in equations (C-21), (C-22), and (C-23) were used to study the influence of mesh boundary conditions on the accuracy of the solutions of the finite difference equations.

APPENDIX D

FOURIER ANALYSIS OF TWO STEP FUNCTIONS OSCILLATING ON OPPOSITE SIDES OF A PLATE

Consider a jump in pressure across a plate produced by two pressure step functions representing shocks on the two sides of a flat zero thickness airfoil. For the two step functions 90° out of phase, the pressure jump is given

$$\Delta C_p = f(t) = H(x - a \sin \omega t) - H(x - a \cos \omega t) \tag{D-1}$$

where H(x) is the unit function defined by

$$H(x) = 0 \text{ for } x < 0$$

$$H(x) = 1 \text{ for } x > 0$$

Note that $\Delta C_p = 0$ for $x > a$ and $x < -a$. This produces a pulse of oscillating width about the range $-a < x < a$. Furthermore, the center of this pulse also oscillates about x = 0.

We shall now represent equation (D-1) by a Fourier expansion of the form

$$f(t) = \sum_{n=1}^{\infty} b_n \sin n\omega t + \sum_{n=0}^{\infty} c_n \cos n\omega t \tag{D-2}$$

For $0 < x < a$, the coefficients b_n are given by

$$\pi b_n = \int_{-\pi}^{\sin^{-1}(x/a)} \sin n\theta \, d\theta + \int_{\pi - \sin^{-1}(x/a)}^{\pi} \sin n\theta \, d\theta - \int_{-n}^{-\cos^{-1}(x/a)} \sin n\theta \, d\theta - \int_{\cos^{-1}(x/a)}^{\pi} \sin n\theta \, d\theta \tag{D-3}$$

Integration yields

$$b_n = \left\{(-1 + \cos n\pi) \cos \left[n \sin^{-1}(x / a)\right]\right\} / (n\pi) \tag{D-4}$$

Replacing $\sin n\theta$ by $\cos n\theta$ in equation (D-3) yields

$$\pi c_n = \left\{(1 + \cos n\pi) \sin \left[n \sin^{-1}(x / a)\right]\right\} / n + 2 \sin \left[n \cos^{-1}(x / a)\right] / n \tag{D-5}$$

The preceding equations also hold for negative x. Since we are concerned with the amplitude of the fundamental frequency, we set n = 1 and obtain

$$\pi b_1 = -2 \cos \left[\sin^{-1}(x / a)\right] = -2\sqrt{1 - (x / a)^2} \tag{D-6}$$

$$\pi c_1 = 2 \sin \left[\cos^{-1}(x / a)\right] = 2\sqrt{1 - (x / a)^2} \tag{D-7}$$

In the complex form of the amplitude, b_1 is the imaginary part of $\exp(i\omega t)$, while c_1 is the real part. Equations (D-6) and (D-7) are plotted in figure 5. Note that the pressure pulse is similar to the example in figure 2.

Thus it appears that the present frequency domain method may well produce the pulse amplitude and movement of the fundamental resulting from moving shocks without additional treatment such as computing the actual shock motion by a linear analysis and performing the Fourier analysis.

REFERENCES

1. Ehlers, F. E.: "A Finite Difference Method for the Solution of the Transonic Flow Around Harmonically Oscillating Wings." NASA CR-2257, January 1974.

2. Weatherill, W. H.; Ehlers, F. E.; and Sebastian, J. D.: "Computation of the Transonic Perturbation Flow Fields Around Two- and Three-Dimensional Oscillating Wings." NASA CR-2599, December 1975.

3. Weatherill, W. H.; Sebastian, J. D.; and Ehlers, F. E.: "The Practical Application of a Finite Difference Method to the Analysis of Transonic Flow Over Oscillating Airfoils and Wings." NASA CR-2933, December 1977.

4. Tijdeman, H.: "Investigations of the Transonic Flow Around Oscillating Airfoils." NLR TR 77090 U, December 1977.

5. Ashley, H.: "On the Role of Shocks in the 'Sub-Transonic' Flutter Phenomenon." AIAA Paper 79-0765, presented at the AIAA/ASME/ASCE/AHTS 20th Structures, Structural Dynamics, and Materials Conference, St. Louis, Mo., April 4–6, 1979. Printed in conference proceedings, *A Collection of Technical Papers on Design and Loads*, CP795.

6. Ehlers, F. E.; Sebastian, J. D.; and Weatherill, W. H.: "An Investigation of Several Factors Involved in a Finite Difference Procedure for Analyzing the Transonic Flow About Oscillating Airfoils and Wings." NASA CR-159143, December 1979.

7. Weatherill, W. H.; and Ehlers, F. E.: "A User's Guide for A344 – A Program Using a Finite Difference Method to Analyze Transonic Flow Over Oscillating Airfoils." NASA CR-159141, December 1979.

8. Yip, E. L.: "FORTRAN Subroutines for Out-of-Core Solutions of Large Complex Linear Systems." NASA CR-159142, December 1979.

9. Krupp, J. A.; and Murman, E. M.: "Computation of Transonic Flows Past Lifting Airfoils and Slender Bodies." *AIAA Journal*, vol. 10, July 1972, pp. 880–887.

10. Krupp, J. A.: "The Numerical Calculation of Plane Steady Transonic Flows Past Thin Lifting Airfoils." Doctor of Philosophy Thesis, University of Washington, 1971; also Boeing Scientific Research Laboratories document D180-12958-1, June 1971.

11. Klunker, E. B.: "Contributions to Methods for Calculating the Flow About Thin Lifting Wings at Transonic Speeds." NASA TN D-6530, November 1971.

12. Rowe, W. S.; Redman, M. C.; Ehlers, F. E.; and Sebastian, S. D.: "Prediction of Unsteady Aerodynamic Loadings Caused by Leading Edge and Trailing Edge Control Surface Motions in Subsonic Compressible Flow – Analysis and Results." NASA CR-2543, August 1975.

REFERENCES (concluded)

13. Redman, M. C.; and Rowe, W. S.: "Predictions of Unsteady Aerodynamic Loadings Caused by Leading Edge and Trailing Edge Control Surface Motions in Subsonic Compressible Flow – Computer Program Description." NASA CR-132634, May 1975 1975.

14. Stahara, S. S.: "Operational Manual for Two-Dimensional Transonic Code TSFOIL." NASA CR-3064, December 1973.

15. Traci, R. M.; Albano, E. D.; and Farr, J. L., Jr.: "Small Disturbance Transonic Flows About Oscillating Airfoils and Planar Wings." AFFDL-TR-75-100, August 1975.

16. Bailey, F. R.; and Ballhaus, W. F.: "Relaxation Methods for Transonic Flow About Wing-Cylinder Combinations and Lifting Swept Wings." *Proceedings of the 3rd International Conference on Numerical Methods in Fluid Mechanics*, 3–7 July 1972, Paris, France, Spring-Verlag, Berlin, Germany, (A74-16951).

17. Axelson, O.; and Gustaffson, I.: "A Modified Upwind Scheme for Convective Transport Equations and the Use of Conjugate Gradient Methods for the Solution of Non-symmetric Equations." *J. Inst. Math. App.*, vol. 23, pp. 321-337, 1979.

18. Rodrigue, G. H.; Madsen, N. K.; and Karush, J. I.: "Odd-Even Reductions for Banded Linear Equations." *J. of the Association for Computing Machines*, vol. 26, No. 1, January 1979, pp. 72–81.

1 Report No	2 Government Accession No.	3 Recipient's Catalog No
NASA CR-3195		

4 Title and Subtitle	5 Report Date
Further Investigation of a Finite Difference Procedure for Analyzing the Transonic Flow About Harmonically Oscillating Airfoils and Wings	May 1980
	6 Performing Organization Code
7 Author(s) W. H. Weatherill, F. E. Ehlers, E. Yip, and J. D. Sebastian	8 Performing Organization Report No D6-48851
	10 Work Unit No
9 Performing Organization Name and Address Boeing Commercial Airplane Company P.O. Box 3707 Seattle, Washington 98124	11 Contract or Grant No NAS1-15128
	13 Type of Report and Period Covered Contractor report
12 Sponsoring Agency Name and Address National Aeronautics and Space Administration Washington, D.C. 20546	14 Sponsoring Agency Code

15 Supplementary Notes
Langley technical monitor: Robert M. Bennett
Final report

16 Abstract

Analytical and empirical studies of a finite difference method for the solution of the transonic flow about harmonically oscillating wings and airfoils are presented. The procedure is based on separating the velocity potential into steady and unsteady parts and linearizing the resulting unsteady equations for small disturbances. The steady velocity potential is obtained first from the well-known nonlinear equation for steady transonic flow. The unsteady velocity potential is then obtained from a linear differential equation in complex form with spatially varying coefficients. Since sinusoidal motion is assumed, the unsteady equation is independent of time.

An out-of-core direct solution procedure has been developed and applied to two-dimensional sections. Results are presented for a section of vanishing thickness in subsonic flow and an NACA 64A006 airfoil in supersonic flow. Good correlation is obtained in the first case at values of Mach number and reduced frequency of direct interest in flutter analyses. Reasonable results are obtained in the second case.

Comparisons of two-dimensional finite difference solutions with exact analytic solutions indicate that the accuracy of the difference solution is dependent on the boundary conditions used on the outer boundaries. Homogeneous boundary conditions on the mesh edges that yield complex eigenvalues give the most accurate finite difference solutions. The plane outgoing wave boundary conditions meet these requirements.

17 Key Words (Suggested by Author(s))	18 Distribution Statement
Unsteady flow Transonic flow Oscillating airfoil Flutter	Unclassified - unlimited Subject Category 02

19 Security Classif. (of this report)	20 Security Classif. (of this page)	21 No. of Pages	22 Price*
Unclassified	Unclassified	81	$6.00

*For sale by the National Technical Information Service, Springfield, Virginia 22161

NASA-Langley, 1980